CHAPTER 1

Survey of Small Antenna Theory

Jeffrey Chalas, Kyohei Fujimoto, John L. Volakis, and Kubilay Sertel

1.1 Introduction

Antenna miniaturization has long been discussed as one of the most significant and interesting subjects in antenna and related fields. Since the beginning of radio communications, the desire for small and versatile antennas has been ever increasing. Today's needs for more multifunctional systems further drive requirements for small mobile terminals, including cell phones, handheld portable wireless equipment for internet connection, short- and long-range communication devices, RFIDs (radio frequency identification), etc. Similarly, small equipment and devices used for data transmission and navigation (GPS systems) require small antennas. These applications and continuing growth of wireless devices will continue to challenge the community to create smaller and more multifunctional antennas.

This chapter is intended to provide a chronological review of past theoretical work crucial to antenna miniaturization. Throughout, we shall refer to the small antennas as "electrically small antennas," or ESAs, implying that their size is much smaller than a wavelength at the operational frequency.

Wheeler [1] proposed the ESA definition as an antenna whose maximum dimension is less than $\lambda/2\pi$, referred to as a "radianlength." Another commonly used (and equivalent) definition of an ESA is an

antenna that satisfies the condition

$$ka < 0.5 \tag{1.1}$$

where k is the wave number $2\pi/\lambda$, and a is the radius of the minimum size sphere that encloses the antenna (see Fig. 1.1). We shall refer to this spherical enclosure as the "*Chu sphere*." Small antennas fitting the Wheeler definition radiate the first order spherical modes of a Hertzian dipole (see Fig. 1.2) and have radiation resistances, efficiencies, and bandwidths. As is well known, these parameters typically decrease with electrical size ka.

Another commonly accepted definition of a small antenna is $ka < 1$, [2]. This definition can be interpreted as an antenna enclosed inside a sphere of radius equal to one radianlength. Such a sphere is referred to as a "radiansphere" [33], and represents the boundary between the near- and far-field radiation for a Hertzian dipole. Hansen [2] notes that for antennas of this size, higher order spherical modes ($n > 1$) are evanescent.

In the sections to follow, the small antenna performance will be characterized by their size ka, quality factor Q, fractional bandwidth B, and gain G. It is therefore important to have an understanding of these parameters. Of particular interest is how antenna bandwidth (or Q) is related to the antenna size. As will see, there is an optimum Q

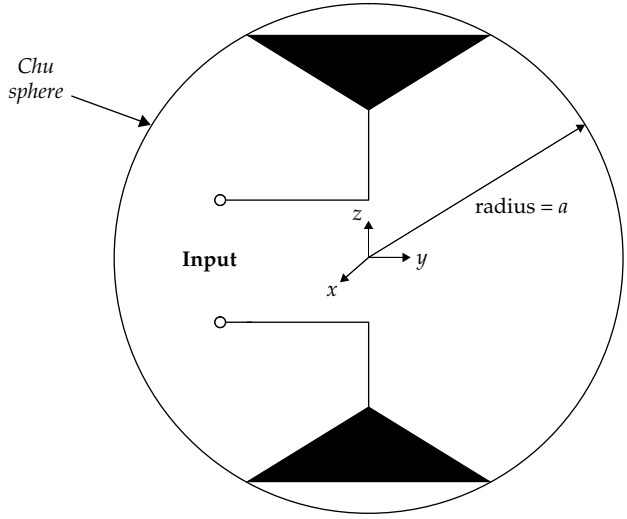

FIGURE 1.1 *Chu sphere* of radius "*a*" centered about the origin.
The *Chu sphere* is the minimum circumscribing sphere enclosing the antenna of maximum dimension $2a$.

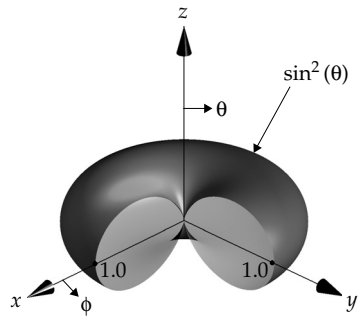

FIGURE 1.2 TM_{10} or TE_{10} mode power pattern with the region ($0^\circ < \phi < 90^\circ$, $0^\circ < \theta < 90^\circ$) omitted for clarity.

(smallest possible Q) for a given antenna size. Following a review of some basic antenna parameters, a short discussion on lumped resonant circuits and circuit Q is presented, which lays the foundation for small antenna analysis. A chronological review of the significant contributions to small antennas will then be presented, with a focus on the theoretical development of the field.

1.2 Small Antenna Parameters

To establish a foundation for discussing small antennas, an overview of their most important characteristics is presented below.

1.2.1 Directivity

It is often stated that small antennas have the familiar doughnut-shaped (see Fig. 1.2) omni-directional radiation pattern of a Hertzian dipole of directivity $D = 1.5$. This pattern may be also thought as the radiation of TE_{10} or TM_{10} spherical modes. However, this is not the only possible pattern for a small antenna, as seen in the work presented by Harrington [3], Kwon [4, 5], and Pozar [6]. By superposing various electric and magnetic Hertzian dipole arrangements, unidirectional and bidirectional patterns are theoretically possible, along with directivities ranging from $D = 1.5$ to 3 (see Sec. 1.3.11 in this chapter). We can state that antennas having significant spherical TE_{nm} and TM_{nm} mode radiation with $n > 1$ are generally not of the small type. Small antennas are also classified as superdirective antennas, since for decreasing size ka, their directivity D remains constant [2,7].

1.2.2 Radiation Efficiency

Radiation efficiency is a critical topic for small antennas but has not been studied rigorously. Antenna radiation efficiency factor η is simply the ratio of the power radiated by the antenna to the power delivered to the input terminals of the antenna. Often the efficiency factor is seen in the formula $G = \eta(1 - |\Gamma|^2)D$ where G is the realized gain that includes the mismatches between the source and matching network (see Fig. 1.3). We assume the matching network of Fig. 1.3 is lossless. The losses in the antenna apart from radiation are frequently modeled through a series loss resistor R_{loss}, in which case the radiation efficiency η can be represented as

$$\eta = \frac{R_{\text{rad}}}{R_{\text{rad}} + R_{\text{loss}}} = \frac{R_{\text{rad}}}{R_A} \tag{1.2}$$

where R_A is the total antenna input resistance $R_{\text{rad}} + R_{\text{loss}}$ (see Fig. 1.3).

It has been observed that as antenna size ka decreases, R_{rad} decreases and the loss resistance R_{loss} dominates the efficiency expression of Eq. (1.2). This decrease in efficiency is primarily due to frequency-dependent conduction and dielectric losses within the antenna. As mentioned later, Harrington [3] quantified the efficiency for an ideal spherical antenna, showing that losses are extremely prominent for smaller ka values.

A simple method to find the radiation efficiency η and separate R_{rad} from R_A is to use the Wheeler Cap [8] method (see Fig. 1.4). The Wheeler Cap (shown in Fig. 1.4) is a hollow perfectly electric conducting (PEC), enclosing sphere of the same size as the radiansphere. Wheeler noted that the size and shape of the Wheeler Cap is not critical. However, it must be electrically large enough so that the near-zone-antenna fields are not disturbed while still preventing radiation, and small enough so that cavity resonances are not excited. Indeed,

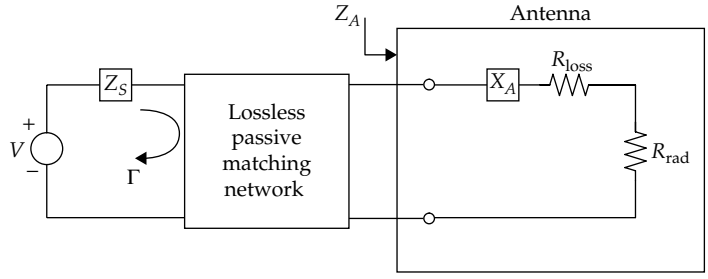

FIGURE 1.3 Lossless passive matching network with antenna load and input reflection coefficient Γ.

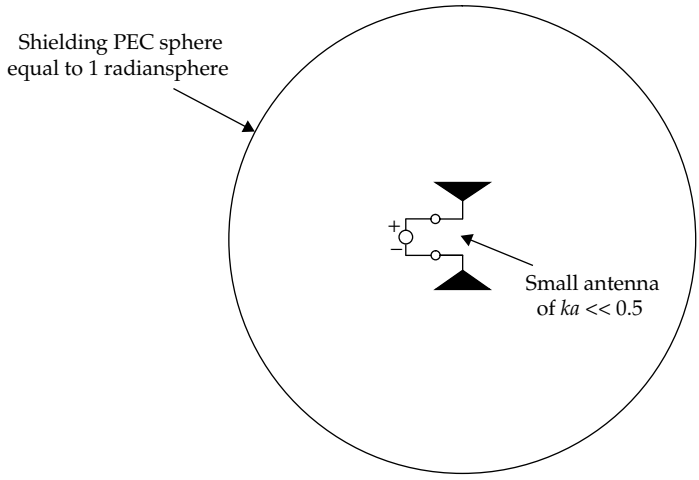

FIGURE 1.4 Wheeler Cap for small antenna efficiency measurement. *(After Wheeler* [8].)

Huang [9] proved rigorously that using the radiansphere-sized spherical Wheeler Cap does not significantly affect the near fields excited.

To measure the radiation efficiency η using the Wheeler Cap method, first a computation or measurement is done at the antenna resonant frequency in the absence of the Wheeler Cap to obtain R_A. If the antenna is not self-resonant, it must be tuned to resonance by a reactive element at the input. The tuned antenna is then enclosed inside the Wheeler Cap, and the measured input resistance then yields R_{loss}. Substitution of R_A and R_{loss} in Eq. (1.2) then gives $\eta = R_{\text{rad}}/R_A$.

1.2.3 Quality Factor

1.2.3.1 Antenna Quality Factor

An intrinsic quantity of interest for a small antenna is the Q factor, defined in [3] as

$$Q = \frac{2\omega_0 \max(W_E, W_M)}{P_A} \tag{1.3}$$

W_E and W_M are the time averaged stored electric and magnetic energies, and P_A is the antenna received power. The radiated power is related to the received power through $P_{\text{rad}} = \eta P_A$, where η is the

antenna efficiency. It is assumed in Eq. (1.3) that the small antenna is tuned to resonance at the frequency ω_0, either through self-resonance or by using a lossless reactive tuning element.

Antenna Q is a quantity of interest and can be also evaluated using equivalent circuit representations of the antenna. Another important characteristic of Q is that it is inversely proportional to antenna bandwidth (approximately). A commonly used approximation between Q and the 3 dB fractional bandwidth B of the antenna is

$$Q \approx \frac{1}{B} \quad \text{for} \quad Q \gg 1 \tag{1.4}$$

Equation (1.4) is based on resonant circuit analysis and tends to become more accurate as Q increases. An explicit relationship between Q and bandwidth is given later (see Sec. 1.3.10 or Yaghjian and Best [10]). For the moment let us review the lumped resonant circuit analysis used for computing Q in this chapter.

The reader may wonder why Q is the quantity of interest rather than bandwidth itself. One practical reason is that bandwidth remains an ambiguous term. Though it is often implied that bandwidth refers to the 3 dB bandwidth, this is not always the case for antennas. It is desirable to find an independently derived quantity Q that is also related to bandwidth. This idea is given in Sec. 1.3.10 by Yaghjian and Best [10]. However, the most important reason that Q remains of interest for small antennas is that a fundamental lower limit on Q can be found using a number of techniques (and consequently the max bandwidth of a small antenna). This fundamental limitation on Q (or max bandwidth) drives the majority of the work examined later on small antennas.

1.2.3.2 Quality Factor for Lumped Circuits

Wheeler [1] recognized that a small antenna radiating the single spherical TE_{10} mode can be accurately represented as a RLC combination of Fig. 1.5*a*. We note the series capacitor represents the ideal tuning element in Eq. (1.3) which brings the antenna to resonance. Similarly, a small antenna radiating only a spherical TM_{10} mode can be accurately represented by the parallel RLC combination as in Fig. 1.5*b*, where the shunt inductor represents the ideal tuning element in Eq. (1.3) that brings the antenna to resonance. More complicated, high-Q circuits can be accurately represented as a series [for $X'_{\text{in}}(\omega_0) > 0$] or parallel [for $X'_{\text{in}}(\omega_0) < 0$] RLC circuits within the neighborhood of their resonant frequencies.

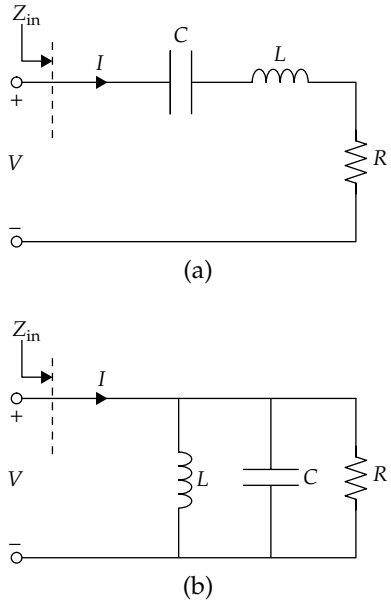

FIGURE 1.5 Series and parallel RLC circuits. (a) Series RLC, (b) Parallel RLC.

Series RLC Circuit For the series RLC circuit of Fig. 1.5*a*, the input impedance is

$$Z_{\text{in}} = R + j\omega L - \frac{j}{\omega C} = R + j\omega L\left(\frac{\omega^2 - \omega_0^2}{\omega^2}\right) \text{ with } \omega_0 = \frac{1}{\sqrt{LC}} \quad (1.5)$$

where ω_0 represents the resonant frequency at which the input impedance is purely real. This resonance occurs when the average stored electric energy is equal to the average stored magnetic energy in the circuit. Using the general definition of Q in Eq. (1.3) and recognizing the current is the same in all circuit components, we find that

$$Q = \frac{2\omega_0 W_H}{P_a} = \frac{2\omega_0\left(\frac{1}{4}LI^2\right)}{\frac{1}{2}I^2R} = \frac{\omega_0 L}{R} = \frac{1}{\omega_0 RC} \quad (1.6)$$

where I is the current through the series RLC circuit in Fig. 1.5*a*. The bandwidth of the series RLC circuit can be estimated after introducing the approximation

$$F(\omega) = \omega^2 - \omega_0^2 \approx F(\omega_0) + (\omega - \omega_0)F'(\omega_0) = 2\omega\Delta\omega \quad (1.7)$$

valid for small $\Delta\omega = \omega - \omega_0$. With this Taylor series, Eq. (1.5) becomes

$$Z_{\text{in}} \approx R + j\omega L\left(\frac{2\omega(\omega - \omega_0)}{\omega^2}\right) = R + j2L\,\Delta\omega \tag{1.8}$$

From Eq. (1.8), it is then evident that the 3 dB points occur when

$$2L\,\Delta\omega_{3\,\text{dB}} = \pm R \tag{1.9}$$

where $\Delta\omega_{3\,\text{dB}}$ is the difference between the 3 dB frequency and resonant frequency. Using Eqs. (1.6) and (1.9) we can now write

$$2Q\frac{\Delta\omega_{3\,\text{dB}}}{\omega_0} = QB = 1 \tag{1.10}$$

since by definition, $2\Delta\omega_{3\,\text{dB}}/\omega_0 = B$ for an antenna having ω_0 as its operational frequency. From this result, we then have the relationship $B = 1/Q$ as mentioned in Eq. (1.4). Figure 1.6 depicts the impedance as a function of frequency for a typical series RLC circuit for various $Q \gg 1$ values.

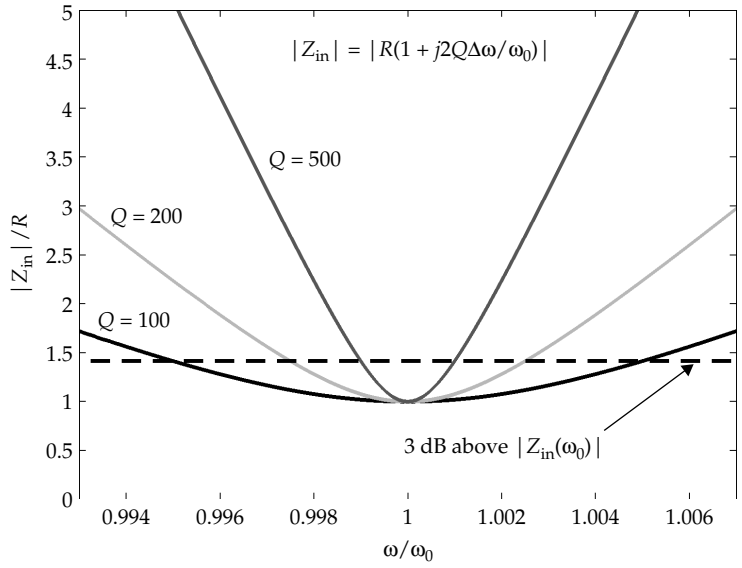

FIGURE 1.6 Normalized impedance magnitude for a series RLC circuit near resonance.

Parallel RLC Circuit For the parallel RLC circuit of Fig. 1.5*b*, the input admittance is

$$Y_{\text{in}} = G + j\omega C - \frac{j}{\omega L} = G + j\omega C\left(\frac{\omega^2 - \omega_0^2}{\omega^2}\right) \text{ with } \omega_0 = \frac{1}{\sqrt{LC}} \quad (1.11)$$

where ω_0 is again the resonant frequency for which the input admittance is purely real. Using the general definition of Q and recognizing for the parallel RLC circuit the voltage V across each component is the same, the Q for the parallel RLC circuit at resonance is found to be

$$Q = \frac{2\omega_0 W_E}{P_a} = \frac{2\omega_0\left(\frac{1}{4}CV^2\right)}{\frac{1}{2}V^2G} = \frac{\omega_0 C}{G} = \frac{1}{\omega_0 GL} \quad (1.12)$$

From the dual nature of the series and parallel RLC circuits, the same bandwidth relations obtained in Eq. (1.10) hold for the parallel RLC circuit. Figure 1.7 depicts the impedance as a function of frequency for a typical parallel RLC circuit having $Q \gg 1$.

Arbitrary Lumped Networks In many cases, tuning the antenna impedance to resonance using a single lossless reactive element does not give a suitable value for the input resistance to match the transmission line. To minimize mismatches (reflections) and deliver maximum power to the antenna, two degrees of freedom are needed to provide

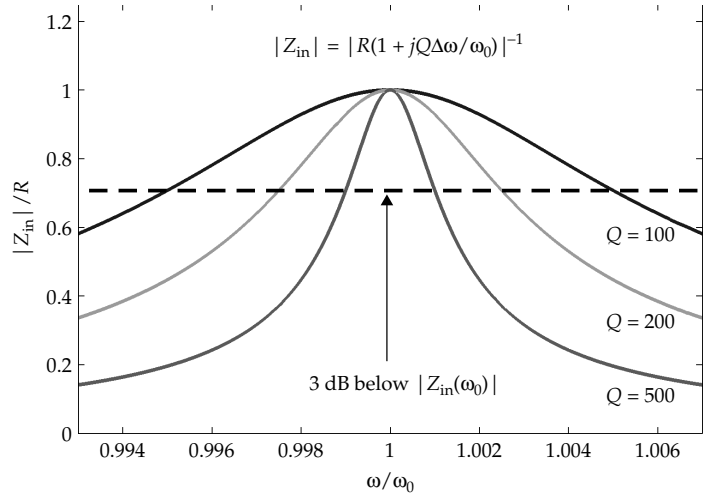

FIGURE 1.7 Normalized impedance magnitude for a parallel RLC circuit near resonance.

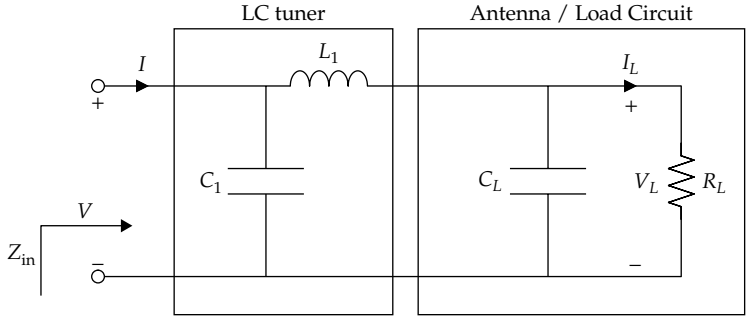

FIGURE 1.8 Antenna circuit with LC tuner.

an impedance match to a transmission line. Figure 1.8 shows an example of a lumped matching network with two degrees of freedom—one series and another shunt element. With these two degrees of freedom, an arbitrary load impedance can be transformed to a real impedance value, and matched to the transmission line.

To find the Q for the circuit configuration in Fig. 1.8, we note that at resonance

$$Z_{\text{in}} = \text{Re}(Z_{\text{in}}) = R_{\text{in}}$$
$$P_{\text{in}} = P_L = \frac{1}{2}|I_L|^2 R_L$$

where Z_{in} is the input impedance, P_{in} is the input power, and P_L is the power at the load. Using these conditions, we can find Q from Eq. (1.3). To employ Eq. (1.3), we note

$$P_{\text{in}} = \frac{1}{2}\frac{|V|^2}{R_{\text{in}}} = P_L = \frac{1}{2}\frac{|V_L|^2}{R_L} \tag{1.13}$$

$$W_{E1} = \frac{1}{4}|V|^2 C_1 \tag{1.14}$$

$$W_{EL} = \frac{1}{4}|V_L|^2 C_L = \frac{1}{4}C_L\frac{R_L}{R_{\text{in}}}|V|^2 \tag{1.15}$$

Substituting these quantities into Eq. (1.3), we get

$$Q = \frac{2\omega_0 W_E}{P_L} = \frac{2\omega_0 (W_{E1} + W_{EL})}{P_L} = \omega_0 C_1 R_{\text{in}} + \omega_0 C_L R_L \tag{1.16}$$

Finding Q for arbitrary circuit topologies can become a cumbersome procedure. Formulating the topology using approximate RLC circuits can therefore be beneficial. One method used by Chu [11] is to equate the input resistance, reactance, and reactance frequency derivative of

a more complicated passive circuit to those of a series RLC circuit at the resonant frequency.

1.2.3.3 External and Loaded *Q*

The Q described thus far is an intrinsic circuit quantity known as the unloaded Q, and is independent of the source. Figure 1.9 shows the more realistic situation of a source of impedance R_S driving a resonant circuit characterized by the unloaded quality factor Q. If the resonant circuit is a series RLC, the source impedance R_S combines in series with the input resistance R. Thus, to find the overall Q in Eq. (1.6), R is replaced with $R + R_S$. Similarly, for a parallel RLC circuit, the value of G in Eq. (1.12) need be replaced with $G + G_S$. It is nevertheless clear from Eqs. (1.6) and (1.12) that the source resistance has the effect of reducing the overall quality factor. To account for this Q reduction, the external quality factor Q_S is introduced and defined by

$$Q_S = \begin{cases} \dfrac{\omega_0 L}{R_S} & \text{Series resonator} \\ \dfrac{R_S}{\omega_0 L} & \text{Shunt resonator} \end{cases} \tag{1.17}$$

The total circuit Q, now referred to as the loaded quality factor Q_L, can then be defined by the known relation (adding Q_S in parallel)

$$\frac{1}{Q_L} = \frac{1}{Q} + \frac{1}{Q_S} \tag{1.18}$$

We observe that when the source is matched to the resonant circuit (typically at resonance) then $Q_L = Q/2$, implying double the bandwidth.

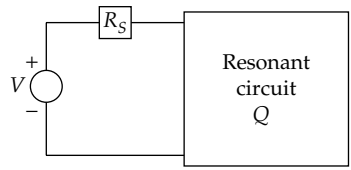

FIGURE 1.9 Resonant circuit with unloaded Q driven by a source of impedance R_S.

1.2.4 Input Impedance and Matching

In general, the input impedance of small antennas is typically characterized by low resistance and high reactance [12]. As the antenna size decreases, the radiation resistance R_{rad} decreases, causing the antenna reactance X_A to dominate. With respect to Fig. 1.10, a convenient proportionality relationship for small monopole antennas was given by [12] and [13] as

$$R_{\text{rad}} \propto \left(\frac{h}{\lambda}\right)^2 \tag{1.19}$$

Here, h is the monopole height and λ is the wavelength, implying that the input resistance decreases quadratically with electrical size. Matching circuits are therefore needed to improve the small antenna efficiency over a wide range of frequencies. But this imposes a significant practical design challenge as the matching network must also be physically small. It is therefore important to design self-resonant antennas with high radiation resistances that can be matched to standard transmission lines. In this context, certain self-resonant (folded) antenna structures have been shown to have input resistances that approach those of standard transmission lines [13].

Several texts [14–16] have sections dedicated to both lumped and distributed matching networks, and in Chap. 2 we consider matching as an essential component to achieving optimal size narrowband and wideband antennas. For the narrowband antennas, the fundamental bounds on lossless passive matching networks were derived by Fano [17] as

$$BQ \leq \frac{\pi}{\ln\left(\dfrac{1}{\Gamma_{\max}}\right)} \tag{1.20}$$

where B is the 3 dB fractional bandwidth, $\Gamma_{\max}$ is the maximum allowable reflection coefficient in the passband, and Q is the quality factor of the load to be matched.

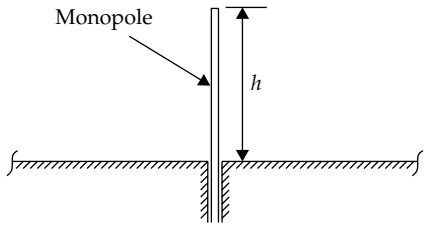

FIGURE 1.10 Monopole antennas.

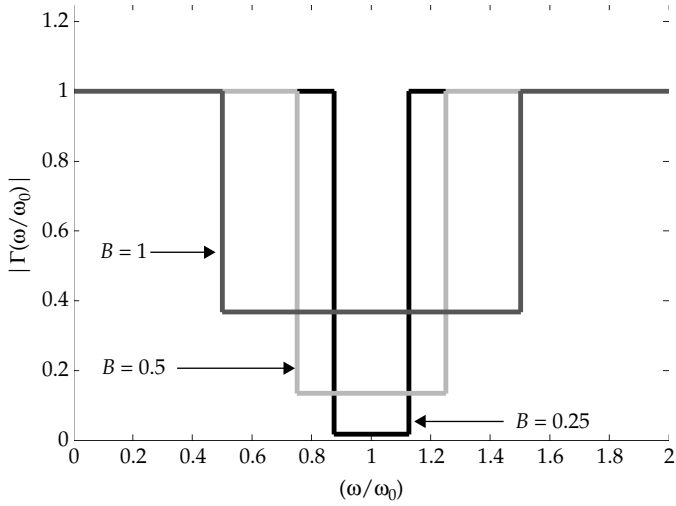

FIGURE 1.11 Bode limit on reflection coefficient Γ for various B values.

The interpretation of Eq. (1.20) is depicted in Fig. 1.11 (see Chap. 2 as well) for $B = 0.25$, 0.5, and 1, with $Q = \pi$. The fundamental limitation given by Eq. (1.20) indicates that greater bandwidth can only be achieved at the cost of increased maximum reflection coefficient (less realized gain).

1.3 Small Antenna Theory

Work on small antennas can be first traced back to the treatments done by Wheeler in 1947 [1]. Wheeler later discussed the fundamental limitations of small antennas using a simple model that approximates the small antenna with a lumped capacitance or inductance and a radiation resistance. He applied the concept of the radiation power factor (RPF)—a ratio of the radiated power to reactive power—to the antenna model [1] in an attempt to find a relationship between antenna size and radiation properties. He was the first to note that the reduction in the antenna size imposes a fundamental limitation on bandwidth. Wheeler concluded that the RPF was directly proportional to the physical antenna volume. To a degree, we can say that the RPF was the precursor to the commonly used quantity, Q. In Wheeler's circuit model, Q is the inverse of RPF (implying that RPF represents the small antenna bandwidth).

Wheeler's work was a rough approximation that was accurate only for extremely small antenna sizes. This is because it did not take into

account the radiated spherical modes as the antenna size increased. Nevertheless, his treatment can be recognized as the first intense study of small antennas, and encouraged many followers to investigate fundamental properties and limitations proposed in his work. It also inspired advances in the theory of the small antennas and also the development of practical small antennas.

In 1948, Chu derived the minimum possible Q for an omni-directional antenna enclosed in a *Chu sphere* (see Fig. 1.1 for definition) along with the maximum G/Q [11]. He accomplished this by using spherical mode wavefunction expansions outside the mathematical sphere enclosing the antenna (by expressing the radiated field as a sum of spherical modes). Each mode was then expressed in terms of an equivalent circuit, and through lumped circuit analysis the Q for each mode was found. Though Chu restricted his analysis to a specific type of omni-directional antenna, his contributions would lay the groundwork for many future authors that refined these limits. Chu's expression for calculating the minimum Q was later simplified by Hansen [2] (1981). Harrington [3] followed much of Chu's analysis (1960), and was the first to consider the antenna as radiating both TE and TM modes. As a result, his work led to lower minimum Q values.

As noted, the analysis done by Chu and Harrington involved equivalent circuit approximations for representing each generated mode. Collin and Rothschild (1964) pursued a field-based technique calculating the exact radiation Q [18] for an antenna radiating only TM or TE modes, and found the minimum Q possible for such an antenna enclosed in a *Chu sphere*. Their analysis was later generalized by Fante [19] to include both TE and TM modes. Fante [19] derived an exact Q expression for an arbitrary TM and TE mode configuration.

McLean (1996) used another method to calculate Q, and his results were in agreement with those presented by Collin and Rothschild [37]. McLean felt that Wheeler's method was too rough an approximation, and Chu's equivalent circuit approximations were not accurate enough to establish a fundamental limit on Q. Later, Foltz and McLean (1999) recognized that their lower Q bounds were not close to the verifiable values for many antennas, especially dipoles. As a result they repeated Chu's analysis using a prolate spheroidal wavefunction expansion outside a prolate spheroid. Their intention was to more accurately represent the geometry of many practical antennas such as dipoles [20]. They discussed the minimum possible Q associated with antennas enclosed in such a prolate spheroid, assuming only TM or only TE modes. Foltz and McLean concluded that Q increases as the spheroid becomes thinner, further reinforcing the concept that Q is inversely proportional to physical antenna volume.

Thiele (2003) observed that the exact lower limit for Q derived in earlier works was far from that of actual antennas and conjectured that the current distribution on the antenna had strong effect on the

value of Q [7]. His method for determining Q utilized an extension of the superdirective ratio concept. Thus, his analysis was unique in determining Q from the far-field pattern and not a modal expansion. Thiele applied his approach to a dipole antenna having non-uniform current distribution, and obtained favorable results as compared to practical dipole antennas with a similar current distribution.

Geyi (2003–2005) thought, as previous authors, that Chu's treatment was not adequately accurate, and pointed out that Collin's analysis involved integrations which were not feasible for many applications. Geyi began by reinvestigation the antenna Q and directivity limits [21]. He also presented an approximate method for calculating Q using less taxing integrations than those derived by Collin and Rothschild.

More recently, Best (2003–2008), Yaghjian, and their colleagues [10,13,23–26] carried out extensive work both on the theory of small antennas and their design. Among the theoretical topics pursued by Best are the exact and approximate expressions for Q in terms of fields and impedance, and the relationship between Q and bandwidth [10]. He also considered specific self-resonant wire antennas that approach the Q limits. His work explored the effect of wire geometry, wire folding, and volume utilization on radiation resistance and Q. Best's [24] folded spherical helix antenna was shown to deliver nearly the lowest possible Q for a single radiating mode antenna. This design of the folded spherical helix is reminiscent of the spherical inductor antenna proposed decades earlier by Wheeler [27].

While previous theoretical work focused on finding the physical limitations on antenna Q, Kwon and Pozar (2005–2009) noted that many authors were not consistent in defining the TM and TE modes, the antenna gain, Q, and directionality. With this motivation, Kwon [4,5] performed extensive analytical work on the gain and Q associated with electric and magnetic dipoles in varying configurations. Pozar [6] summarized the results of Kwon and others, and pointed out inconsistencies among previous small antennas authors.

Thal (2006–2009) set out to determine a more restrictive Q than previously derived for a class of antennas represented by a surface current distribution over a sphere and radiating both TE and TM modes [28]. His work extended the equivalent mode circuit method of Chu by introducing an additional equivalent circuit to account for energy storage inside the sphere (previously assumed by Chu and others to be zero). The Q of Best's spherical helix antenna [24] was found to be nearly identical to the minimum Q limit found by Thal. Thal also considered the relationship between gain, Q, and the energy inside the *Chu sphere* for a small antenna, and concludes that these quantities are not independent of one another [29].

The more recent work of Gustafsson and associates (2007) [30] provided Q and gain expressions for small antennas having arbitrary shape. Specifically, Gustafsson took an approach radically different

than previous authors using scattering theory and representing the antenna in terms of material dyadics. His work seems to indicate that accurate gain and Q limitations on antenna geometries such as prolate and oblate spheroids, disks, needles, and cylinders are now possible through numerical computations.

In the following sections we proceed to examine the aforementioned works in more detail.

1.3.1 Work of Wheeler (1947–1975)

The first widely published paper (in 1947) on small antennas was by H. A. Wheeler entitled "Fundamental Limitations of Small Antennas" [1]. Wheeler approximated the small antenna as a lumped capacitance or a lumped inductance, with a radiation resistance. He claimed that the physical limitations on small antenna design could then be found based on this simplified representation.

Wheeler explored the limitations of small antennas in [27] providing an analysis of the properties for a spherical coil antenna. Wheeler introduced the fundamental limitations of small antennas using the lumped element models which closely match the work of later authors based on rigorous field analysis. Wheeler's 1975 review paper [8] on small antennas stressed the importance of the small antenna's spherical "effective volume." He interpreted the latter as a "sphere of influence" for nonspherical antenna structures.

Much of Wheeler's work was reviewed and verified through computer simulation in Lopez's work [31], and later by many authors.

1.3.1.1 The Radiation Power Factor

In [1], Wheeler recognized that small antennas had far-field patterns and stored energy properties similar to those of electric and magnetic dipoles. Figure 1.12 presents a simplified lumped circuit for small L-type (magnetic) antenna and a small C-type (electric) antenna. Wheeler recognized that a small antenna used as an electric dipole would have far greater capacitively stored energy (as compared to inductive energy). Thus, the antenna could be represented

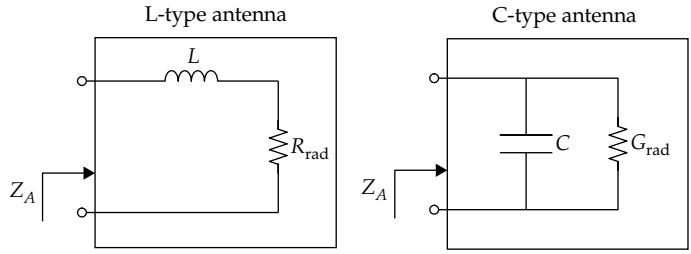

FIGURE 1.12 Small L-type antenna and C-type antenna models. (*See* [1].)

as a capacitance in parallel with a radiation conductance G_{rad}. Similarly, if the small antenna behaves as a magnetic dipole, the stored inductive energy is far greater. Thus it can be represented by a circuit having an inductance in series with a radiation resistance R_{rad}. Ohmic losses R_{loss} were neglected in his analysis as the goal was to gain insight on the behavior of the antenna Q. As such, in Wheeler's analysis the only real power dissipation was due to the radiation resistance, representing the radiated power.

With respect to the circuits in Fig. 1.12, Wheeler introduced the quantity he referred to as the *radiation power factor* (RPF). RPF is defined as the ratio of the radiated power P_{rad} to the reactive power P_{react} at the feed point of the antennas. He also introduced the definitions p_e = RPF for the capacitive (C-type) antenna and p_m = RPF for the inductive (L-type) antenna. His specific definitions are

$$p_m = \frac{R_{\text{rad}}}{\omega L} \tag{1.21}$$

$$p_e = \frac{G_{\text{rad}}}{\omega C} \tag{1.22}$$

Using the expressions (1.6) and (1.12) for the lumped RLC resonators, one can express the quality factors Q_m and Q_e of the magnetic and electric dipole circuits of Fig. 1.12 as

$$Q_m = \frac{2\omega W_M}{P_{\text{rad}}} = \frac{\omega L}{R_{\text{rad}}} = \frac{1}{p_m} \tag{1.23}$$

$$Q_e = \frac{2\omega W_E}{P_{\text{rad}}} = \frac{\omega C}{G_{\text{rad}}} = \frac{1}{p_e} \tag{1.24}$$

By inspection, one can see that Wheeler's RPF is equal to the inverse of the Q for the circuit models in Fig. 1.12. As Q has become the commonly used parameter today, it is appropriate to employ Q (rather than p_e and p_m) from here on.

In order to analyze the effect of antenna size to Q, Wheeler examined the circuit parameters for a cylindrically shaped capacitor and inductor representing the C-type or L-type dipole antennas (as depicted in Fig. 1.13), respectively. Wheeler also considered the cases where the C-type antenna may be filled with dielectric material of relative permittivity ε_r, and the L-type antenna may be filled with magnetic material of relative permeability μ_r.

Wheeler approximated the capacitance and inductance of the C-type and L-type antennas in Fig. 1.13 using the formulae

$$C = \varepsilon_0 \frac{k_a\, A}{b} \tag{1.25}$$

and

$$L = \mu_0\, n^2\, \frac{A}{k_b\, b} \tag{1.26}$$

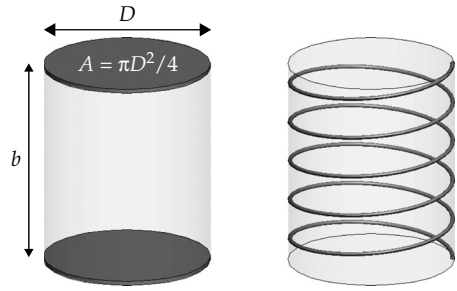

FIGURE 1.13 Small C-type and L-type cylindrical antennas occupying equal volume. (*See* [1].)

where n indicates the number of turns in the coil. We note that the Eqs. (1.25) and (1.26) differ from the standard formulas found in most texts through the additional factors k_a and k_b (which Wheeler defines as the shape factors). The capacitor shape factor k_a multiplies the physical area A to yield the effective area, taking into account the electric field outside the capacitor volume on the overall capacitance. The inductor shape factor k_b multiplies the inductor physical length to provide an effective length, taking into account the return path of the magnetic flux produced by the inductor. We note that these effective capacitance and inductances are larger and smaller, respectively, than the idealized ones ($k_a = k_b = 1$). Of course, if basic capacitor (no electric flux outside cylinder volume) and inductor models (no magnetic flux outside the inductor interior) are used, the shape factors will both become unity and the presented models will no longer be accurate. Therefore, it is critical to include the contributions of the fields outside the cylindrical structure to modify the L and C values to their more accurate representations.

Wheeler gave the radiation resistances derived from [32] of the C-type and L-type antennas as

C-type antenna	L-type antenna	
$R_{\text{rad}} = 20\left(\dfrac{b}{(\lambda/2\pi)}\right)^2$	$R_{\text{rad}} = 20\left(\dfrac{nA}{(\lambda/2\pi)^2}\right)^2$	(1.27)
$G_{\text{rad}} = \dfrac{1}{6\pi\, Z_0}\left(\dfrac{k_a\, A}{(\lambda/2\pi)^2}\right)^2$	$G_{\text{rad}} = \dfrac{1}{6\pi\, Z_0 n^2}\left(\dfrac{k_b\, b}{(\lambda/2\pi)}\right)^2$	(1.28)

From the radiation resistance and reactance values in Eqs. (1.25) to (1.27), the radiation conductances G_{rad} can be found by representing the series RC (C-type antenna) or RL (L-type antenna) circuits as shunt GC (C-type) or GL (L-type) circuits. We note that there are

no correction factors k_a and k_b in the radiation resistance formulas (1.27) and (1.28). Wheeler notes that this is because the electric current radiation for both antenna types is confined to the physical dimensions of the small antenna. This is unlike the electric and magnetic flux paths which extend beyond the antenna structure and modify the reactance values.

Substituting the parameters of Eqs. (1.25) to (1.28) into the definitions of Q given in Eqs. (1.23) and (1.24) yields

$$Q_e = \frac{\omega C}{G_e} = \frac{6\pi}{k_a Ab}\left(\frac{\lambda}{2\pi}\right)^3 = \frac{9}{2}\frac{V_{\text{RS}}}{V_{\text{eff}}} \tag{1.29}$$

$$Q_m = \frac{\omega L}{R_m} = \frac{6\pi}{k_b Ab}\left(\frac{\lambda}{2\pi}\right)^3 = \frac{9}{2}\frac{V_{\text{RS}}}{V_{\text{eff}}} \tag{1.30}$$

where V_{RS} is the volume of the radiansphere

$$V_{\text{RS}} = \frac{4\pi}{3}\left(\frac{\lambda}{2\pi}\right)^3 \tag{1.31}$$

and V_{eff} is the effective volume, defined as the physical volume of the antenna scaled by a physical and material dependent shape factor

$$V_{\text{eff}} = \sigma V_{\text{physical}} \quad \text{where} \quad \sigma = k_a, k_b \tag{1.32}$$

The final forms of Eqs. (1.29) and (1.30) provide two essential relations between Q and all small antennas:

(1) Q is inversely proportional to the effective antenna volume V_{eff} (and therefore physical antenna volume V_{physical}).

(2) Q is inversely proportional to the cubic power of frequency.

The effective volume is a concept frequently used in small antennas. In Eq. (1.32) it is seen that the effective volume is simply the physical volume multiplied by the material and structurally dependent shape factor σ. To explore the effect of shape factors have on Q (for the cylindrical antennas in Fig. 1.13), Wheeler introduced the shape factor for the C-type cylindrical antenna with radius a and height b as

$$k_a = \frac{k_{\text{SC}}^2}{k_{\text{SC}} + \varepsilon_r - 1} \qquad k_{\text{SC}} = 1 + \frac{8}{\pi}\frac{b}{D} \tag{1.33}$$

The corresponding shape factor for the L-type cylindrical antenna is

$$k_b = \frac{k_{\text{SL}}^2}{k_{\text{SL}} + \dfrac{1}{\mu_r} - 1} \qquad k_{\text{SL}} = 1 + 0.45\frac{D}{b} \tag{1.34}$$

Material filling effects can be seen in Eqs. (1.33) and (1.34), where filling the C-type antenna with a dielectric ε_r has the effect of decreasing the

effective volume and concurrently increasing Q. However, filling the L-type antenna with a magnetic material μ_r results in an increase in effective volume, concurrently decreasing Q. Wheeler also notes in [1] that the C-type and L-type shape factor physical dependences are inversely related. As an example, a short and wide coil ($D/2 \gg$ b, a spiral is such an example) has a higher effective volume as compared to a short and wide dipole. Similarly, a long and thin dipole (b $\gg D/2$) has a higher effective volume as compared to a long and thin coil.

Figure 1.14 gives another interpretation of the effective volume as described by in [8]. Wheeler states that the effective volume can be thought of as a "sphere of influence," providing a convenient reference to the radiansphere. From Eqs. (1.29) and (1.30), the effective volume is thus a sphere of radius

$$a' = \frac{\lambda}{2\pi}\left[\frac{9}{2Q}\right]^{1/3} \tag{1.35}$$

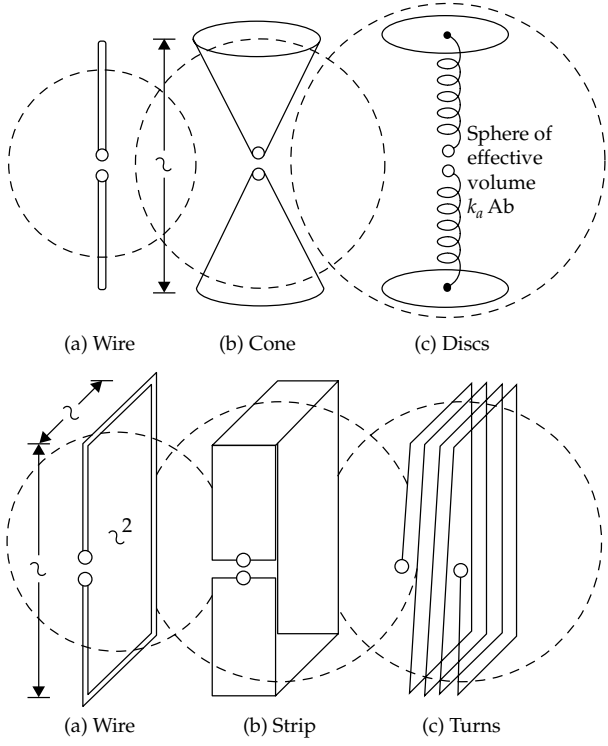

FIGURE 1.14 Effective volumes for C-type and L-type small antennas. (*After Wheeler ©IEEE, 1975* [8].)

1.3.1.2 The Spherical Coil

Constant Pitch Spherical Coil To determine which small antennas utilize their volumes most efficiently (or equivalently have the highest effective volume and lowest Q), Wheeler explored the constant pitch spherical coil antenna shown in Fig. 1.15, where the excitation voltage is across the poles of the coil.

The inductance of the spherical coil in Fig. 1.15 was derived starting with the familiar formula for an n-turn, air-filled cylindrical coil of radius a and length $2a$, surrounded by a perfect magnetic medium

$$L_{\text{cylinder}}(\mu_r = 1,\ \mu_{r,\text{external}} = \infty) = \frac{\pi}{2}\mu_0 a n^2 \tag{1.36}$$

Wheeler states that similarly to the cylindrical coil, a constant magnetic field is present inside the spherical volume of Fig. 1.15 when a ϕ-directed constant surface current is assumed over the sphere surface [27] (for a detailed analysis see Simpson [33,34]). Consequently, he then notes that since sphere volume $= 2/3$ cylinder volume, the stored magnetic energy is also two-thirds that of the cylinder. He then proceeds to correct the inductance formula by considering mediums other than air or perfectly magnetic. By integrating over the coil currents, he found the magnetic field along the axis perpendicular to the loops, and used this field to find the magnetic potential as a function of position along the z-axis. Wheeler concluded that two-thirds of the magnetic potential is inside the coil and one-third is external to it. This indicates that the magnetic reluctance outside the sphere is half the magnetic reluctance inside the sphere.

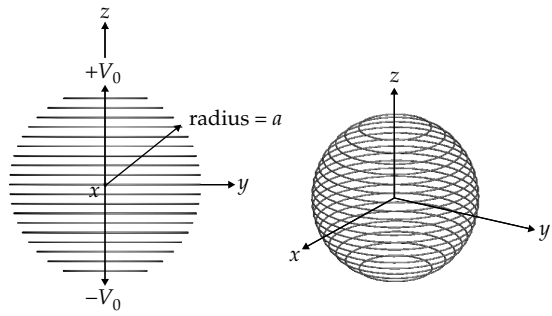

FIGURE 1.15 Wheeler's spherical coil antenna with constant pitch. (*See Wheeler* [27].)

From the above analysis, Wheeler proceeded to give the inductance formula for the spherical coil antenna in Fig. 1.15 with constant pitch as

$$L = \frac{2\pi}{9}\mu_0 a n^2 \frac{1}{\dfrac{2}{3\mu_r} + \dfrac{1}{3\mu_{r,\text{external}}}} = \frac{2\pi}{9}\mu_0 a n^2 \frac{3}{\dfrac{2}{\mu_r} + \dfrac{1}{\mu_{r,\text{external}}}} \tag{1.37}$$

As usual, μ_r is the relative permeability inside the spherical coil and $\mu_{r,\text{external}}$ is the relative permeability outside the spherical coil. Wheeler frequently includes shaping factors such as these to modify inductance and capacitance to account for shape and material variances. This was also noted in the cylindrical C-type and L-type antennas.

To determine the quality factor of the spherical coil antenna, initially Wheeler assumed an air surrounding medium and a magnetic medium (relative permeability μ_r) filling. The feed-point reactance of this antenna can be written as

$$\omega L = \frac{4\pi^2}{9} Z_0 \frac{a n^2}{\lambda} \frac{3}{1 + 2/\mu_r} \tag{1.38}$$

For the radiation resistance, Wheeler again started with the corresponding formula for a cylinder coil of n turns, radius a, and length $2a$. He then used the same volume and material correction factors as in Eq. (1.37) to obtain

$$R = 20\left(\frac{2\pi\sqrt{A}}{\lambda}\right)^4 \tag{1.39}$$

where

$$A = \frac{2}{3}\pi a^2 n \frac{3}{1 + 2/\mu_r} \tag{1.40}$$

From Eq. (1.30) it then follows that

$$Q = \frac{\omega L}{R} = \frac{1}{(ka)^3}(1 + 2/\mu_r) = \frac{V_{\text{RS}}}{\sigma V_{\text{physical}}} \tag{1.41}$$

We observe that this expression for Q is simply the ratio of the volume of the radiansphere to that of the structure multiplied by the shape factor $\sigma = (1 + 2/\mu_r)^{-1}$. Clearly, the minimum Q for this spherical coil antenna is obtained when $\mu_r \to \infty$. This is also the same conclusion noted earlier for the L-type cylindrical coil antenna in Fig. 1.13. The condition of $\mu_r \to \infty$ corresponds to zero magnetic energy storage inside the volume, and since no capacitive component exists in Wheeler's model, the total energy storage inside the spherical volume is zero. Further, as the radiated fields are those of a TE_{10} mode, the

spherical coil antenna with constant pitch and infinite permeability core can be thought of as giving the lower bound Q for single mode operation. From Eq. (1.41), this limit can be expressed as

$$Q_{\min,\text{Wheeler}} = \frac{1}{(ka)^3} \tag{1.42}$$

Self-Resonant Spherical Coil Wheeler [27] gave an example of a self-resonant spherical coil antenna depicted in Fig. 1.16, excited by a voltage across the coil poles. Wheeler gave a new wire arrangement on the sphere to realize constant electric and magnetic fields inside the structure for self-resonance. This is accomplished by using a tapered coil pitch arrangement (see Fig. 1.16).

Wheeler corrected the constant pitch inductance formula (1.37) by introducing a shape factor to account for the change in voltage along the wire due to tapering. He also determined the capacitance of the structure using the excitation potential difference between the two poles of the sphere. The equivalent inductance of the tapered spherical coil and coil length (necessary for self-resonance) are derived by Wheeler as

$$L = \frac{2}{9\pi^3}\mu_0 \frac{l^2}{a} \frac{3}{1+2/\mu_r} \tag{1.43}$$

$$l = \frac{\lambda}{2}\sqrt{\frac{1+2/\mu_r}{1+\varepsilon_r/2}} = \frac{\lambda}{2}\alpha \tag{1.44}$$

As seen, the equivalent length of the tapered coil is equal to $l = \alpha\lambda/2$, where α is the scale factor dependent on the enclosed material. For the case when no energy is stored within the sphere

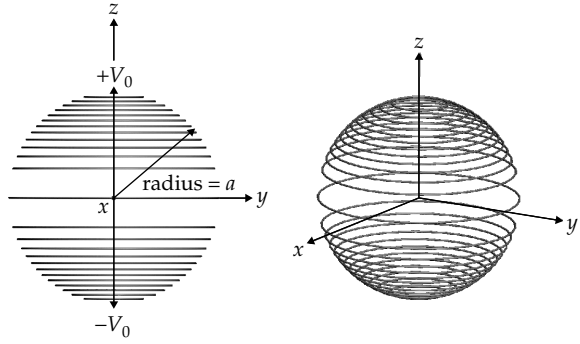

FIGURE 1.16 Wheeler's self-resonant tapered pitch spherical coil antenna. (*See* [2].)

($\varepsilon_r = 0$, $\mu_r = \infty$), the resonant length is exactly $\lambda/2$. This zero energy self-resonant spherical coil presents an important limiting case for a small antenna radiating both TM_{10} and TE_{10}. As in [27], it is stated that the Q of this self-resonant coil is half of the Q for constant pitch spherical coil (with zero internal stored energy). Wheeler states that this is a result of equal electric and magnetic stored energy outside the sphere, and the radiated power is now twice the single mode case. The Q for this self-resonant coil with a tapered pitch is therefore equal to

$$Q(\varepsilon = 0, \mu = \infty) = \hat{Q}_{\text{min,Wheeler}} = \frac{1}{2(ka)^3} \tag{1.45}$$

In terms of the definition of Q given in Eq. (1.3), this means that the $max(W_M, W_E)$ remains the same in the single mode case, but P_A is twice its original value.

Equivalent Spherical Coil Wheeler states that any coil formed by a loop winding in the same direction and with the loops located parallel to one another can be represented by an equivalent spherical coil as in Fig. 1.15. The equivalent spherical coil will have the same inductance and the radiation pattern as that of the original coil. He then gave the appropriate formulas for the equivalent spherical coil of radius a_{eq} and turns n_{eq} as

$$a_{\text{eq}} = \left(\frac{\mu_0 A^2}{2\pi L}\right)^{1/3} \tag{1.46}$$

$$n_{\text{eq}} = \left(\frac{6L^2}{\pi\mu_0^2 A}\right)^{1/3} \tag{1.47}$$

In this, $A = A_1 + A_2 + \cdots + A_n$ where A_i is the area of the ith turn in the original coil, and L is the inductance of the original coil. These results illustrate another key conclusion made by many authors and seen in much empirical evidence but never explicitly shown. That is, Wheeler's results imply that the diameter of the equivalent spherical coil is always less than the maximum dimension of the original coil. Concurrently, the equivalent spherical coil will retain the same Q and radiation resistance as that of the original coil. This demonstrates that the spherical coil makes more efficient use of the *Chu sphere* as compared to the class of coils described above.

Though this conclusion was only shown comparing different coils represented by an equivalent spherical coil, it holds for all small antennas. That is, *antennas which utilize more of their Chu sphere tend to have smaller values of Q*. Most of the empirical work in demonstrating this property is with surface current distributions over the *Chu sphere*.

1.3.1.3 Comments

Using the concept that a small antenna behaves as a lumped capacitor or inductor with a radiation resistance component, Wheeler expressed these parameters in terms of modified versions of well known capacitance, inductance, and radiation resistance formulae. This representation is, of course, an approximation as the single reactance lumped element model breaks down as antenna size increases. As the antenna size increases, other techniques for representing the properties of small antennas including multimode analysis are more appropriate.

The primary conclusion reached by Wheeler is that the Q of a small antenna is inversely proportional to its physical volume. A shape factor σ was also introduced to account for variances in the effective area or length of the antenna, giving

$$Q = \frac{V_{\text{RS}}}{\sigma V_{\text{physical}}} \tag{1.48}$$

Wheeler obtained two important limiting cases for the small antenna Q. For the coil in Fig. 1.15 with infinite permeability core, Wheeler gave the radiation characteristics as a series RL circuit. Recognizing that the mode radiated by this structure is a TE_{10} type and that an infinite permeability core results in zero stored energy inside the sphere, he reached the limiting value for Q given by

$$Q_{\text{min,Wheeler}} = Q_{\text{TE10}}\,(\mu_r = \infty) = \frac{1}{(ka)^3} \tag{1.49}$$

For the second limiting case, Wheeler considered the self-resonant coil of Fig. 1.16 supporting TE_{10} and TM_{10} modes, with zero stored internal energy. He found the limiting value for Q as

$$\hat{Q}_{\text{min,Wheeler}} = Q_{\text{TE10+TM10}}\,(\varepsilon_r = 0,\, \mu_{\text{r}} = \infty) = \frac{1}{2(ka)^3} \tag{1.50}$$

Wheeler's conclusions on small antenna limitations were later verified analytically by Thal [28] and experimentally by Best [13]. It is important to note that Wheeler's analysis is all based on equivalent circuit model of the small antenna. That is, he did not perform any full-wave analysis. Through his circuit analysis, Wheeler was the first to show that the Q of a small antenna is decreased with the increasing volume. The associated formula is in Eq. (1.48) and leads to the conclusion that *antennas which best utilize their minimum enclosing sphere tend to have small Q values as compared to other geometries within the same volume*. Wheeler also concluded that as the antenna size decreases, the ratio of reactance to radiation resistance increases even more rapidly. This reality exemplifies the issue of impedance matching for very small antennas.

1.3.2 Work of Chu (1948)

While Wheeler carried out his analysis using lumped circuit models for the small antenna itself, Chu [11] came to similar conclusions using spherical vector wavefunctions to evaluate the gain and bandwidth of omnidirectional antennas. Figure 1.1 shows the mathematical sphere of radius a enclosing the small antenna structure. This is the minimum sphere that encloses the antenna structure, and will be referred to hereafter as the *"Chu Sphere."* Chu [11] notes that the field configuration external to the *Chu sphere* is not uniquely defined by the interior source. Also he notes that an infinite number of source distributions are possible inside the *Chu sphere* for a single external field configuration.

1.3.2.1 Spherical Waves

Chu begins his analysis by assuming a vertically polarized, omnidirectional antenna of maximum dimension $2a$. Thus, the structure can be enclosed by the *Chu sphere* of radius a. With a spherical coordinate system (r, θ, ϕ), the transmitted/received fields are TM_{n0} waves of order n (the azimuthal index m is zero due to the omni-directional field nature). The nonzero electromagnetic field components associated with TM_{n0} modes are

$$H_\varphi = \sum_n A_n P_n^1(\cos\theta) h_n^{(2)}(kr) \tag{1.51a}$$

$$E_r = -jZ_0 \sum_n A_n n(n+1) P_n(\cos\theta) \frac{h_n^{(2)}(kr)}{kr} \tag{1.51b}$$

$$E_\theta = jZ_0 \sum_n A_n P_n^1(\cos\theta) \frac{1}{kr} \frac{d}{dr} \left(h_n^{(2)}(kr)\right) \tag{1.51c}$$

where A_n are constants determined by the source distribution of the antenna
$P_n^1(\cos\theta)$ is the associated Legendre polynomial of order $m = 1$ and degree n. This polynomial has a behavior similar to that of Fourier series with n terms. Several associated Legendre polynomials $P_n^1(x)$ are plotted in Fig. 1.17.
$P_n(\cos\theta)$ is the Legendre polynomial of degree n.
$h_n^{(2)}(kr)$ is the spherical Hankel function of the second kind, representing the outward traveling wave.
$Z_0 = \sqrt{\frac{\mu}{\varepsilon}}$ is the plane wave impedance of the homogeneous, isotropic medium represented by (μ, ε).

Chu then further restricted his analysis to an omni-directional antenna whose maximum gain lies in the equatorial plane $\theta = \pi/2$.

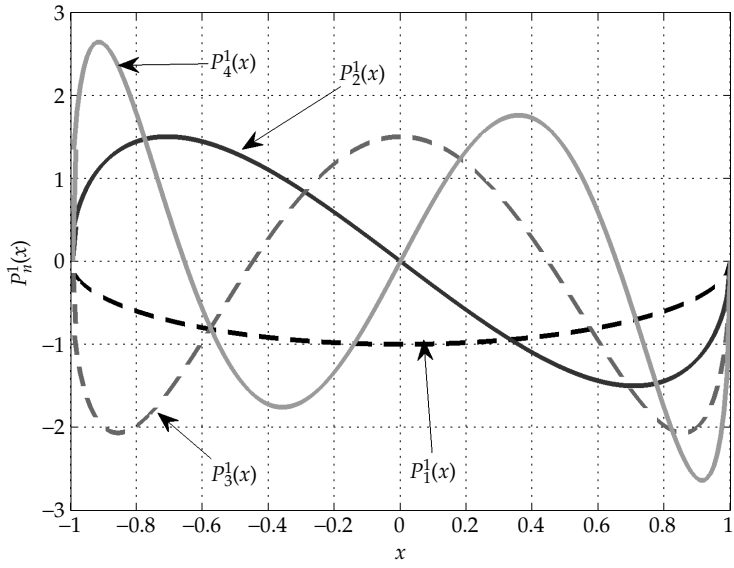

FIGURE 1.17 Associated Legendre polynomials $P_n^1(x)$ for $n = 1$ to 4.

We can see from Fig. 1.17 that $P_n^1(0)$ vanishes for n even and is finite for n odd. Therefore, for maximum gain in the equatorial plane it is necessary that A_n is zero for n even, and the A_n values for n odd combine in phase.

1.3.2.2 Chu Equivalent Circuit

To separate the total antenna energy into components associated with radiation, nonpropagating electric energy, and nonpropagating magnetic energy, Chu devised an equivalent circuit for the wave impedance of each propagating TM_{n0} wave. This circuit approach to determine the radiated and stored fields provides many benefits over a field approach using the Poynting theorem. Among them, the passive circuit provides greater insight into the nature of the spherical mode and their contribution to the overall antenna performance. Chu notes that the significant drawback in using a field approach to find the radiated power and stored energies is the nonlinear nature of the field components. As such, superposition cannot be directly applied to separate the electric and magnetic stored energy components in the near field.

To derive the equivalent circuits for spherical TM_{n0} mode, Chu begun by recognizing mode orthogonality among the modes. As such, the overall antenna power or energy can be viewed as a superposition of the corresponding powers and energies for each mode. Figure 1.18

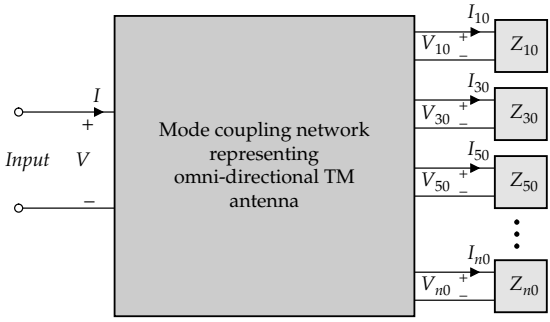

FIGURE 1.18 Chu's equivalent circuit network to represent the omni-directional TM_{n0} antenna. (*See Chu* [11].)

represents the equivalent circuit used to represent the modes generated by the omni-directional TM_{n0} antenna.

Chu proceeds to define the equivalent voltage and current for each TM_{n0} mode network on the following assumptions:

1. The input impedance of the TM_{n0} network is equal to the normalized wave impedance in the outward radial direction of the TM_{n0} mode at the surface of the *Chu sphere* of radius $= a$.
2. The complex power at the input terminals of the TM_{n0} mode circuit is equal to the complex power of the TM_{n0} mode exiting the *Chu sphere*.

The normalized wave impedance in the outward radial direction for the TM_{n0} mode can be written using the recurrence relations among Bessel functions. Specifically,

$$
\begin{aligned}
Z_{n0} &= \frac{j\left(kah_n^{(2)}(ka)\right)'}{kah_n^{(2)}(ka)} \\
&= \frac{n}{jka} + \cfrac{1}{\cfrac{2n-1}{jka} + \cfrac{1}{\cfrac{2n-3}{jka} \bullet \\
&\qquad \bullet \\
&\qquad \bullet \cfrac{1}{\cfrac{3}{jka} + \cfrac{1}{\cfrac{1}{jka} + 1}}}}
\end{aligned}
\tag{1.52}
$$

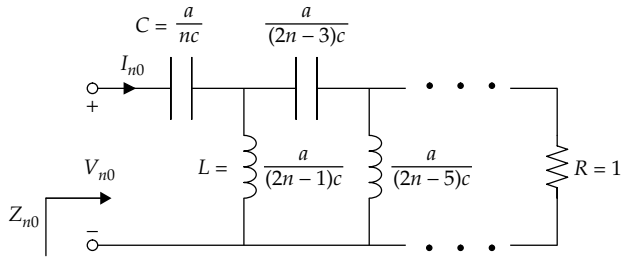

FIGURE 1.19 Equivalent impedance circuit for the TM_{n0} mode of the *Chu antenna* with a = sphere radius and c = velocity of light. (*See Chu* [11].)

This continued fraction expansion implies that Z_{n0} can be represented in terms of the circuit network shown in Fig. 1.19.

It is important to recognize that the equivalent circuit for any TM_{n0} wave (Fig. 1.19) behaves as a high-pass filter and stores capacitive energy. Thus, increasing the radius a of the *Chu sphere* has the same effect as increasing the frequency. By itself, the circuit models the impedance seen by a wave propagating outward from the *Chu sphere* surface. As the distance from the *Chu sphere* becomes larger, the wave impedance (for the TM_{n0} mode) approaches that of the intrinsic impedance Z_0 (as would be expected). Since there are an infinite set of source configurations that can generate any mode, *Chu chose the excitation leading to zero dissipation for the antenna and zero stored energy inside the Chu sphere*. This type of spherical, zero internal stored energy antenna will be referred to as a *"Chu antenna."*

With respect to Fig. 1.19, the Q of the omni-directional TM_{n0} *Chu antenna* can be determined rather easily. Since the antenna is assumed to have no losses other than those due to radiation, the total power delivered (P_A) is the sum of the real powers delivered to each of the mode circuits. Further, since we assume zero energy inside the *Chu sphere*, W_E is the total stored electric energy in each of the mode circuits. With these considerations in mind, the total Q of the omni-directional TM_{n0} *Chu antenna* can be expressed as

$$Q = \frac{2\omega W_E}{P_a} = \frac{\sum_{n=odd} |A_n|^2 \dfrac{n(n+1)}{2n+1} Q_n}{\sum_{n=odd} |A_n|^2 \dfrac{n(n+1)}{2n+1}} \tag{1.53}$$

where Q_n is the quality factor of the TM_{n0} mode circuit (see Fig. 1.19). As Chu did not have access to efficient methods for computing the total electric energy in each of the mode circuits, he approximated each mode circuit in Fig. 1.19 as an RLC series circuit, a valid approximation near the operating frequency.

In summary, Chu restricts his analysis to an antenna with the following properties:

- Vertically polarized
- Omni-directional
- Even n modes are not excited ($A_n = 0$ for n even)
- For n odd, A_n has the same phase angle for each mode
- No conducting losses in the antenna structure
- No stored energy inside the *Chu sphere* (*Chu antenna*)

Chu examines three cases for this type of antenna: (1) maximum gain antenna, (2) minimum Q antenna, and (3) maximum G/Q antenna. These quantities are examined in the following sections.

1.3.2.3 Maximum Gain Omni-directional Chu Antenna

Using the standard antenna gain definition, the gain G (in the equatorial plane of the *Chu antenna*) is given by

$$G\left(\theta = \frac{\pi}{2}\right) = \left.\frac{4\,\pi\,|E_\theta|^2}{\int\int |E_\theta|^2 \sin\theta\; d\theta\; d\varphi}\right|_{\theta=\frac{\pi}{2}}$$

$$= \frac{\left|\sum_{n=1,odd}^{N} A_n(-1)^{\frac{n+1}{2}} P_n^1(0)\right|^2}{\sum_{n=1,odd}^{N} |A_n|^2 \frac{n(n+1)}{2n+1}} \tag{1.54}$$

For maximum achievable gain, the A_n coefficients remain to choose appropriately. To do so we differentiate Eq. (1.54) with respect to A_n and set the result to zero. Solving the resulting $N \times N$ system yields the A_n values. Table 1.1 gives the maximum gain in the equatorial plane when $N = 1$, 3, and 5.

From Table 1.1, we can conclude that in theory any desired gain can be realized independent of antenna size as long as the source

N	1	3	5 ---------- N
G_{max} ($\theta = \pi/2$)	1.5	3.81	4.10 ---------- $2N/\pi$

TABLE 1.1 G_{max} Versus N in the Equatorial Plane (After Chu [11])

distribution can be constructed. Equation (1.54) shows how the antenna gain increases with the inclusion of higher order modes (again with proper excitation coefficients). However, in order to excite these higher order modes, the source distribution complexity increases dramatically. As such, the needed excitation configurations may not be realizable in practice.

1.3.2.4 Minimum *Q* Omni-directional Chu Antenna

To determine the set of mode coefficients A_n that give minimum Q for the *Chu antenna*, we proceed to differentiate Eq. (1.53) with respect to A_n and set the result to zero, giving

$$Q_n \sum_{n=1,odd}^{N} |A_n|^2 \frac{n(n+1)}{2n+1} = \sum_{n=1,odd}^{N} \left\{ |A_n|^2 \frac{n(n+1)}{2n+1} Q_n \right\} \qquad (1.55)$$

From Eq. (1.55) it is obvious that the only nontrivial solution to minimizing Q is to excite only a single mode (i.e., $A_n = 0$ except for $n = 1$). From Fig. 1.19, it is clear that the TM_{10} mode (see Fig. 1.20) gives the lowest Q for the omni-directional *Chu antenna*, and we observe that it also represents the mode generated by an infinitesimal (Hertzian) electric dipole.

1.3.2.5 Maximum *G/Q* Omni-directional Chu Antenna

The maximum G/Q ratio can be determined by using the derived formulas for G and Q in Eqs. (1.54) and (1.53), respectively. After dividing (1.54) by (1.53), the resultant G/Q ratio is again differentiated with respect to A_n and set to zero to create a system of equations. Solving these yields the A_n coefficients giving the max G/Q as plotted in Fig. 1.21.

Figure 1.21 shows the plot of the maximum G/Q ratio versus ka ($2\pi a/\lambda$). The asymptotic nature of the curves in Fig. 1.21 demonstrates another fundamental limitation of omni-directional antennas. Specifically, for a given antenna supporting N modes, there is an upper bound

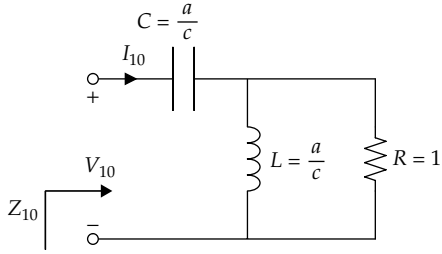

FIGURE 1.20 Equivalent impedance network for the TM_{10} mode with a = *Chu sphere* radius and c = velocity of light. (*See Chu* [11].)

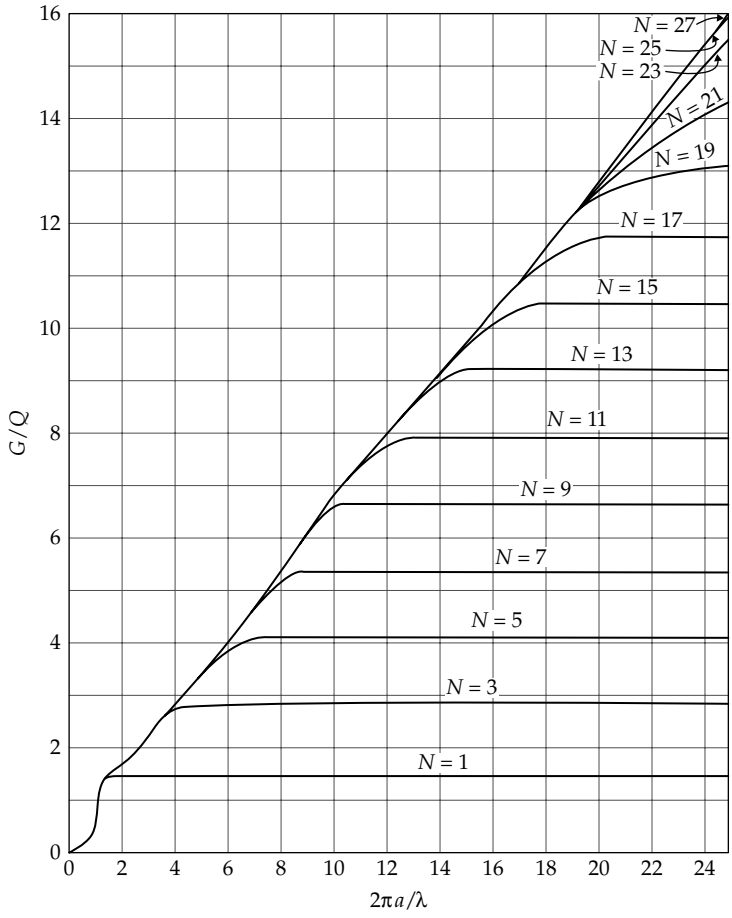

FIGURE 1.21 Maximum *G/Q* ratio for vertically polarized *Chu antenna* versus antenna size *ka* for various *N*. (*After Chu ©J. App. Phys., 1948* [11].)

of the *G/Q* ratio. Alternatively, we can state that as *Q* is reduced, the *G/Q* ratio reaches a maximum bound.

1.3.2.6 Horizontally Polarized Omni-directional Chu Antenna

The previous analysis was restricted to a *Chu antenna*, vertically polarized and having an omni-directional pattern with maximum gain in the equatorial plane. If this *Chu antenna* is now horizontally polarized as well as omni-directional and with maximum gain in the equatorial plane, the transmitted/received waves will be the superposition of the TE_{n0} waves. Once again, the *m* index is zero due to

TM	TE
H_ϕ	$-E_\phi$
E_R	H_R
E_θ	H_θ
Z_0	$1/Z_0$

TABLE 1.2 TM-TE Duality

the omni-directional nature of the fields. It is a straightforward task to identify the three nonzero field components associated with the TE_{n0} waves. They are listed in Table 1.2 along with their dual TM mode quantities [36].

The horizontally polarized TE_{n0} *Chu antenna* can also be represented by an equivalent circuit similar to Fig. 1.19. However, in this case each circuit outside the sphere must represent the TE_{n0} modes generated by the sources inside the *Chu sphere*. Chu noted that the normalized wave admittance of the TE_{n0} mode is equal to the normalized wave impedance of the TM_{n0} modes as given in Eq. (1.3.2.2). The TE_{n0} mode equivalent circuits can similarly be found by defining the unique mode voltages and currents such that the input admittance of each TE_{n0} equivalent circuit is equal to the normalized wave admittance of the corresponding TE_{n0} mode. This can be done by equating the complex power at the input terminals of each TE_{n0} circuit to the complex power of the TE_{n0} mode crossing the *Chu sphere*. The equivalent admittance circuit for the TE_{n0} mode is shown in Fig. 1.22.

It is important to note that the equivalent admittance circuit for any TE_{n0} wave behaves as a high-pass filter with inductive energy storage. Increasing the radius a of the *Chu sphere* has the same effect as increasing the frequency. It is also evident that as the distance from the *Chu sphere* increases, the intrinsic wave admittance approaches that of free space. Invoking the dual nature between the TE_{n0} and TM_{n0} fields, all

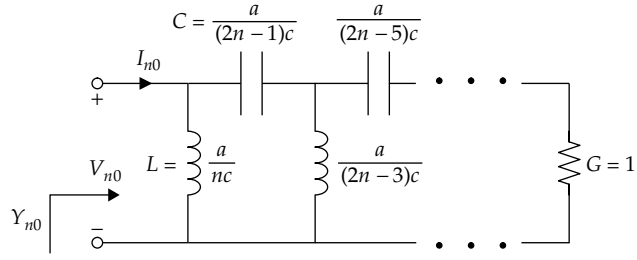

FIGURE 1.22 Equivalent admittance circuit for the TE_{n0} mode of the *Chu antenna* with a = sphere radius and c = velocity of light. (*See Chu* [11].)

previously derived results for a *Chu antenna* with vertical polarization also apply to the *Chu antenna* with horizontal polarization.

1.3.2.7 TE and TM Circularly Polarized Omni-directional Chu Antenna

Chu stated that a circularly polarized, omni-directional *Chu antenna* with maximum gain in the equatorial plane can be realized with 90° phasing between the TM_{n0} and TE_{n0} modes (provided the TE_{n0} and TM_{n0} pairs radiate equal power). Under these conditions, the stored electric and magnetic energies are also equal. The nth mode Q for such a *Chu antenna* can be found using the standard definition of Q given in Eq. (1.3). That is,

$$Q_n = \frac{2\omega W_n}{P_n} \tag{1.56}$$

with W_n being the total stored electric (see Fig. 1.19) *or* magnetic energy (see Fig. 1.22) in the networks, and P_n is the total real power delivered to both TE_{n0} and TM_{n0} circuits. For this type of circularly polarized antenna, we recognize that for small ka the TM_{10} equivalent circuit has predominantly electric stored energy. Likewise, the corresponding TE_{10} network has predominantly magnetic stored energy. However, since the total real powers delivered to both circuits are equal, Chu states that the resulting quality factor for the TM_{10}/TE_{10} circularly polarized antenna $Q_{CP,TM_{10}-TE_{10},Chu}$ is appropriately given by

$$Q_{CP,TM10-TE10,Chu} \approx \frac{1}{2} Q_{TM10,Chu} = \frac{1}{2} Q_{TE10,Chu} \tag{1.57}$$

Here, the *Chu* subscript indicates we refer to a *Chu antenna*.

1.3.2.8 Comments

Chu's work introduced many of the fundamental ideas used in modern analysis of small antennas. The concept of the *Chu antenna* (an antenna with zero energy storage inside its *Chu sphere*) is central to finding a lower bound on Q. Practical antennas exciting a given mode configuration must, of course, have nonzero energy storage inside their *Chu sphere*, to give a Q value larger than that of the *Chu antenna*. However, since Chu used a series RLC for each of his mode circuits there are inherent approximations, and much of the later work in small antennas is dedicated to finding more accurate and simpler closed form expressions for the Q limits.

The absolute lower bound on Q for a linearly polarized antenna (denoted as Q_{min}) radiating *only* TM or *only* TE modes was shown to be the Q of a *Chu antenna* radiating a pure TM_{10} or TE_{10} mode. The corresponding Q for a circularly polarized (CP) antenna radiating

equal parts TM_{10} and TE_{10} modes was shown to have its lowest bound equal to half of the single mode Q

$$\hat{Q}_{\min} = Q_{\text{CP,TM10-TE10,Chu}} \tag{1.58}$$

Chu also noted that in theory any gain can be realized with proper mode excitation coefficients. Additionally, Chu noted that there is a theoretical upper limit on G/Q, indicating that higher gain is possible at the cost of reduced bandwidth and increased antenna complexity.

The TM_{n0} and TE_{n0} mode high-pass networks proposed by Chu in Figs. 1.19 and 1.22, respectively, show the difficulty in radiating higher order modes using smaller antennas. For small antennas these modes are not practically realizable for two reasons: (1) the source complexity increases and (2) the large Q associated with higher order modes leads to large amounts of stored energy as compared to radiated power. This can be seen in the TM_{n0} and TE_{n0} mode networks as they operate well into their stopband for small antenna sizes. As is well known, in most cases, it is desirable to have minimal higher order mode excitation to maximize bandwidth. However, higher order modes can serve to tune out reactance (see Sec. 1.3.12).

1.3.3 Work of Harrington (1960)

Harrington [3] expanded Chu's [11] work, focusing on the gain and Q properties of a unidirectional *Chu antenna* radiating equally excited TE and TM modes along the $\theta = 0^\circ$ direction. He also introduced the dissipation factor d_F in an attempt to quantify antenna losses as a function of size and number of modes excited.

1.3.3.1 Maximum Gain for a Directional Chu Antenna

As stated in Sec. 1.3.2 (Chu), the fields outside the *Chu sphere* can be written as the superposition of orthogonal TE_{nm} and TM_{nm} modes. Harrington [3] used the known TE_{nm} and TM_{nm} wavefunction representation

$$\Psi_{\text{TE}} = \sum_{m,n} A_{\text{nm}} h_n^{(2)}(kr)\, P_n^m(\cos\theta)\cos(m\varphi + \alpha_{\text{TEnm}}) \tag{1.59a}$$

$$\Psi_{\text{TM}} = \sum_{m,n} B_{\text{nm}} h_n^{(2)}(kr)\, P_n^m(\cos\theta)\cos(m\varphi + \alpha_{\text{TMnm}}) \tag{1.59b}$$

$$\boldsymbol{E} = -\nabla \times (\hat{\boldsymbol{r}}\Psi_{\text{TE}}) + \frac{1}{j\omega\varepsilon}\nabla \times \nabla \times (\hat{\boldsymbol{r}}\Psi_{\text{TM}}) \tag{1.60a}$$

$$\boldsymbol{H} = \nabla \times (\hat{\boldsymbol{r}}\Psi_{\text{TM}}) + \frac{1}{j\omega\mu}\nabla \times \nabla \times (\hat{\boldsymbol{r}}\Psi_{\text{TE}}) \tag{1.60b}$$

In these equations, $h_n^{(2)}(kr)$ is the spherical Hankel function of the second kind, and $P_n^m(\cos\theta)$ is the associated Legendre polynomial. Harrington used these expressions to derive the directive gain in the $\theta = 0^\circ$ direction. His derivation finds that $G(\theta = 0)$ is independent of the phase constants $\alpha_{TE_{nm}}$ and $\alpha_{TE_{nm}}$, implying that $G(\theta = 0)$ is independent of polarization [3]. Harrington's gain expression has the A_{n1} and B_{n1} coefficients on the numerator, and all of the mode coefficients in the denominator. Thus, G increases when all mode coefficients with $m \neq 1$ vanish. The gain is further maximized when the A_{n1} and B_{n1} coefficients are chosen so that the TE_{n1} and TM_{n1} powers are equalized, implying

$$A_{n1} = Z_0 B_{n1} \tag{1.61}$$

Even higher gain is obtained when the phases of A_{n1} are chosen to maximize the numerator. Upon applying each of these conditions, Harrington proceeded to maximize G by differentiating it with respect to A_{n1} and solving for the A_{n1} values. His resulting maximum gain expression for a unidirectional *Chu antenna* for $n \leq N$ is

$$G_{\max} = N^2 + 2N \tag{1.62}$$

1.3.3.2 Minimum *Q* for a Directional Chu Antenna

Using the same equivalent circuits employed by Chu [11], Harrington recognized that the Q of the nth mode (denoted as Q_n) for a linearly polarized, unidirectional, equally excited TE and TM mode *Chu antenna* is the same as that of the circularly polarized, omni-directional, equally excited TE and TM mode antenna in [11]. As usual, Q_n can be computed from

$$Q_n = \frac{2\omega W_{nm}^{\text{Electric}}}{P_{nm}} = \frac{2\omega W_{nm}^{\text{Magnetic}}}{P_{nm}} \tag{1.63}$$

where P_{nm} denotes the power contained by the TE_{nm} or TM_{nm} modes and $W_{nm}^{\text{Electric, Magnetic}}$ refer to the corresponding electric or magnetic energy densities. He found that

$$Q_{\text{LP, TE}_{n1}-\text{TM}_{n1},\text{Chu}} = Q_{\text{CP, TE}_{n0}-\text{TM}_{n0},\text{Chu}} \approx \frac{1}{2} Q_{\text{TE}_{n0},\text{Chu}} = \frac{1}{2} Q_{\text{TM}_{n0},\text{Chu}} \tag{1.64}$$

where the notation $Q_{\text{LP,TE1n-TM1n,Chu}}$ refers to the *Chu antenna* Q radiating LP polarized waves due to equally excited TE_{n1} and TM_{n1} modes. Similarly to Chu [11] the minimum Q, denoted by $\hat{Q}_{\min}$, is

$$\hat{Q}_{\min} = Q_{\text{LP,TE11-TM11,Chu}} = Q_{\text{CP,TE10-TM10,Chu}} \tag{1.65}$$

1.3.3.3 Antenna Losses and Efficiency

Harrington also investigated the losses in the antenna structure as a function of antenna size. To do so, he used a figure of merit referred to as the dissipation factor d_F. He considered a spherical antenna of radius a whose radiation can be represented by the equivalent surface magnetic currents

$$\boldsymbol{M} = \boldsymbol{E} \times \hat{\boldsymbol{r}}|_{r=a} \tag{1.66}$$

He also represented the TE_{nm} and TM_{nm} normalized wave impedances looking in the $-\hat{r}$ direction by

$$Z_{nm}^{TE-} \approx Z_{nm}^{TM-} \approx \frac{Z_c}{Z_0} = \frac{(1+j)}{Z_0}\sqrt{\frac{\omega\mu}{2\sigma}} \tag{1.67}$$

That is, he included the conductivity σ into his expression to account for losses.

Harrington proceeded to define an equivalent network with $\boldsymbol{M}$ representing a series voltage discontinuity at the sphere's surface. For each mode, the normalized wave impedance looking into the $+\hat{\boldsymbol{r}}$ direction is given by the Chu equivalent circuit. Additionally, the impedance in the $-\hat{\boldsymbol{r}}$ direction (interior to the sphere) is given by Eq. (1.67). This equivalent network problem is depicted in Fig. 1.23.

Denoting the powers dissipated inside the *Chu sphere* by $P_{diss}^{TE_{nm},TM_{nm}}$ and the radiated mode powers as $P_{rad}^{TE_{nm},TM_{nm}}$, the dissipation factor for each equally excited TE_{nm}/TM_{nm} mode pair is

$$d_{F_n} = \frac{P_{diss}^{TE_{nm}} + P_{diss}^{TM_{nm}}}{P_{rad}^{TE_{nm}} + P_{rad}^{TM_{nm}}} \tag{1.68}$$

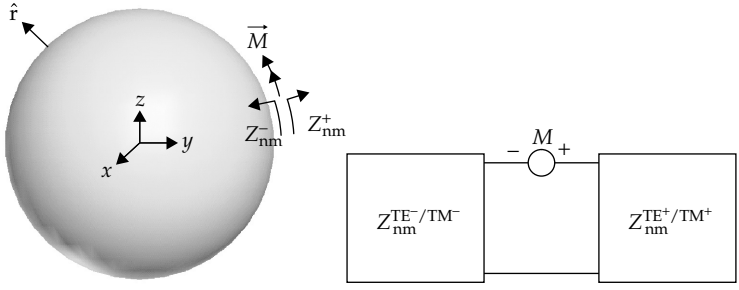

FIGURE 1.23 Circuit model for a lossy antenna structure used to compute the dissipation factor d_F.

The overall dissipation factor is then given by

$$d_F = \frac{\sum_{m,n} \left[\left(P_{\text{rad}}^{\text{TE}_{mn}} + P_{\text{rad}}^{\text{TM}_{mn}} \right) d_{F_n} \right]}{\sum_{m,n} \left(P_{\text{rad}}^{\text{TE}_{mn}} + P_{\text{rad}}^{\text{TM}_{mn}} \right)} \tag{1.69}$$

As expected, higher order modes are evanescent for small antennas. So, the dominant dissipation factor is d_{F1}. The efficiency is then given by

$$\textit{Efficiency}(\%) = \frac{100}{1 + d_F} \tag{1.70}$$

and plotted in Fig. 1.24.

Though simplified models were used for the conductor losses, the dissipation factor provides an insight in the behavior of small antennas. We can state that *as antenna size decreases, its efficiency also decreases*. This is also the reason that low Q values for small antennas are primarily the result of material losses rather than radiation loss.

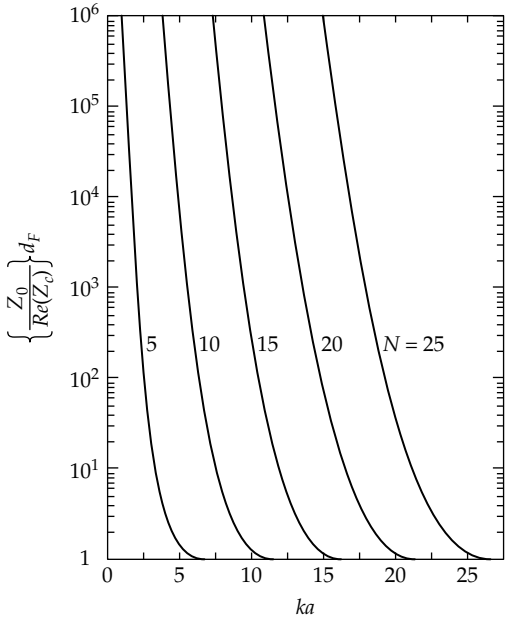

FIGURE 1.24 Dissipation factor d_F versus ka for various $N = \max(n)$ in Eq. (1.69). (*See Harrington* [3].)

1.3.3.4 Comments

Unlike Chu, Harrington focused on linearly polarized, unidirectional *Chu antennas* with equal excitation of TE_{nm} and TM_{nm} modes. In the small antenna limit, Eq. (1.1), the maximum gain or directivity of this antenna was derived to be 3. Also, the lower bound on Q was found to be approximately half that of the same *Chu antenna* supporting only TM or TE modes. This further reinforces the idea that reduction of Q from a linearly polarized antenna is a result of introducing TE and TM modes and not due to change in polarization. The reader may wonder why it was stressed in earlier sections that small antennas have the same pattern as that of a Hertzian dipole, yet Harrington's work focused on a unidirectional antenna. It will later be shown [4, 5] that these patterns can be realized in the small antenna limit using certain arrangements of electric and magnetic monopoles.

We close this discussion by nothing that Fig. 1.24 clearly shows the inverse relationship between antenna size and antenna efficiency. Though this analysis was performed for one specific case, the principle generally holds for all small antennas.

1.3.4 Work of Collin, Rothschild, and Fante (1964–1969)

Collin and Rothschild [18] sought to examine the antenna limits on Q by using a different method than Chu [11], based purely on the spherical TM_{nm} and TE_{nm} fields generated by a *Chu antenna*. Their work [18] was restricted to an antenna radiating either TM_{nm} modes or TE_{nm} modes. The authors also extended their analysis to cylindrical modes. However, the cylindrical mode analysis is not of relevance to small antennas since they focused on antennas of finite radius but of infinite extent.

1.3.4.1 Exact Q for a TM or TE Propagating Chu Antenna

Collin and Rothschild considered a *Chu antenna* of radius a (as defined in Sec. 1.3.2). The authors note that all antenna radiated fields have stored, nonpropagating reactive energy and a radiation component to carry real power out to infinity. Since the components cannot be easily separated, to evaluate Q Collin and Rothschild devised a method to separate the radiation component from the total stored electric and magnetic energy. The former can, of course, be found using Poynting's theorem.

Without loss of generality, Collin and Rothschild choose to analyze only the TM_{n0} mode of the *Chu antenna*. As discussed in Secs. 1.3.2 and 1.3.3, Q is independent of the azimuthal mode index m (the second

index of the mode). So, it was assumed zero for simplicity. Also, the TE_{nm} modes, being the dual of the TM_{nm} modes, do not need to be considered. The field components of the TM_{n0} mode are given in Eqs. (1.51*a*) to (1.51*c*).

Central to determining the antenna Q, the authors note that the power flow from an antenna can be represented by an energy density multiplied by the energy velocity. That is,

$$\begin{aligned} P_{\text{rad}} &= \textit{Radiated Antenna Power} = (\textit{Energy density})\ (\textit{Speed of light}) \\ &= \rho_{\text{rad}} \cdot c \end{aligned} \tag{1.71}$$

From Poynting's theorem, the power exiting the *Chu antenna* surface S is given by (see Fig. 1.1 for coordinates)

$$\begin{aligned} P_{\text{out}} &= \frac{1}{2} \oint_S (\boldsymbol{E} \times \boldsymbol{H}^*) \bullet d\boldsymbol{S} = \frac{1}{2} \int_0^{2\pi} \int_0^{\pi} E_\theta H_\phi^* a^2 \sin\theta \, d\theta \, d\phi \\ &= P_{\text{rad}} + 2j\omega (W_M - W_E) \end{aligned} \tag{1.72}$$

As usual, $W_{E,M}$ refer to the total stored electric and magnetic energy. Using the energy density ρ_{rad} in Eq. (1.71), we can subtract the total radiation energy from the total energy to yield the total stored energy

$$\begin{aligned} &W_M + W_E \\ &= \int_a^\infty \left\{ \left[\int_0^{2\pi} \int_0^{\pi} (w_e + w_m)\, r^2 \sin\theta \, d\theta \, d\phi \right] - \rho_{\text{rad}} \right\} dr \\ &= \int_a^\infty \left\{ \left[\int_0^{2\pi} \int_0^{\pi} \left(\frac{1}{4}\varepsilon_0 |\boldsymbol{E}|^2 + \frac{1}{4}\mu_0 |\boldsymbol{H}|^2 \right) r^2 \sin\theta \, d\theta \, d\phi \right] - \frac{P_{\text{rad}}}{c} \right\} dr \end{aligned} \tag{1.73}$$

where $\rho_{\text{rad}} = P_{\text{rad}}/c$ refers to radiated power density. Since the stored electric energy is greater than the magnetic one for TM_{nm} modes, W_M can be neglected. Thus, we evaluate on the W_E to get

$$Q_n = \frac{2\omega_0 W_{E,n}}{P_{\text{rad},n}} \tag{1.74}$$

This is the Q for the TM_{n0} mode. Collin and Rothschild evaluate Eq. (1.74) to get the following expressions

$$Q_1 = \frac{1}{ka} + \frac{1}{(ka)^3} \tag{1.75a}$$

$$Q_2 = \frac{3}{ka} + \frac{6}{(ka)^3} + \frac{18}{(ka)^5} \tag{1.75b}$$

$$Q_3 = \frac{6}{ka} + \frac{21}{(ka)^3} + \frac{135}{(ka)^5} + \frac{675}{(ka)^7} \tag{1.75c}$$

We note that the first three of these are the same as those obtained by Chu using the equivalent circuits in Fig. 1.19.

1.3.4.2 Exact *Q* for a TM and TE Propagating Chu Antenna

Fante [19] expanded Collin and Rothschild's work by assuming a *Chu antenna* exciting TE and TM modes (similar to the case considered by Harrington in Sec. 1.3.3). Using Eq. (1.3) and the same procedure as Collin and Rothschild, Fante expressed the quality factor Q for an arbitrarily excited *Chu antenna* with TM and TE mode coefficients A_{nm} and B_{nm}, respectively, as

$$Q = \max \left\{ \frac{\sum_{n=1}^{\infty} \left[a_n^2 Q_n' + b_n^2 Q_n \right]}{\sum_{n=1}^{\infty} \left(a_n^2 + b_n^2 \right)} \quad \text{or} \quad \frac{\sum_{n=1}^{\infty} \left[a_n^2 Q_n + b_n^2 Q_n' \right]}{\sum_{n=1}^{\infty} \left(a_n^2 + b_n^2 \right)} \right\} \tag{1.76}$$

where

$$a_n^2 = \sum_{m=0}^{n} \lambda_{\mathrm{nm}} |A_{\mathrm{nm}}|^2 \tag{1.77}$$

$$b_n^2 = \sum_{m=0}^{n} \lambda_{\mathrm{nm}} |B_{\mathrm{nm}}|^2 \tag{1.78}$$

$$\lambda_{\mathrm{nm}} = \frac{2\pi \hat{\varepsilon}_m}{2n+1} n(n+1) \frac{(n+m)!}{(n-m)!} \tag{1.79}$$

$$\hat{\varepsilon}_m = \begin{cases} 2 & \text{for } m = 0 \\ 1 & \text{for } m = 1 \end{cases} \tag{1.80}$$

In the equations, Q_n is the quality factor derived by Collin and Rothschild for the TM_{nm} or TE_{nm} modes, and Q_n' is an additional contribution. Closed form expressions for Q_n and Q_n' are given in [19] in terms of spherical Bessel functions with arguments of ka, and are plotted in Fig. 1.25 for several n. For the equally excited case, $a_n^2 = b_n^2$

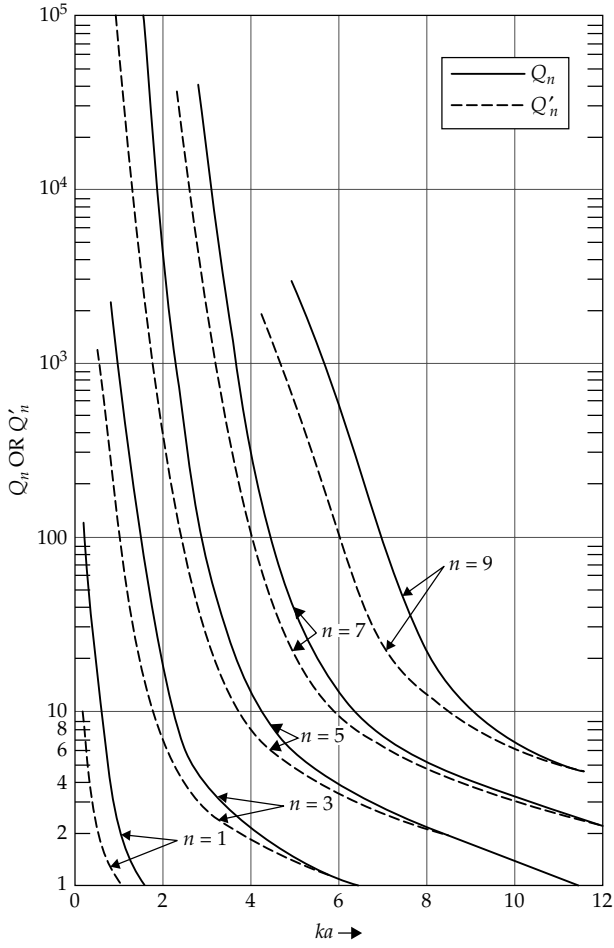

FIGURE 1.25 Quality factor components Q_n (solid) and Q'_n (dashed) for different mode indices n (*After Fante © IEEE, 1969* [19].)

and Eq. (1.76) reduces to

$$Q = \frac{\sum_{n=1}^{\infty} a_n^2 \hat{Q}_n}{\sum_{n=1}^{\infty} a_n^2} \tag{1.81}$$

with

$$\hat{Q}_n = \frac{Q_n + Q'_n}{2} \tag{1.82}$$

ka	$Q_1/2$	$\hat{Q}_{\min}$
0.3	20.00	21.600
0.6	3.16	3.990
1.0	1.00	1.505

TABLE 1.3 $\hat{Q}_{\min}$ and $Q_1/2$ for the *Chu Antenna* (See Fante [19])

From Eq. (1.81), Fante concluded that the minimum possible Q occurs for a *Chu antenna* exciting equal parts TM_{1m} and TE_{1m}

$$\hat{Q}_{\min} = Q_{\text{TM10+TE10,Chu}} = \frac{Q_1 + Q_1'}{2} \tag{1.83}$$

$$\hat{Q}_{\min} \approx \frac{1}{2}Q_1 = \frac{1}{2}Q_{\text{TE10,Chu}} = \frac{1}{2}Q_{\text{TM10,Chu}} \quad \text{for} \quad ka \ll 1 \tag{1.84}$$

Clearly, Eq. (1.84) is the same result as that derived by Harrington [36]. Also, Fig. 1.25 and Eq. (1.83) demonstrate an important issue alluded by Chu [11] and Harrington [4] (though never fully quantified). That is, the Q for a *Chu antenna* exciting equal parts of TM_{1m} and TE_{1m} modes is slightly greater than half the Q associated with either TE or TM modes. Indeed, Fig. 1.25 shows that for small ka, Q_n remains approximately an order of magnitude greater than Q_n'. Fante remarks that Q_n is always greater than Q_n'. Thus, from Eq. (1.83) the Q corresponding to equally excited TM_{1m} and TE_{1m} modes is approximately equal to $Q/2$ for the *Chu antenna*. However, as ka approaches unity, Q_n' can no longer be ignored, and the approximation Eq. (1.84) breaks down. Table 1.3 demonstrates this principle by comparing the actual $\hat{Q}_{\min}$ Eq. (1.83) to the $Q_1/2$ approximation.

1.3.4.3 Relationship Between *Q* and Fractional Bandwidth *B*

In [19] Fante gives the first direct relationship between Q and the 3 dB fractional bandwidth B for small antennas. To do so, Fante begins by assuming a high-Q, perfectly efficient antenna having an input impedance

$$Z_{\text{in}} = R_{\text{rad}} + jX_{\text{A}}(\omega) = \frac{2}{|I|^2}\left[P_{\text{rad}} + j2\omega(W_M - W_E)\right] \tag{1.85}$$

At resonance ($\omega = \omega_0$), Z_{in} can be approximated by the first two terms of its Taylor series expansion about ω_0. Specifically, we have

$$Z_{\text{in}} = R_{\text{rad}} + j(\omega - \omega_0)\left(\frac{dX_A(\omega)}{d\omega}\right)\Bigg|_{\omega_0} \tag{1.86}$$

For this, the 3 dB return loss point occurs when $(\omega - \omega_0) d X_A \omega_0)/d\omega = R_{\text{rad}}$. Therefore, the 3 dB fractional bandwidth B can be identified as

$$B \approx \frac{2R_{\text{rad}}}{\omega_0 \left(\dfrac{d X_A(\omega)}{d\omega} \right) \Big|_{\omega_0}} = \frac{4P_{\text{rad}}}{\omega_0 |I|^2 \left(\dfrac{d X_A(\omega)}{d\omega} \right) \Big|_{\omega_0}} \tag{1.87}$$

To find $X'_A(\omega_0)$, Fante begins by considering a volume Ω bounded by a surface S coinciding with the entire antenna structure (including the feed port A) and the spherical surface S_∞ at infinity (see Fig. 1.26). Fante starts with the identity [36, pp. 394–396]

$$\begin{aligned} &\iint_S \left(\frac{\partial \boldsymbol{E}}{\partial \omega} \times \boldsymbol{H}^* - \frac{\partial \boldsymbol{H}}{\partial \omega} \times \boldsymbol{E}^* \right) \bullet d\boldsymbol{S} + \iint_{S_\infty} \left(\frac{\partial \boldsymbol{E}}{\partial \omega} \times \boldsymbol{H}^* \right. \\ &\left. - \frac{\partial \boldsymbol{H}}{\partial \omega} \times \boldsymbol{E}^* \right) \bullet d\boldsymbol{S} = -j \iiint_\Omega \left(\mu_0 |\boldsymbol{H}|^2 + \varepsilon_0 |\boldsymbol{E}|^2 \right) dv \\ &= -j4 \left(W_{M,\text{total}} + W_{E,\text{total}} \right) \end{aligned} \tag{1.88}$$

where $W_{M,\text{total}}$ and $W_{E,\text{total}}$ represent the total magnetic and electric energy in Ω. For an antenna fabricated of perfect conductor, the

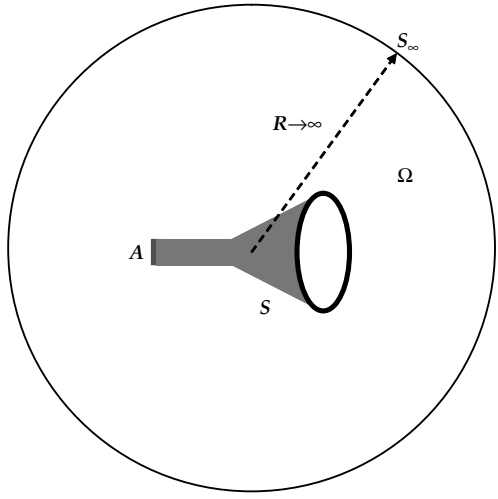

FIGURE 1.26 Volume Ω bounded by surface S coinciding with the entire antenna structure (including the feed port A) and far-field sphere S_∞.

boundary conditions can be applied

$$\left.\begin{aligned} d\boldsymbol{S} \bullet \left[\frac{\partial \boldsymbol{E}}{\partial \omega} \times \boldsymbol{H}^*\right] &= 0 \\ d\boldsymbol{S} \bullet \left[\frac{\partial \boldsymbol{H}}{\partial \omega} \times \boldsymbol{E}^*\right] &= 0 \end{aligned}\right\} \quad \text{on } S, \text{ excluding } A$$

to rewrite Eq. (1.88) as

$$\iint_{S_\infty} \left(\frac{\partial \boldsymbol{E}}{\partial \omega} \times \boldsymbol{H}^* - \frac{\partial \boldsymbol{H}}{\partial \omega} \times \boldsymbol{E}^*\right) \bullet d\boldsymbol{S} - \left(I^* \frac{\partial V}{\partial \omega} + V^* \frac{\partial I}{\partial \omega}\right)$$
$$= -j4(W_{M,\text{total}} + W_{E,\text{total}}) \tag{1.89}$$

where the second term on the left hand side is associated with the feed port equivalent voltage V and equivalent current I. Next, introducing the far zone field expressions valid on S_∞, we get

$$\boldsymbol{E}(r \to \infty) = \boldsymbol{E}_\infty(\omega) \frac{e^{-jkr}}{r} \tag{1.90a}$$

$$\boldsymbol{H}(r \to \infty) = \boldsymbol{H}_\infty(\omega) \frac{e^{-jkr}}{r} \tag{1.90b}$$

Using Eqs. (1.90a) and (1.90b) along with the chain rule for derivatives (with respect to frequency), Eq. (1.89) can be simplified to

$$\left(I^* \frac{\partial V}{\partial \omega} + V^* \frac{\partial I}{\partial \omega}\right) = \iint_{S_\infty} \frac{1}{r^2} \left(\frac{\partial \boldsymbol{E}_\infty}{\partial \omega} \times \boldsymbol{H}_\infty^* - \frac{\partial \boldsymbol{H}_\infty}{\partial \omega} \times \boldsymbol{E}_\infty^*\right) \bullet d\boldsymbol{S}$$
$$+ j4 \left[W_{M,\text{total}} + W_{E,\text{total}} - \frac{r}{2c} \text{Re} \iint_{S_\infty} (\boldsymbol{E} \times \boldsymbol{H}^*) \bullet d\boldsymbol{S}\right] \tag{1.91}$$

As $r \to \infty$ in Eq. (1.91), we immediately identify the bracketed term in the imaginary part as the total stored electric and magnetic energy $W_E + W_M$. Subtracting the conjugate of Eq. (1.91) from itself and utilizing vector identities inside the integrand, Fante derived an equation for the frequency derivative of the reactance $X^{A'}(\omega_0)$ as

$$\frac{\partial X_A}{\partial \omega} = \frac{4(W_E + W_M)}{|I|^2} - \frac{2}{Z_0 |I|^2} \text{Im} \iint_{S_\infty} \left(\boldsymbol{E}_\infty \bullet \frac{\partial \boldsymbol{E}_\infty^*}{\partial \omega}\right) dS \tag{1.92}$$

where it was assumed the current was held constant with frequency. Substituting this into the fractional bandwidth definition of Eq. (1.87) gives

$$B \approx \left[\frac{\omega_0(W_E + W_M)}{P_{\text{rad}}} + P(\omega_0)\right]^{-1} = \left[\frac{2\omega_0 W_E}{P_{\text{rad}}} + P(\omega_0)\right]^{-1}$$
$$= \left[\frac{2\omega_0 W_M}{P_{\text{rad}}} + P(\omega_0)\right]^{-1} \tag{1.93}$$

From Eq. (1.93) it is clear that in the case where $P(\omega_0)$ is small, this expression for B results in the well known relation of $Q \approx 1/B$. To quantify $P(\omega_0)$ in relation to Q, Fante derived the following inequality

$$P(\omega_0) \leq \frac{2}{B}\left[\frac{\sum_{n,m} |\Delta C_{\text{nm}}|^2}{\sum_{n,m} |C_{\text{nm}}|^2}\right]^{1/2} \tag{1.94}$$

where C_{nm} are proportional to the TE and TM mode excitation coefficients present in the far-field, and ΔC_{nm} is the total change in C_{nm} over approximately half the antenna's bandwidth. For this derivation, $R_{\text{rad}}'(\omega_0)$ was assumed nearly zero, implying that the derivative of the radiated power about the resonant frequency is approximately zero. Consequently, there is little change in the C_{nm} coefficients as these are proportional to the TE and TM mode coefficients present in the far-field, and the square root term in Eq. (1.94) is very small with respect to unity.

1.3.4.4 Comments

Collin and Rothschild developed a field-based method for determining the Q of a *Chu antenna* exciting either TM_{nm} or TE_{nm} modes. Their results were shown to be consistent with the results derived by the Chu equivalent circuits. Collin and Rothschild found that the Q associated with TM_{1m} or TE_{1m} modes represents the absolute lower bound on Q for a small antenna radiating only TE or TM modes, given below as

$$Q_{\text{min}} = \frac{1}{(ka)^3} + \frac{1}{ka} \tag{1.95}$$

We do note that compared to Wheeler's result, Eq. (1.95) has the extra term $1/ka$. This extra term is predictably due to the TM_{1m} mode having a small inductive energy component. Likewise, the TE_{1m} mode will have a small capacitive energy component. Nevertheless, both Eqs. (1.42) and (1.95) are very close for $ka \ll 1$.

Fante used the same procedure as Collin and Rothschild, and affirmed the statements made by Harrington and Chu that equal

excitations of TM_{1m} and TE_{1m} modes lead to the lowest possible Q. This Q in Eq. (1.83) is half that in Eq. (1.95) for $ka \ll 1$, and slightly greater than in Eq. (1.95) for $ka \approx 1$. It will be discussed later that an exact expression for this lowest possible Q will be derived by McLean [37] in Sec. 1.3.6.

We remark that Fante was the first to give a direct relationship between Q and the 3 dB fractional bandwidth B. He showed that the approximation $Q \approx 1/B$ remains valid for large Q and assumes that the input resistance does not vary rapidly near the resonant frequency. Another derivation relating Q and fractional bandwidth will be given later in Sec. 1.3.10.

1.3.5 Work of Hansen (1981–2006)

Hansen [2] sought a closed form expression for the minimum Q based on the results of Chu's work. He begins by representing the radiated field as a superposition of spherical vector waves, and notes that all excited modes (TE_{nm} and TM_{nm}) have an associated stored electric and magnetic energy. However, only the propagating modes contribute to radiation. Hansen reiterates that Q_n rises rapidly for $ka < n$.

Hansen [38] has reviewed the performance of many practical small antennas including loaded dipoles and loops, dielectric resonator antennas (DRA), small patches, and partial sleeves. He also analyzed several published small antenna designs which have poor radiation characteristics when compared to traditional designs, as well as a detailed criticism of antennas that claim to beat McLean's [37] Q limits [38].

1.3.5.1 Closed Form *Q* for TM or TE Omni-directional Chu Antenna Using Chu RLC Approximation

Hansen [2] used the series RLC approximation employed by Chu for the TM mode network in Fig. 1.19 to determine a closed form expression for the minimum Q of a *Chu antenna*. Chu's RLC series approximation of the networks in Fig. 1.19 is based on equating the input resistance, reactance, and frequency derivative of the reactance for each mode TM_{nm} to that of an equivalent series RLC circuit. Using Eq. (1.3.2.2), he cites the input resistance and reactance for each mode (as also obtained by Chu) as

$$R_n = \frac{1}{\left|ka\,h_n^{(2)}(ka)\right|^2} \qquad X_n = \mathrm{Re}\left\{\frac{\left(ka\,h_n^{(2)}(ka)\right)'}{ka\,h_n^{(2)}(ka)}\right\} \tag{1.96}$$

where the primes indicate derivatives with respect to ka. Using the series RLC approximation, Q_n for each TE_{nm} and TM_{nm} mode can be found using Eqs. (1.96), (1.3), and the duality principles in Table 1.2 as

$$Q_n = \frac{2\omega_0 \max(W_{En},\, W_{Mn})}{P_{a,n}} = \frac{ka\left|ka\,h_n^{(2)}(ka)\right|^2}{2}(ka\,X_n)' \tag{1.97}$$

The total Q for a pure TE or pure TM antenna system can then be obtained from Eq. (1.76). For $ka < 1$, Hansen states that based on the Chu equivalent circuits of Figs. 1.19 and 1.22, modes with $n > 1$ can be considered evanescent. Accordingly, setting $a_n^2 = 0$ for n $\neq 1$, we get the closed form solution using the series RLC approximation as

$$Q_{\mathrm{TM}1m,\mathrm{Chu}} = Q_{\mathrm{TE}1m,\mathrm{Chu}} \approx \frac{1 + 2(ka)^2}{(ka)^3\left[1 + (ka)^2\right]} \quad \text{for} \quad ka < 1 \qquad (1.98)$$

As mentioned previously, Eq. (1.98) is an approximate minimum possible Q for a TM or TE antenna circumscribed by a *Chu sphere* of radius a. We note that Eq. (1.98) is the corrected result derived by McLean based on Chu's RLC circuit approximation, as the original result [2] has an algebra mistake [3]. Figure 1.27 shows the Chu approximate result Eq. (1.98) alongside the approximate limit derived by Wheeler in Eq. (1.42) and exact limit derived by Collin and Rothschild in Eq. (1.95).

1.3.6 Work of McLean (1996)

In 1996, McLean [3] presented another rigorous method to determine Q for a *Chu antenna* supporting TE_{10}, TM_{10}, or equally excited TE_{10} and TM_{10} modes. McLean focused on this class of modes as they represent the radiated fields by small antennas. In his approach, McLean

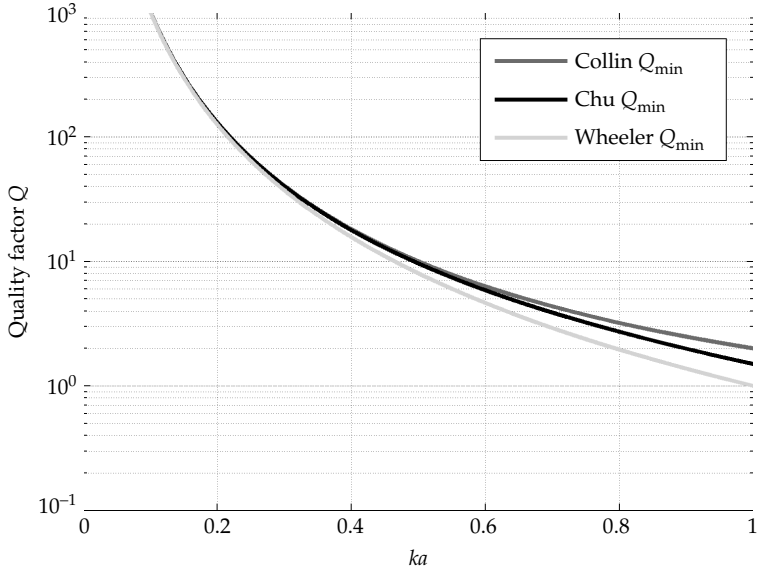

FIGURE 1.27 $Q_{\min}$ comparison for TM or TE antenna circumscribed by a *Chu sphere* of radius a.

challenged the approximate Q limits derived by Wheeler [1], Chu [11], Harrington [3], and Hansen [2].

1.3.6.1 McLean's Exact Q for Chu Antenna Radiating TM_{10} or TE_{10}

McLean starts by using (1.51a) to (1.51c) to compute the near-zone TM_{10} mode radiated fields

$$H_\phi = \sin\theta\, e^{-jkr}\left(\frac{j}{kr^2} - \frac{1}{r}\right) \tag{1.99a}$$

$$E_\theta = \frac{1}{j\omega\varepsilon}\sin\theta\, e^{-jkr}\left(-\frac{1}{r^2} - \frac{jk}{r} + \frac{j}{kr^3}\right) \tag{1.99b}$$

$$E_r = \frac{2}{\omega\varepsilon}\cos\theta\, e^{-jkr}\left(\frac{1}{kr^3} + \frac{j}{r^2}\right) \tag{1.99c}$$

and become

$$H_\phi^{\text{rad}} = -\sin\theta\,\frac{e^{-jkr}}{r} \tag{1.100a}$$

$$E_\theta^{\text{rad}} = -Z_0\sin\theta\,\frac{e^{-jkr}}{r} \tag{1.100b}$$

as $r \to \infty$. As the TM_{10} mode has capacitive energy, McLean used only the electric energy density w_e in his Q computations. It is given by

$$w_e = \frac{1}{4}\varepsilon\,|E|^2 \tag{1.101}$$

which reduces to the radiated energy density

$$w_e^{\text{rad}} = \frac{Z_0^2}{r^2}\sin^2(\theta) \tag{1.102}$$

for $r \to \infty$. Using a method similar to Collin and Rothschild, McLean subtracts the electric energy density Eq. (1.102) from the total electric energy density Eq. (1.101) to obtain the stored electric energy density w_e^s. Integrating w_e^s over all space outside the *Chu sphere* of radius a then gives the stored electric energy W_E to be used in Eq. (1.3) to compute Q. The associated radiated power P_{rad} is readily obtained using the far zone fields Eqs. (1.100a) and (1.100b) and the Poynting theorem. Using P_{rad} and W_E in Eq. (1.3), we have

$$Q_{\text{TM10,Chu}} = Q_{\min} = \frac{2\omega_0 W_E}{P_{\text{rad}}} = \frac{1}{ka} + \frac{1}{(ka)^3} \tag{1.103}$$

Equation (1.103) is the same as that derived by Collin and Rothschild [18] and the same as the TE_{10} or TM_{10} mode Q for the *Chu antenna*.

1.3.6.2 *Q* for Radiating Equally Excited TM_{10} and TE_{10}

For equally excited TM_{10} and TE_{10} modes within the *Chu antenna*, McLean invoked duality to represent the TE_{10} fields (see Table 1.2). He excited the modes to achieve CP polarization by scaling the TE_{10} coefficients with jZ_0. In computing the Q, he used the same procedure to evaluate the W_E and P_{rad}. Doing so, McLean concluded that

$$Q_{\text{TM10-TE10,Chu}} = \hat{Q}_{\text{min}} = \frac{1}{2}\left(\frac{2}{ka} + \frac{1}{(ka)^3}\right) \tag{1.104}$$

We note that Eqs. (1.103) and (1.104) are exact and valid for all *ka*. Also, Eq. (1.104) is the absolute minimum Q, and is approximately half of Eq. (1.103) for $ka \ll 1$. For such small sizes, the TM_{10} contributes primarily all W_E and TE_{10} does the same for W_H. Meanwhile, P_{rad} is doubled when both TE_{10} and TM_{10} are excited, leading to the half factor. However, this approximation breaks down as *ka* approaches unity.

Figure 1.28 compares the Q for TM_{10} and $TM_{10} + TE_{10}$ *Chu antennas* using Chu's RLC approximation [12] versus the exact results in Eqs. (1.103) and (1.104). It is evident that for $ka < 0.5$, the Chu RLC approximation remains accurate.

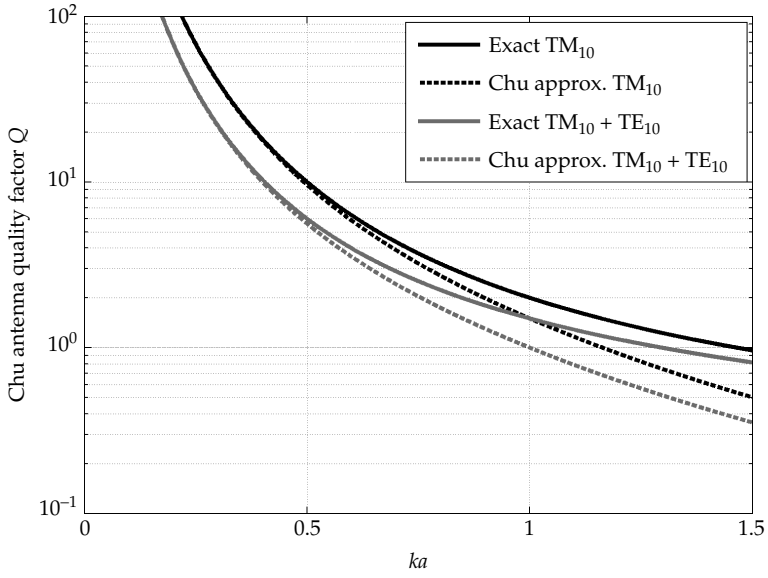

FIGURE 1.28 Comparison between exact and Chu RLC approximated *Chu antenna Q*.

1.3.6.3 Exact *Q* for Chu Antenna Derived from Mode Circuits

The Q values in Eqs. (1.103) and (1.104) can be verified using the equivalent impedance and admittance circuits in Figs. 1.19 and 1.22. For the TM_{10} mode, the circuit is given in Fig. 1.29 having the corresponding stored electric and radiated power given by

$$W_E = \frac{1}{4} C \, |V_C|^2 = \frac{1}{2\omega(ka)} \tag{1.105}$$

$$P_{\text{rad}} = \frac{1}{2} \, |I_r|^2 \, R = \frac{(ka)^2}{1 + (ka)^2} \tag{1.106}$$

Using these in the definition of Q in Eq. (1.3) we get

$$Q_{\text{TM10,Chu}} = Q_{\min} = \frac{2\omega_0 W_E}{P_{\text{rad}}} = \frac{1}{ka} + \frac{1}{(ka)^3} \tag{1.107}$$

Obviously, this is identical to Eq. (1.103) obtained via full-wave analysis. Correspondingly, using the TM_{10} and TE_{10} equivalent circuits, equally excited TM_{10} and TE_{10} modes radiating CP fields lead to the result in Eq. (1.104). The relation $\hat{Q}_{\min} \approx 1/2 \; Q_{\min}$ for $ka \ll 1$ can be easily seen through this circuit method. Specifically, for low frequencies the circuits in Figs. 1.19 and 1.22 ($n = 1$) are dominated by the capacitive and inductive elements, respectively. However, as the frequency increases and ka approaches unity, the contribution of the inductive (Fig. 1.19) and capacitive (Fig. 1.22) elements become more prominent, and the half factor relation begins to break down.

Using Figs. 1.19 and 1.22 for $n = 1$, we further note that mode circuits also demonstrate the breakdown of the often cited Q

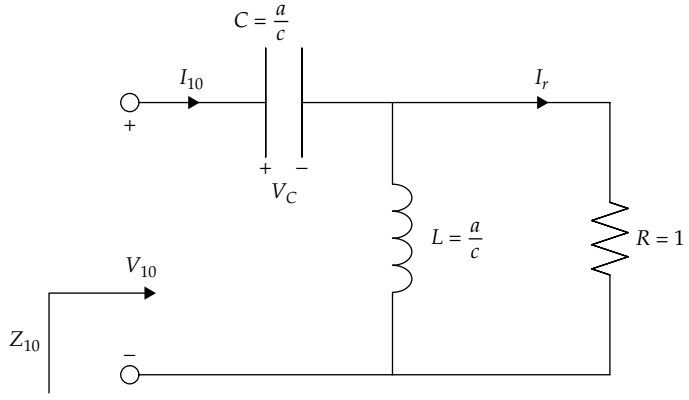

FIGURE 1.29 Equivalent RLC circuit for the TM_{10} mode.

approximation [39] (for small *ka*) given by

$$Q \approx \frac{|X_A|}{R_A} \tag{1.108}$$

For $ka \ll 1$ the net stored energy $|W_M - W_E| \approx |W_E|$, due to negligible inductor reactance. However, as *ka* approaches 1, the inductor's reactance becomes larger and $|W_M - W_E|$ can no longer be approximated by $|W_E|$. Consequently, Eq. (1.108) is no longer a valid approximation of Eq. (1.3). This is depicted in Fig. 1.30, where Yaghjian and Best's computed *Q* [10] [also given in Eq. (1.153)] is compared to Eq. (1.108) for a small dipole and small loop. We can state that Eq. (1.108) remains accurate for a small dipole with $ka < 0.5$, and for a small loop with $ka < 0.3$.

1.3.6.4 Comments

McLean demonstrated two procedures (using fields and circuits) to determine the exact minimum *Q* limits for an antenna circumscribed by a *Chu sphere*. For an antenna exciting only TE modes or TM modes, the fundamental *Q* limit is given by Eq. (1.103) and valid for all *ka*. When both TE and TM modes are excited, the fundamental limit is given by Eq. (1.104) and valid for all *ka*.

In Secs. 1.3.2 through 1.3.6, the minimum *Q* was derived using a *Chu antenna*—an antenna which is enclosed by a *Chu sphere* and has zero stored energy inside the sphere. Though the *Q* given by McLean represents an absolute lower bound, it remains much lower than those of practical antennas. It has been noted that this is due to the nonzero energy stored within the *Chu sphere*. This additional energy component was used by Lopez [31] to define the quality factor ratio (*QR*) for a small antenna

$$QR = \frac{Q}{Q_{\text{Chu}}} \tag{1.109}$$

where *Q* is the actual value and Q_{Chu} is that given by Eqs. (1.103) and (1.104). In essence, *QR* gives the ratio of the total stored energy to that stored external to the *Chu sphere*. If only the TM_{10} or TE_{10} mode is excited, then Q_{Chu} is given as Eq. (1.103). Conversely, if both TM_{10} and TE_{10} modes are excited, Q_{Chu} is given as Eq. (1.104). Lopez gives the *QR* for several practical antennas in Table 1.4.

1.3.7 Work of Foltz and McLean (1999)

Foltz and McLean [21] recognized that the derived fundamental *Q* limit is not close to the verifiable values for many practical antennas (see Table 1.4). Wheeler [9] and Hansen [2] had also noted that dipole antennas deviate from the optimal *Q* as they do not utilize the

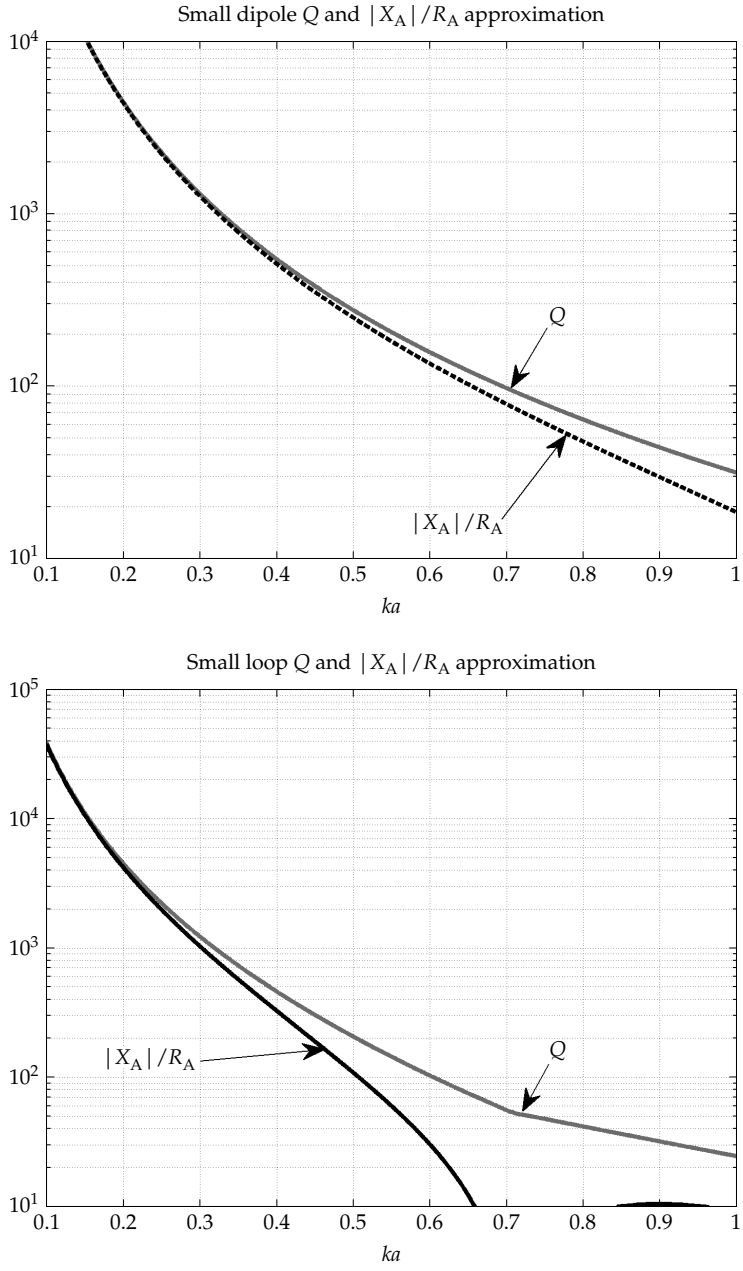

FIGURE 1.30 Yaghjian and Best's [10] computed Q compared to $|X_A|/R_A$ approximation for a small dipole and small loop.

Antenna Type	*QR*
Spherical coil (Fig. 1.15), $\mu_r = \infty$	1
Spherical coil (Fig. 1.15), $\mu_r = 1$	3
L-type cylindrical antenna (Fig. 1.13), $\mu_r = 1$, $D/b = 2.24$	4.4
Disc dipole (Fig. 1.31), $D/b = 0.84$	2.4
Spherical-cap dipole (Fig. 1.32)	1.75

TABLE 1.4 Quality Factor Ratio QR for Several Common Small Antennas (*See Lopez* [31])

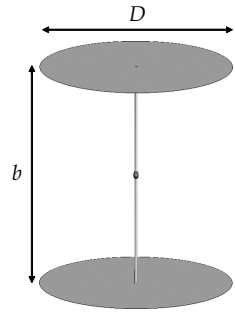

FIGURE 1.31 Disc dipole.

FIGURE 1.32 Spherical-cap dipole.

Chu sphere effectively. To examine this hypothesis, Foltz and McLean considered the Q of an enclosure having the surface of a prolate spheroid (see Fig. 1.33) with zero interior energy. We will refer to this as the *prolate Chu antenna*. Foltz and McLean assume the *prolate Chu antenna* has azimuthal symmetry. This is analogous to setting $m = 0$ for the spherical case.

The minimum Q associated with the *prolate Chu antenna* gives a more restrictive class of limitations. The analysis reported [20] is summarized in the preceding sections.

1.3.7.1 Minimum *Q* for the TM Prolate Chu Antenna

Foltz and McLean represented the geometry of Fig. 1.33 in a prolate spheroidal coordinate system (ξ, η, ϕ), where the surface of the prolate spheroid lies on $\xi = \xi_0$. The relation between ξ_0 and the prolate dimensions are

$$a = \xi_0 f$$
$$b = \left(\xi_0^2 - 1\right)^{1/2} f$$

where $2f$ is the foci distance. Foltz and McLean expanded the fields generated by the TM *prolate Chu antenna* as a superposition of azimuthally symmetric TM (to ξ) spheroidal vector wavefunctions.

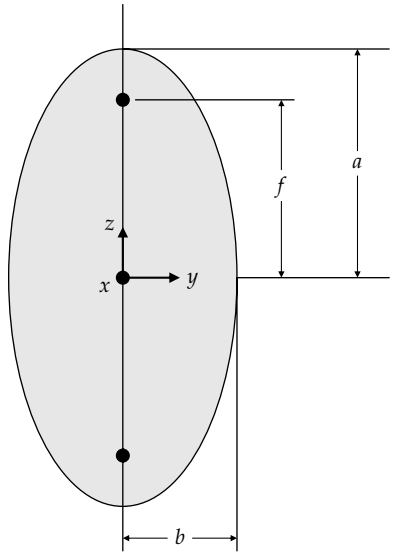

FIGURE 1.33 Cross-section of a prolate spheroid volume and coordinates, used in [20].

The wave admittance of these modes looking out from the surface ξ_0 was computed to be

$$Y_{n+1} = -jc_x\omega\varepsilon \frac{\sqrt{\xi_0^2 - \eta^2}\, R_{n,n+1}^{(4)}(\xi_0)}{\dfrac{d}{d\xi}\left(\sqrt{\xi^2 - 1}\, R_{n,n+1}^{(4)}(\xi)\right)\Big|_{\xi_0}} \tag{1.110}$$

where $c_x = fk$, and $R_{n,n+1}^{(4)}$ is the (outward) radial spheroidal function of the fourth kind. This is analogous to the second kind spherical Hankel function used in spherical wavefunction analysis. The transition from a prolate spheroid to an oblate spheroid can be achieved by simply replacing c_x with $\pm jc_x$. The reader is referred to Stratton [40] and Flammer [41] for more details on spheroidal wavefunctions.

Foltz and McLean state that Eq. (1.110) cannot be easily represented as an exact lumped network as was done by Chu [11]. Instead, for $ka < 0.5$ they fitted Eq. (1.110) to the numerical representation

$$Y_{n+1} \approx \frac{(j\omega)a_1 + (j\omega)^2 a_2 + \cdots}{1 + (j\omega)b_1 + (j\omega)^2 b_2 + \cdots} \tag{1.111}$$

Foltz and McLean derived an equivalent high-pass network for Eq. (1.110) based on Eq. (1.111). They also noted that the minimum Q for the TM *prolate Chu antenna* is associated with the first order TM (to ξ) mode $n = 1$, which we denote as $Q_{\text{min, prolate}}$.

1.3.7.2 Comments

Foltz and McLean plotted their results for $Q_{\text{min, prolate}}$ versus ka for varying a/b ratios of the prolate spheroid (see Fig. 1.34). The longest dimension for this spheroid is $2a$. In general, $Q_{\text{min, prolate}}$ increases as the length/diameter ratio increases (spheroid gets thinner). However, as the length/diameter ratio is further increased, $Q_{\text{min, prolate}}$ changes much less drastically than the physical volume of the prolate spheroid. This relationship is depicted in Fig. 1.35.

1.3.8 Work of Thiele (2003)

Thiele and his associates Detweiler and Penno [7] also recognized that the theoretical lower limits on Q described in previous sections are far from the results attained for actual antennas. Thiele also addresses an ambiguity in Foltz and McLean [20], stating that multiple prolate spheroid shapes can qualify as minimally enclosing a given antenna structure, resulting in various minimum Q limits.

In an attempt to find the Q for more practical small antennas, Thiele et al. take a much different approach to determine the Q of an ESA based purely on the far-fields. Central to their method is the concept of

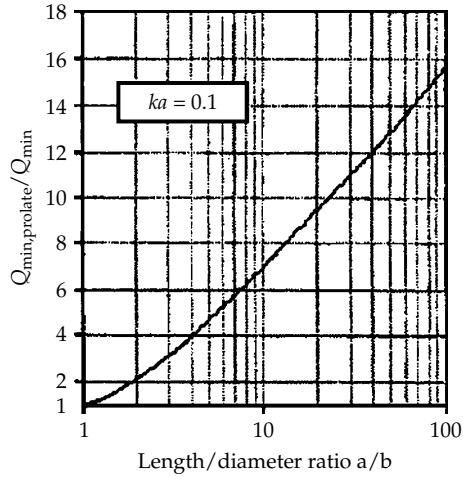

FIGURE 1.34 $Q_{\min,\text{prolate}}$ versus ka for various length/diameter ratios for the prolate *Chu antenna*. (*After Foltz and McLean ©IEEE, 1999* [20].)

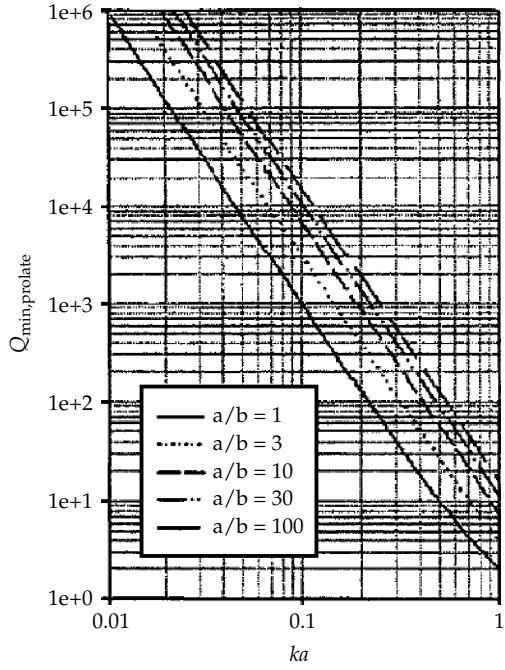

FIGURE 1.35 $Q_{\min,\text{prolate}}/Q_{\min}$ length/diameter ratio with $Q_{\min}$ given in Eq. (1.103) and $ka = 0.1$. (*After Foltz and McLean ©IEEE, 1999* [20].)

superdirectivity, stated by many authors [42–45] to be directly related to the antenna Q. Thiele et al. computed the Q of a dipole supporting a sinusoidal current, and compared their results to the minimum Q in Eq. (1.103) as derived by McLean.

1.3.8.1 Superdirectivity and *Q*

To determine Q using [7], we first review the superdirective ratio R_{SD}. We begin by introducing the variable transformation

$$u = \frac{kd}{2}\cos(\theta) \tag{1.112}$$

where

$$\frac{\pi d}{\lambda} \le u \le \frac{\pi d}{\lambda} \quad \text{is the visible region}$$

and

$$\begin{bmatrix} -\infty \le u \le -\dfrac{\pi d}{\lambda} \\ \dfrac{\pi d}{\lambda} \le u \le \infty \end{bmatrix} \quad \text{is the invisible region}$$

For an antenna array (see Fig. 1.36), the array factor is then given by

$$f(u) = \frac{\sin\left(\dfrac{Nu}{2}\right)}{N\sin\left(\dfrac{u}{2}\right)} \tag{1.113}$$

and R_{SD} is given by

$$R_{SD} = \frac{\displaystyle\int_{-\infty}^{\infty} |f(u)|^2\, du}{\displaystyle\int_{-\pi\, d/\lambda}^{\pi\, d/\lambda} |f(u)|^2\, du} \tag{1.114}$$

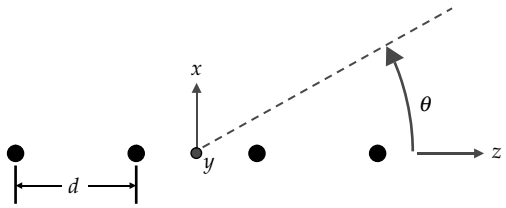

FIGURE 1.36 Linear array along z-axis with element spacing d.

This superdirective ratio has also been used to measure the realizability of an antenna. Superdirective antennas are antennas that exhibit higher directivity than nominal, and an "electrically small antenna (ESA)" can be classified as superdirective since its directivity stays approximately constant as $ka \to 0$. Thiele et al. noted that Rhodes [45] compared R_{SD} to "somewhat similar to $Q + 1$." If R_{SD} is assumed to be equal to $Q + 1$ as in [42–44], then Q can be represented as

$$Q = \frac{\displaystyle\int_{-\infty}^{-\pi\, d/\lambda} |f(u)|^2\, du + \int_{\pi\, d/\lambda}^{\infty} |f(u)|^2\, du}{\displaystyle\int_{-\pi\, d/\lambda}^{\pi\, d/\lambda} |f(u)|^2\, du} \tag{1.115}$$

We may also replace $f(u)$ in Eq. (1.115) by the array's normalized electric field $E(u)$

$$|E(u)| = |g(u)\, f(u)| \tag{1.116}$$

where $g(u)$ is the element pattern. Using this in Eq. (1.115) gives

$$Q = \frac{\displaystyle\int_{-\infty}^{-\pi\, d/\lambda} |E(u)|^2\, du + \int_{\pi\, d/\lambda}^{\infty} |E(u)|^2\, du}{\displaystyle\int_{-\pi\, d/\lambda}^{\pi\, d/\lambda} |E(u)|^2\, du} \tag{1.117}$$

In Fig. 1.37, Thiele et al. used Eq. (1.117) for a dipole element pattern (of sinusoidal distribution) and compared it to Eq. (1.103). Unlike Eq. (1.103), Eq. (1.117) does not assume TM mode propagation, but is instead based on the far fields of the actual antenna. The computed Q for a bowtie and end-loaded dipole are also given in Fig. 1.37 (see Figs. 1.38 and 1.39 for the antenna geometries), as well as the Q associated with dipoles of radius $a_0 = 0.0005\lambda$ and 0.001λ.

Of importance in Fig. 1.37 is that the Thiele et al. Q values for the bowtie and end-loaded dipole (enclosed in a *Chu sphere*) are closer to the far-field Q in Eq. (1.117). In contrast, McLean's minimum Q Eq. (1.103) is often an order of magnitude smaller. We note that Thiele makes a significant approximation (see Fig. 1.30) in using $Q \approx |X_A|/R_A$ to compute Q for the two dipole curves ($a_0 = 0.0005\lambda$ and 0.001λ), the bowtie antenna, and the end-loaded dipole antenna. Thiele remarks that the patterns of the sinusoidally distributed dipoles are slightly narrower than that of a Hertzian (constant current) dipole (see Fig. 1.2). Thus, from Eq. (1.117) the sinusoidal dipoles are more

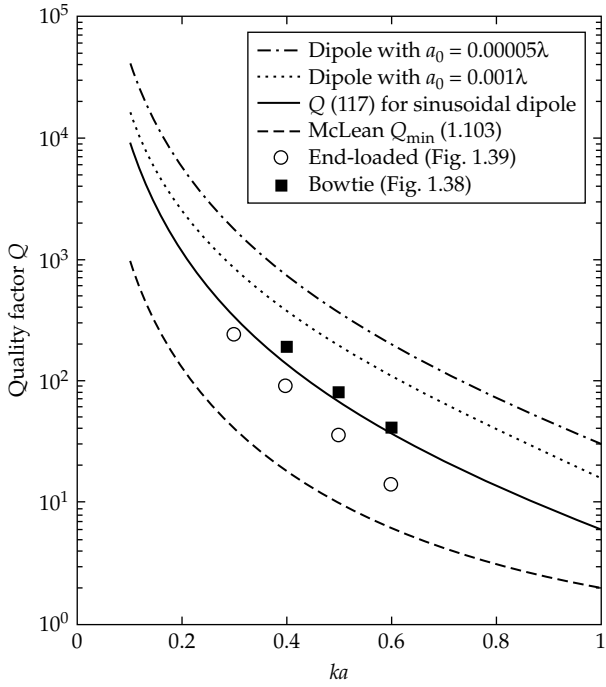

FIGURE 1.37 Computed bowtie, end-loaded, and sinusoidal dipole Q with Eqs. (1.103) and (1.117). (*After Thiele et al. ©IEEE, 2003* [7].)

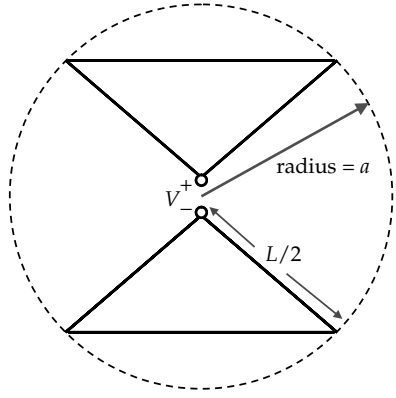

FIGURE 1.38 Bowtie dipole circumscribed by *Chu sphere*.

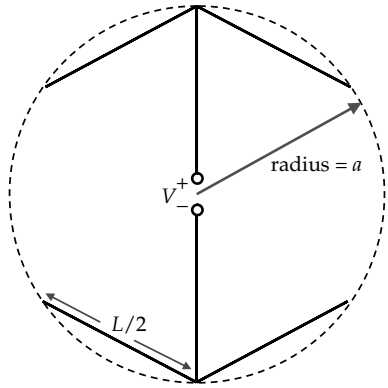

FIGURE 1.39 End-loaded dipole circumscribed by *Chu sphere*.

superdirective and as a result have a higher Q. This is also seen in the current distributions of the bowtie and end-loaded dipoles [7]. From Fig. 1.37 we also observe that as the dipole thickness decreases, the Q value increases. This effect was also predicted in Fig. 1.34 by Foltz and McLean.

1.3.8.2 Comments

The approach used by Thiele et al. [7] is solely based on the antenna or array far field, regardless of its shape and form. Therefore, it can be readily used to compute the Q for any other antenna. However, it is important to examine Eq. (1.117) and verify that it agrees with standard definition of Q Eq. (1.3). Indeed, the denominator of Eq. (1.117) involves integration of the normalized field pattern over the visible region. Thus, it is proportional to the radiated power. So, for Eq. (1.117) to be equivalent to Eq. (1.3), the numerator of Eq. (1.117) must represent twice the reactive electric power in the space surrounding the antenna (assuming the proportionality factor is the same as in the numerator). For that we refer to Rhodes [46]. Rhodes determined that the stored electric and magnetic energies generated by a planar aperture can be found using the field pattern given in Eq. (1.116). His result is indeed twice the reactive electric power in [46] making it consistent with the numerator of Eq. (1.117).

Rhodes [46] also examined the fields of a planar dipole (of sinusoidal distribution) to validate his method. He remarked that the input reactance of the planar dipole using his method closely matches that derived by King [12]. He later verified the approximate relationship between Q and the 3 dB fractional bandwidth B for this planar dipole using his far-field integrals over the visible and invisible regions to determine real and reactive electric power, respectively (see Fig. 1.40).

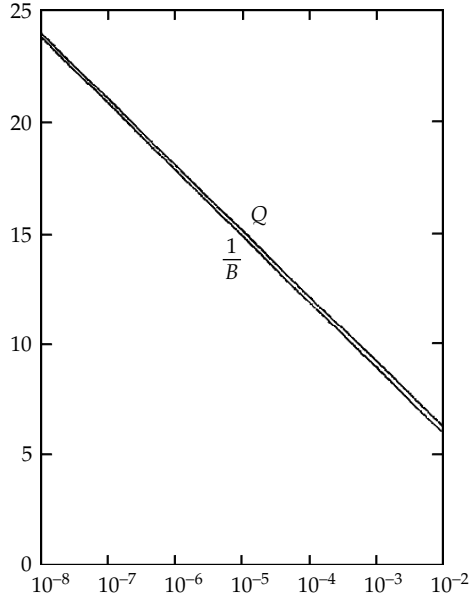

FIGURE 1.40 Q and $1/B$ for a sinusoidal current planar dipole of width "W." (*After Rhodes ©IEEE, 1966* [46].)

1.3.9 Work of Geyi (2003)

Geyi [22] stated that direct calculation of the exact Q using the Collin and Rothschild method [18] is difficult in practice, as it involves numerical integrations over an infinite spatial domain. To overcome this, Geyi formulated an approximate field-based method applicable for the small antenna range ($ka < 0.5$) using the Poynting theorem in both the time and frequency domains. Specifically, he determined Q by integrating the current distribution of the antenna structure. This simplifies numerical integrations significantly as the domain of integration is on the antenna only. Geyi derived the Q for several simple antennas and compared his results to other independent methods. He further reconsidered the fundamental Q limits for omni-directional and directional small antennas in a straightforward manner using spherical wavefunctions [21].

Geyi, along with Jarmuszewski and Qi [47], calculated Q as a function of input impedance via Maxwell's equations extended to the complex frequency domain. Essential to Geyi's results is the assertion that the Foster reactance theorem is valid for general antenna systems. However, several aspects of this derivation has been criticized by Best [48] and Andersen [49] under the premises that the frequency derivatives of the antenna input reactance $X'_A(\omega)$ and input susceptance

$B'_A(\omega)$ at resonance and antiresonance are not always positive. Additionally, Andersen [49] notes that the Cauchy-Reimann (C-R) equation is improperly applied in the derivation of Q, as the complex function for which the C-R theorem is used is not analytic. Due to the controversy surrounding [47], we choose to omit this derivation of Q as a function of input impedance and only state the result used by Geyi et al. [47] as

$$Q = \frac{\omega\left[\dfrac{\partial X_A}{\partial \omega} \pm \dfrac{X_A}{\omega}\right]}{2R_A} \tag{1.118}$$

where $\pm$ is chosen to yield the larger Q. In a later section, we will provide the derivation of the Q in terms of input impedance as given by Yaghjian and Best [10]. This Q will be shown to be

$$\begin{aligned} Q &= \frac{\omega}{2R_A(\omega)}\left|\frac{dZ_{\text{in}}(\omega)}{d\omega}\right| \\ &= \frac{\omega}{2R_A(\omega)}\left[\left(\frac{dR_A(\omega)}{d\omega}\right)^2 + \left(\frac{\partial X_A}{\partial \omega} + \frac{|X_A|}{\omega}\right)^2\right]^{1/2} \end{aligned} \tag{1.119}$$

We remark that if the derivative for the input resistance in Eq. (1.119) is negligible, then Eq. (1.119) can be reduced to Eq. (1.118) as given by Geyi [47]. Indeed, in practice, the frequency derivative of the reactance dominates for small antennas operating away from their natural antiresonance regions [10].

1.3.9.1 Field-Based Evaluation of Antenna *Q*

To find a practical method of computing Q for $ka < 0.5$, Geyi [22] begins by assuming a perfectly conducting small antenna with volume V_0. For his derivations, he approximates the near-zone-antenna fields by introducing a power series expansion for the exponential $\exp(-jk|\boldsymbol{r}-\boldsymbol{r}'|)$ term in the frequency domain scalar and vector potentials. This low frequency approximation for $\exp(-jk|\boldsymbol{r}-\boldsymbol{r}'|)$ remains accurate under the condition that $ka < 0.5$. The Poynting theorem (in the frequency domain) is then used to find the radiated power (P_{rad}) and the difference of the average electric and magnetic energies ($W_E - W_M$). To represent the near-zone fields in the time domain, the charge and current density sources, $\rho(\boldsymbol{r}', T)$ and $\boldsymbol{J}(\boldsymbol{r}', T)$, can be approximated in a power series with respect to retarded time $T = t - |\boldsymbol{r} - \boldsymbol{r}'|/c$ about the point t. With this, the time domain scalar and vector potentials can then be found, and subsequently the Poynting theorem (in the time domain) is used to compute the sum of the average electric and magnetic energies ($W_E + W_M$).

The actual expressions for W_E, W_M, and P_{rad} used by Geyi [22] are

$$W_E \approx \frac{cZ_0}{16\pi}\int_{V_0}\int_{V_0}\frac{1}{R}\left[\rho(\boldsymbol{r})\rho^*(\boldsymbol{r}')\right]\, dv(\boldsymbol{r})dv(\boldsymbol{r}') \tag{1.120}$$

$$W_M \approx \frac{cZ_0}{16\pi}\left[\frac{1}{c^2}\int_{V_0}\int_{V_0}\frac{\boldsymbol{J}(\boldsymbol{r})\bullet\boldsymbol{J}^*(\boldsymbol{r})}{R}dv(\boldsymbol{r})dv(\boldsymbol{r}') + \frac{k^2}{2}\int_{V_0}\int_{V_0}R\left[\rho(\boldsymbol{r})\rho^*(\boldsymbol{r}')\right]\, dv(\boldsymbol{r})dv(\boldsymbol{r}')\right] \tag{1.121}$$

$$P_{\text{rad}} \approx \frac{Z_0k^4}{12\pi}\left[c^2\left|\boldsymbol{p}\right|^2+\left|\boldsymbol{m}\right|^2\right] \tag{1.122}$$

with the electric and magnetic dipole moments $\boldsymbol{p}$ and $\boldsymbol{m}$ defined as

$$\boldsymbol{p} = \int_{V_0}\boldsymbol{r}'\rho(\boldsymbol{r}')dv(\boldsymbol{r}') \tag{1.123}$$

$$\boldsymbol{m} = \int_{V_0}\frac{\boldsymbol{r}\times\boldsymbol{J}(\boldsymbol{r})dv(\boldsymbol{r})}{2} \tag{1.124}$$

Using the above in Eq. (1.3), Geyi computed the following Q expressions for the three antennas in Fig. 1.41

Dipole antenna
$$Q = \frac{2\omega W_E}{P_a} \approx \frac{6\left[\ln\left(\frac{a}{a_0}\right)-1\right]}{(ka)^3} \tag{1.125}$$

Loop antenna
$$Q = \frac{2\omega W_M}{P_a} \approx \frac{6\ln\left(\frac{a}{a_0}\right)}{\pi\,(ka)^3} \tag{1.126}$$

Inverted-L antenna
$$Q = \frac{2\omega W_E}{P_a} = \frac{6\left\{\left[\ln\left(\frac{h}{a_0}\right)-1\right]+b\left[\ln\left(\frac{2b}{a_0}\right)-1\right]\right\}}{k^3h^2\,(h+b)^2} \tag{1.127}$$

1.3.9.2 Reinvestigation of Small Antenna Gain and *Q* Limitations

Geyi [21] reconsidered the small antenna physical limits. To find the minimum Q for a *Chu antenna*, Geyi directly minimized Eq. (1.76)

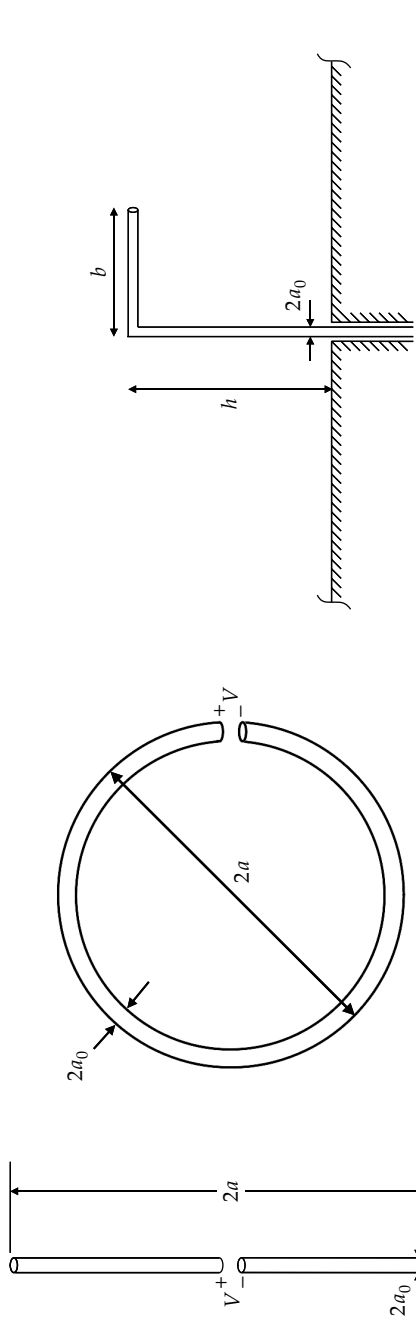

FIGURE 1.41 Small dipole, loop, and inverted *L* antennas.

in terms of spherical vector wavefunctions. His results conclude that the minimum Qs for TM, TE, or TM + TE mode antennas are exactly those derived previously by McLean [3] in Eqs. (1.103) and (1.104), and correspond to only first order mode ($n = 1$) excitations. Furthermore, he notes that the minimum Q TE + TM mode antenna is a *Chu antenna* with equally excited TM_{1m} and TE_{1m} modes.

Geyi believed that Fante's treatment [19] on the maximum G/Q for a directional antenna was incorrect, as Fante ignored a constraint on the mode coefficients necessary to maintain consistency with W_M or W_E in Eq. (1.3). Geyi then examines the maximum G/Q ratio by using the general form of Q given in Eq. (1.76) along with the definition of directivity written in terms of the spherical vector wavefunctions. Through a maximization process of this G/Q ratio, Geyi confirms that for both the omni-directional and directional case, the G/Q ratio is maximized when the TE and TM modes of a *Chu antenna* are equally excited (as already noted by several authors). For $ka \ll 1$, Geyi's formulas indicate that contributions from higher order modes can be ignored, and they are given by

$$\max\left(\frac{G}{Q}\right)\Big|_{\text{directional},ka<<1} \approx \frac{6(ka)^3}{2(ka)^2+1} \tag{1.128a}$$

$$G^{\max}_{\text{directional}}\big|_{ka<<1} \approx 3 \tag{1.128b}$$

$$Q^{\min}_{\text{directional}}\big|_{ka<<1} \approx \frac{1}{ka} + \frac{1}{2(ka)^3} \tag{1.128c}$$

and

$$\max\left(\frac{G}{Q}\right)\Big|_{\text{omni},ka<<1} \approx \frac{3(ka)^3}{2(ka)^2+1} \tag{1.129a}$$

$$G^{\max}_{\text{omni}}\big|_{ka<<1} \approx 1.5 \tag{1.129b}$$

$$Q^{\min}_{\text{omni}}\big|_{ka<<1} \approx \frac{1}{ka} + \frac{1}{2(ka)^3} \tag{1.129c}$$

In these equations, the superscript *max* indicates that gain is maximized under the constraint that antenna Q is at its minimum value. The superscript *min* similarly indicates that Q is minimized under the constraint that G has its maximum value. From Eqs. (1.128) and (1.129), Geyi concludes that in theory a small antenna can have maximum gain and minimum Q simultaneously [21]. We remark that this claim will later be challenged by Thal [29] in Sec. 1.3.12. Figs. 1.42 to 1.44 plot $Q_{\min}$, $G_{\max}$, and $(G/Q)_{\max}$, for the omni-directional and directional antennas as determined through Geyi's optimization procedure. We note that the "min Q" in Fig. 1.42 is that in Eq. (1.104)

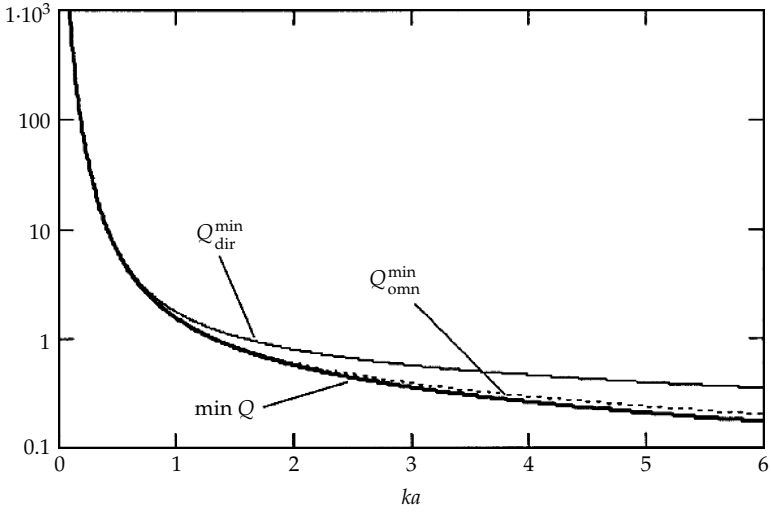

FIGURE 1.42 Minimum possible Q for directional and omni-directional antennas subject to maximum gain constraint; the min Q curve refers to Eq. (1.103) given by McLean [3]. (*After Geyi ©IEEE, 2003* [21].)

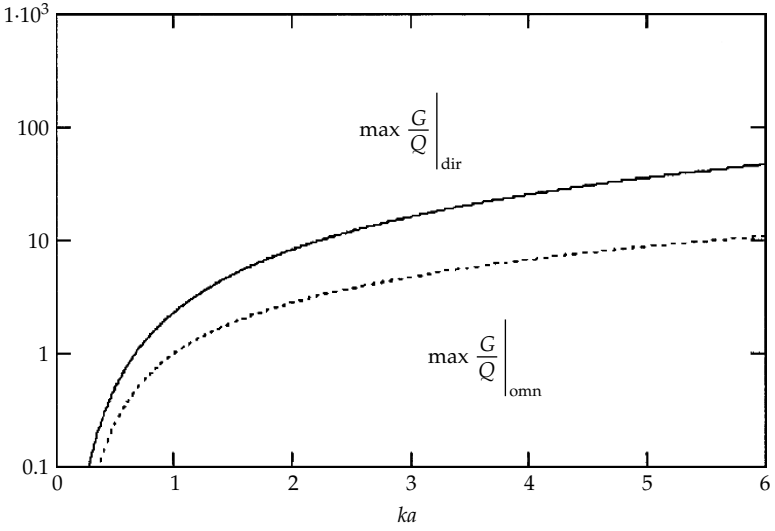

FIGURE 1.43 Maximum G/Q for directional and omni-directional antennas. (*After Geyi ©IEEE, 2003* [21].)

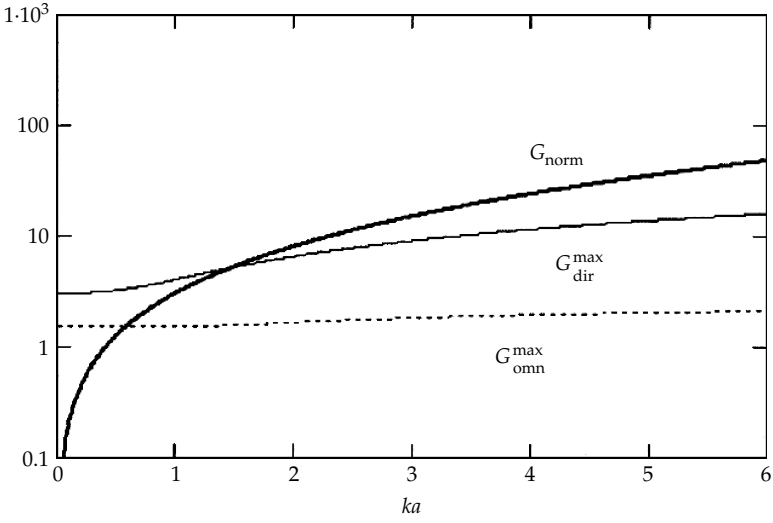

FIGURE 1.44 Maximum possible gain under minimized Q constraint. (*After Geyi ©IEEE, 2003* [21].)

derived by McLean [3]. Figure 1.44 plots the maximum G versus ka (Harrington [4] states that any antenna with a gain higher than the normal gain G_{norm} can be classified as a supergain antenna; see also Chu [11]).

1.3.10 Work of Best (2003–2008)

Yaghjian [10] and Best [10,13,23–26] reconsidered past developments on small antenna theory. A key contribution by Yaghjian and Best [10] is the new expression of Q in terms of input impedance, valid at all frequencies. They also formulated a relationship between the antenna Q and the matched voltage standing wave ratio (VSWR) bandwidth, allowing for antenna bandwidth to be defined in a more flexible manner. Yaghjian and Best first derived the approximate expression for the matched VSWR fractional bandwidth (B_V) of a tuned antenna in terms of its input impedance in resonance and antiresonance ranges. They detail the advantages in using matched VSWR bandwidth over conductance bandwidth, demonstrating that the conductance bandwidth definition breaks down as the impedance approaches antiresonance. Best [23] also gave the limiting relationships between B_V and antenna Q. The validity and accuracy of the derived expressions were confirmed with numerical data for several antennas, including lossy and lossless tuned antennas over a wide range of frequencies.

Best also considered several wire antennas and their Q limits. He showed that a spherical helix antenna [25] has the lowest realized Q to date. Best also explored the folding of small antennas to minimize their Q [14], the relationship between wire antennas and their resonant properties [14,25–26], and antenna volume utilization issues [14].

1.3.10.1 B_V and Antenna Input Impedance

With respect to the transmitting antenna system in Fig. 1.45, we define the following parameters:

- V_P - Shielded power supply and waveguide volume consisting of perfectly conducting walls
- V_A - Antenna volume, including the volume of the tuning reactance bringing the antenna to resonance
- V_0 - Entire volume outside the shielded power supply, including V_A
- S_0 - Antenna input feed port
- X_S - Series tuning reactance bringing the antenna to resonance
- Z_{in} - Input impedance looking into the feed port S_0
- Γ - Input reflection coefficient

Yaghjian and Best [10] begin their study by noting that antennas can be tuned to resonance (zero reactive impedance) by including a series reactance (see Fig. 1.45). Thus, we can represent the input impedance

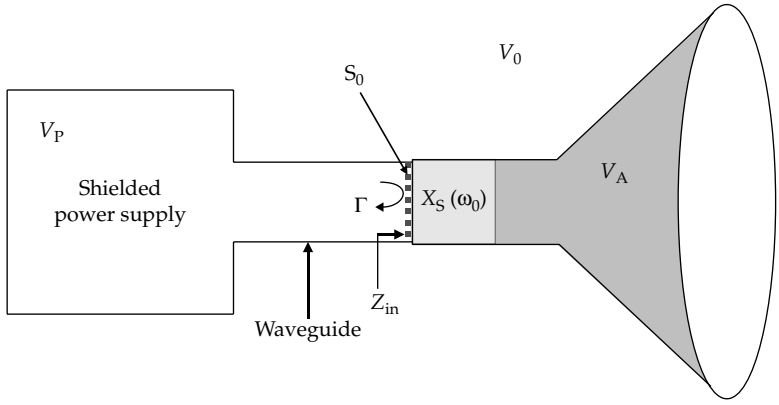

FIGURE 1.45 General transmitting antenna system. (*See Yaghjian and Best* [10].)

at the feed port as

$$Z_{\text{in}}(\omega) = R_A(\omega) + j\,[X_A(\omega) + X_S(\omega)] = R_A(\omega) + j\,X_{\text{in}}(\omega) \quad (1.130)$$

Here, the antenna input impedance is $Z_A(\omega) = R_A(\omega) + j\,X_A(\omega)$, and the series tuning reactance $X_S(\omega)$ is

$$X_S(\omega) = \begin{cases} \omega L_S & \text{for} \quad X_A(\omega_0) < 0 \\ -1/(\omega C_S) & \text{for} \quad X_A(\omega_0) > 0 \end{cases} \quad (1.131)$$

in which L_S and C_S correspond to the associated inductance and capacitance values. For resonance ($\omega = \omega_0$)

$$X_{\text{in}}(\omega_0) = X_A(\omega_0) + X_S(\omega_0) = 0 \quad (1.132)$$

The frequency derivative of the tuned impedance at resonance can then be written as

$$X'_{\text{in}}(\omega_0) = X'_A(\omega_0) + \frac{|X_A(\omega_0)|}{\omega_0} \quad (1.133)$$

This derivative will be used later in computing matched VSWR fractional bandwidth B_V.

The matched VSWR fractional bandwidth (B_V) is defined as the band between frequencies ω_+ and ω_- having a prescribed VSWR, given $Z_C = R_A(\omega_0)$, where Z_C is the feed line characteristic impedance. A parameter associated with the reflection coefficient Γ (see Fig. 1.45) is given by

$$\Gamma_{\max} = \Gamma(\omega_+) = \Gamma(\omega_-) = \left[\frac{VSWR - 1}{VSWR + 1}\right]^2 \quad (1.134)$$

Using Eq. (1.130) and $Z_C = R_A(\omega_0)$, we have

$$|\Gamma(\omega)|^2 = \frac{X^2_{\text{in}}(\omega) + [R_A(\omega) - R_A(\omega_0)]^2}{X^2_{\text{in}}(\omega) + [R_A(\omega) + R_A(\omega_0)]^2} \quad (1.135)$$

Since Eq. (1.135) is valid at any resonance location, Eq. (1.135) is valid for both resonant and antiresonant frequency ranges of the antenna. Following an algebraic manipulation of Eq. (1.135) and a Taylor series expansion of $X^2_{\text{in}}(\omega) + [R_A(\omega) - R_A(\omega_0)]^2$ about ω_0, Yaghjian and Best obtain the equation

$$\left|Z'_{\text{in}}(\omega_0)\right|^2 (\Delta\omega_+)^2 = \left|Z'_{\text{in}}(\omega_0)\right|^2 (\Delta\omega_-)^2 \approx 4\beta R^2_A(\omega_0) \quad (1.136)$$

where

$$\sqrt{\beta} = \frac{|\Gamma_{\max}|^2}{1 - |\Gamma_{\max}|^2} = \frac{VSWR - 1}{2\sqrt{VSWR}} \quad (1.137)$$

and

$$\Delta\omega = \omega_+ - \omega_- \approx \pm\frac{4\beta R_A(\omega_0)}{\omega_0 \left|Z_0'(\omega_0)\right|} \tag{1.138}$$

Using these values in the expression for the fractional bandwidth, we have

$$B_V(\omega_0) = \frac{\omega_+ - \omega_-}{\omega_0} \approx \frac{4\beta R_A(\omega_0)}{\omega_0 \left|Z_0'(\omega_0)\right|} \tag{1.139}$$

Yaghjian and Best remark that Eq. (1.139) remains valid when $B_V(\omega_0) \ll 1$, or equivalently β small enough (stated as $\beta \leq 1$) [10].

Yaghjian and Best stressed that the value of B_V is that it uses impedances as opposed to conductances. The conductance bandwidth at a resonant frequency ω_0 is defined as the difference between the two frequencies about ω_0 such that the power delivered to the antenna is a chosen fraction of the power delivered at resonance. Yaghjian and Best noted that the conductance will only reach its maximum at resonance when $R_A'(\omega)$ is zero [10]. But this is not generally true for small antennas. They also recognized that away from resonance there may be a conductance maximum. Thus the conductance bandwidth cannot be properly defined.

1.3.10.2 Exact *Q* Derived from Maxwell's Equations

Assuming a feed port impedance described by Eq. (1.130), the computation of Q requires $P_A = 1/2|I_{\text{in}}|^2 R_A$ and the stored energy. A convenient form for the stored energy can be found using the frequency derivative of the input reactance $X'_{\text{in}}(\omega_0)$. By coupling Maxwell's equations to the frequency derivative of Maxwell's equations for the antenna system in Fig. 1.45, Yaghjian and Best derive (see [10, App. A])

$$\begin{aligned} |I_{\text{in}}|^2 X'_{\text{in}}(\omega_0) = \lim_{r\to\infty} \Bigg[&\text{Re} \int_{V_0} (\boldsymbol{B}^* \bullet \boldsymbol{H} + \boldsymbol{D}^* \bullet \boldsymbol{E}) dv \\ &- 2\varepsilon_0 r \int_{S_\infty} |\boldsymbol{E}_\infty|^2 \, dS \Bigg] + \omega_0 \text{Re} \int_{V_A} \left(\left(\boldsymbol{B}'\right)^* \bullet \boldsymbol{H} - \boldsymbol{B}^* \bullet \boldsymbol{H}' + \left(\boldsymbol{D}'\right)^* \bullet \boldsymbol{E} \right. \\ &\left. - \boldsymbol{D}^* \bullet \boldsymbol{E}' \right) dv + \frac{2}{Z_0} \text{Im} \int_{S_\infty} \boldsymbol{E}'_\infty \bullet \boldsymbol{E}_\infty^* dS \end{aligned} \tag{1.140}$$

where primes indicate differentiation with respect to frequency, S_∞ is the far field sphere, and $\boldsymbol{E}_\infty$ is defined as

$$\lim_{r\to\infty} \boldsymbol{E}(\boldsymbol{r}) = \boldsymbol{E}_\infty \frac{e^{-jkr}}{r} \tag{1.141}$$

Assuming a linear, isotropic antenna radiating into free space, we can use the constitutive relations

$$\boldsymbol{B} = \mu \boldsymbol{H} \qquad \boldsymbol{D} = \varepsilon \boldsymbol{E} \tag{1.142}$$

and

$$\mu = \mu_r - j\mu_i \qquad \varepsilon = \varepsilon_r - j\varepsilon_i \tag{1.143}$$

Equation (1.140) can then be written as

$$|I_{\text{in}}|^2 \, X'_{\text{in}}(\omega_0) = 4\left[W_E(\omega_0) + W_M(\omega_0) + W_L(\omega_0) + W_R(\omega_0)\right] \tag{1.144}$$

with

$$W_E(\omega_0) = \frac{1}{4} \lim_{r\to\infty} \left[\int_{V_0} (\omega_0 \varepsilon_r)' \, |\boldsymbol{E}|^2 \, dV - \varepsilon_0 r \int_{S_\infty} |\boldsymbol{E}_\infty|^2 \, dS \right] \tag{1.145}$$

$$W_M(\omega_0) = \frac{1}{4} \lim_{r\to\infty} \left[\int_{V_0} (\omega_0 \mu_r)' \, |\boldsymbol{H}|^2 \, dV - \varepsilon_0 r \int_{S_\infty} |\boldsymbol{E}_\infty|^2 \, dS \right] \tag{1.146}$$

$$W_L(\omega_0) = \frac{\omega_0}{2} \text{Im} \int_{V_A} (\mu_i \boldsymbol{H}' \bullet \boldsymbol{H}^* + \varepsilon_i \boldsymbol{E}' \bullet \boldsymbol{E}^*) dv \tag{1.147}$$

$$W_R(\omega_0) = \frac{1}{2Z_0} \text{Im} \int_{S_\infty} \boldsymbol{E}'_\infty \bullet \boldsymbol{E}^*_\infty dS \tag{1.148}$$

$$\lim_{r\to\infty} \boldsymbol{E}(\boldsymbol{r}) = \boldsymbol{E}_\infty \frac{e^{-jkr}}{r} \tag{1.149}$$

where primes indicate differentiation with respect to the resonant frequency. W_E and W_M are as defined before, and the second terms in Eqs. (1.145) and (1.146) are due to the fact that the electric and magnetic energy densities of the radiated fields must be equivalent. This was an essential aspect of McLean's [3] analysis. The dispersive energies $W_L(\omega_0)$ and $W_R(\omega_0)$ are associated with the total dissipated and radiated power in the antenna structure, respectively. However, $W_L(\omega_0)$ and $W_R(\omega_0)$ do not represent the actual energy dissipated or radiated in the antenna structure itself. Furthermore, their sum can be either positive or negative and $X'_0(\omega_0)$ can take different signs. Due to this, Yaghjian and Best state that Eq. (1.144) proves the Foster reactance theorem does not hold for antennas.

Using Eq. (1.144) and the aforementioned P_A expression, we get

$$Q(\omega_0) = \frac{\omega_0 \left[W_M(\omega_0) + W_E(\omega_0)\right]}{P_A} = \frac{\omega_0}{2R_A(\omega_0)} X'_{\text{in}}(\omega_0) - \frac{2\omega_0}{|I_{\text{in}}|^2 R_A(\omega_0)} \left[W_L(\omega_0) + W_R(\omega_0)\right] \tag{1.150}$$

Note that the dispersive energy term $W_L + W_R$ is not present in Geyi's controversial expression (1.118).

1.3.10.3 Representing *Q* as a Function of Antenna Input Impedance

To obtain a useful representation of Eq. (1.150) as a function of the input impedance $Z_{\text{in}}(\omega_0)$ and bandwidth, the dispersion energies associated with dissipation W_L and radiation W_R must be evaluated. Yaghjian and Best choose to model these dispersion energies in terms of a series RLC circuit away from antiresonant frequencies, and as a parallel RLC circuit near the antiresonant frequency ranges. In both cases, the resistance at resonance is assumed to be frequency dependent. Using the models derived in the appendix of [10], they conclude that away from antiresonance regions $|R'_A(\omega_0)| \ll X'_{\text{in}}(\omega_0)$. Thus,

$$Q(\omega_0) \approx \frac{\omega_0}{2R_A(\omega_0)} X'_{\text{in}}(\omega_0) \approx \frac{\omega_0}{2R_A(\omega_0)} \left|Z'_{\text{in}}(\omega_0)\right| \tag{1.151}$$

However, when $X'_{\text{in}}(\omega_0) < 0$, the parallel RLC model approximates the dispersion energies as

$$X'_{\text{in}}(\omega_0) - \frac{4}{|I_{\text{in}}|^2} \left[W_L(\omega_0) + W_R(\omega_0)\right] \approx \sqrt{\left(X'_{\text{in}}(\omega_0)\right)^2 + \left(R'_A(\omega_0)\right)^2} = \sqrt{\left(X'_A(\omega_0) + \frac{|X_A(\omega_0)|}{\omega_0}\right)^2 + \left(R'_A(\omega_0)\right)^2} \tag{1.152}$$

Using Eqs. (1.151) and (1.152), Yagjian and Best [10] note that Q can be accurately represented in both the resonance and antiresonance frequency ranges as

$$Q(\omega_0) \approx \frac{\omega_0}{2R_A(\omega_0)} \left|Z'_{\text{in}}(\omega_0)\right| = \frac{\omega_0}{2R_A(\omega_0)} \sqrt{\left(R'_A(\omega_0)\right)^2 + \left(X'_A(\omega_0) + \frac{|X_A(\omega_0)|}{\omega_0}\right)^2} \tag{1.153}$$

Comparing Eqs. (1.153) and (1.139) gives the relationship between Q and B_V

$$Q(\omega_0) \approx \frac{2\sqrt{\beta}}{B_V(\omega_0)} \tag{1.154}$$

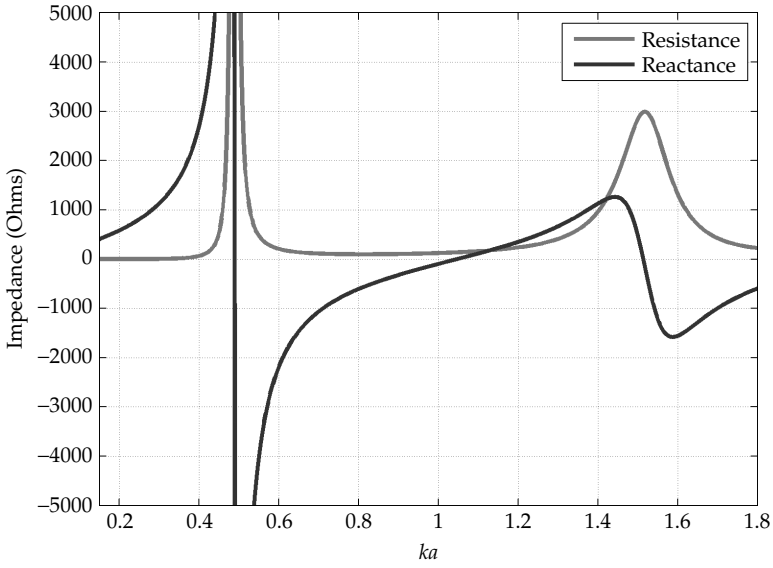

FIGURE 1.46 Impedance for a lossless circular loop of diameter 70 cm and wire diameter 1 mm. (*See Yaghjian and Best* [10].)

Equation (1.154) remains a good approximation when Q is greater than 4 [10]. In [10], method of moments simulations were used to determine the Q for a straight-wire antenna, a lossless or lossy circular loop, a lossless yagi, and a straight-wire embedded in a lossy dispersive dielectric. In each case the approximated Q from Eq. (1.153) remains highly accurate as compared to the rigorous Q values in Eq. (1.150) for all frequencies. However, Geyi's Eq. (1.118) breaks down near the antiresonance regions. Figures 1.46 and 1.47 show the impedance and Q for a lossless circular loop of diameter 70 cm with 1 mm wire diameter. The breakdown of Eq. (1.118) is clearly seen in the bands where $X'_{\text{in}}(\omega_0) < 0$ (antiresonance band).

1.3.10.4 Fundamental Limitations on B_V

Best [23] provided an upper bound for the matched VSWR fractional bandwidth B_V. This is similar to the minimum achievable value for Q. To do so, we begin by the lower bound on Q for an antenna radiating only TE or TM modes including the radiation efficiency η

$$Q_{\text{min}} = \eta \left(\frac{1}{(ka)^3} + \frac{1}{ka} \right) \tag{1.155}$$

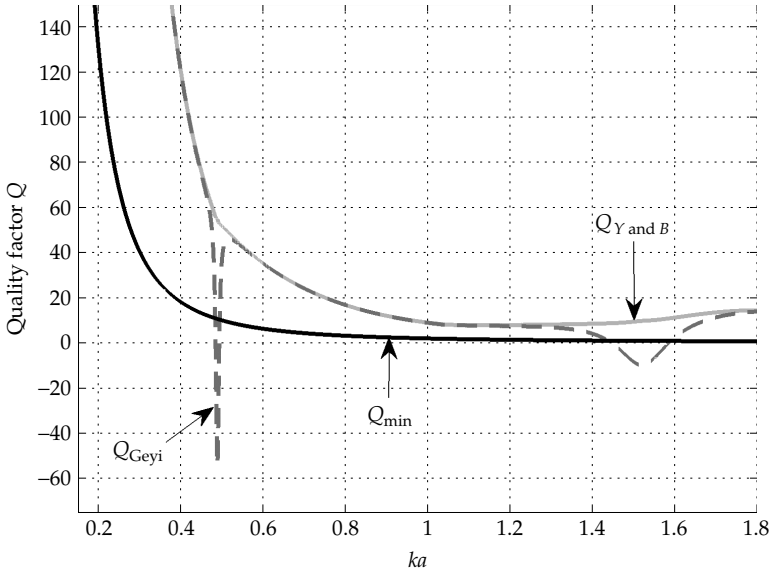

FIGURE 1.47 Q for the lossless circular loop using Geyi's method Q_{Geyi} in Eq. (1.118), Yaghjian and Best's method $Q_{Y \text{ and } B}$ in Eq. (1.153), along with McLean's $Q_{\min}$ in Eq. (1.103). (*See Yaghjian and Best* [10].)

This is a generalization of McLean's expression in Eq. (1.103). Using Eqs. (1.154) and (1.155), and assuming 100% radiation efficiency, the upper bound of B_V is

$$B_{V,\,\text{UB}} = \frac{(ka)^3}{1+(ka)^2}\,\frac{VSWR-1}{\sqrt{VSWR}} \tag{1.156}$$

Best [23] mentioned two methods for maximizing the bandwidth of a small antenna: (1) increasing the number of tuning circuits to approach the Bode-Fano limits (see Chap. 2), and (2) designing for multiple antenna resonances. He first considered maximizing B_V for a case where the small antenna is matched to a load using a number of lossless tuned circuits. From Sec. 1.2.3, it is known that the Q of the antenna itself does not change (as it is an intrinsic quantity). However, the operating bandwidth can change depending on the external Q. Best showed that by applying Eq. (1.156) to the Bode-Fano upper limit relationship in Eq. (1.20), the maximum B_V using an infinite number

of lossless tuning circuits gives

$$B_{V,\,\mathrm{UB,\,Bode}} = \frac{\pi}{Q\ln\left(\dfrac{VSWR+1}{VSWR-1}\right)} = \frac{(ka)^3}{1+(ka)^2}\frac{\pi}{\ln\left(\dfrac{VSWR+1}{VSWR-1}\right)} \tag{1.157}$$

Best then examined the second method (viz. using multiband with closely spaced resonances or wideband antennas) for maximizing B_V, and the validity of Eq. (1.156) and the minimum Q limit in Eq. (1.103) for such antennas. From the numerical computations of a wideband disk-loaded antenna, Best found that Eq. (1.103) was never violated through the entire frequency band and the measured B_V falls below Eq. (1.157) when evaluating at the center frequency.

1.3.10.5 The Spherical Helix Antenna

Apart from the minimum Q and maximum B_V limits discussed earlier, Best [13] also pursued Wheeler's suggestion to better utilize the volume of the antenna's *Chu sphere* to minimize Q. He showed that the resonant properties of small wire antennas are a much heavier function of utilized *Chu sphere* volume rather than conductor arrangement, and that the resonant frequency can be easily decreased by increasing the effective inductance or capacitance seen at the feed point. The latter can be accomplished by techniques such as adding longer wire lengths to fill the *Chu sphere* (increases inductance) or top-loading (increases capacitance). Doing so, the resonance ($X_{\mathrm{in}}(\omega_0) = 0$) shifts, but the resistance curve remains relatively unchanged (as predicted by $R \propto h^2/\lambda^2$ for a monopole height h). This holds as long as the small antenna is far enough away from its initial, first natural antiresonant frequency [14]. Consequently, a great deal of flexibility is available to the designer for choosing the resonant properties of a small antenna.

One monopole design that fills well the *Chu sphere* volume is that of the four-arm spherical helix [24], shown in Fig. 1.48. This is a realization of the coupled TM_{10} – TE_{20} mode equivalent circuit given in Fig. 1.57. This four-arm design by Best [24] in Fig. 1.48 is an extension of the single arm case, where four folded arms are used to increase the resonant resistance to values approaching practical transmission line impedances. Using the usual resistance for wire loop antennas, the resistance of the geometry in Fig. 1.48 can be approximated as

$$R_{N\,\mathrm{arm}} \approx N^2 R_{1\,\mathrm{arm}} \rightarrow R_{4\,\mathrm{arm}} \approx 16 R_{1\,\mathrm{arm}} \tag{1.158}$$

where N refers to the number of arms making up the helix in Fig. 1.48. It is important to note that the four-arm antennas in Fig. 1.48 have efficiencies greater than 97% when copper wires are used [24].

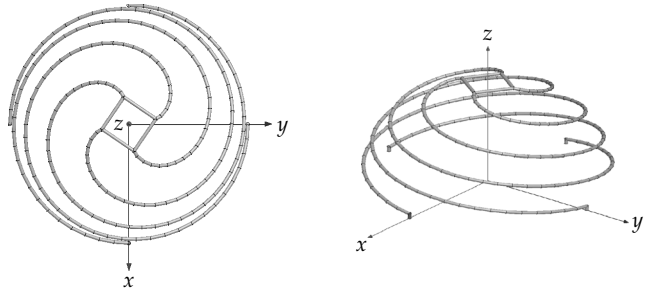

FIGURE 1.48 Four-arm spherical helix. (*See Best* [24].)

Apart from the four-arm spherical helix by Best [24], other shapes can be considered to fill up the *Chu sphere* volume. Examples are shown in Figs. 1.49 and 1.50. These are staircase spherical helices (SSH) and were considered due to their more practical realization. To take advantage of Best's [24] four-arm properties, the design in Fig. 1.49 was constructed using the same design equations given in [24, Eqs. 2–5], with eight vertical jumps of height 2/3 cm between planar layers at the angles

$$\phi_{\text{step}} = 45i\,N(\text{degrees}) \quad \text{for} \quad i = 1, 2, \ldots, 8 \tag{1.159}$$

(ϕ is measured from the x-axis, see Fig. 1.49). As can be understood, the angles and vertical jump heights were chosen so that the SSH would fully utilize the *Chu sphere* using eight layers. Without any dielectric substrate, the SSH was simulated using HFSS [50] for various values of turns N.

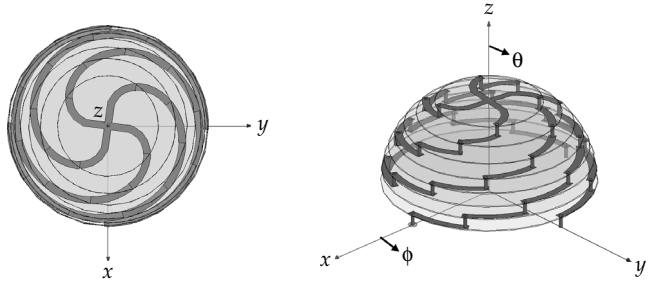

FIGURE 1.49 Top and isometric views of the $N = 0.75$ turn spherical staircase helix (SSH) antenna.

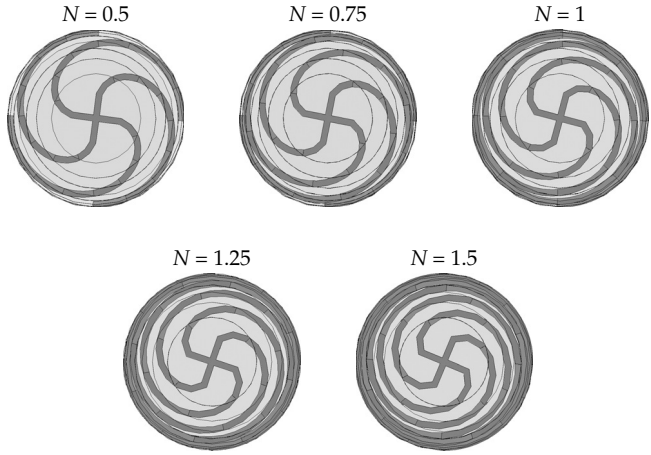

FIGURE 1.50 Top view of SSH antenna with varying turns.

Figures 1.51 and 1.52 give the quality factor and resonant resistance for the SSH for various values of turns N. As depicted, the efficiency for all SSH antennas using copper conductors is greater than 94%.

As seen from Figs. 1.51 and 1.52, the Q of the SSH closely follows that of the two-arm case [24]. However, the resonant resistance follows the four-arm [24] values. The differences between the four-arm Q values in [24] and those of the SSH are likely due to increased stored energy within the SSH *Chu sphere*. We do note, that unlike the four-arm antenna by Best [24], the SSH antenna does not utilize the entire *Chu sphere* surface (see Fig. 1.49). Concurrently, the SSH radiates much better than the two-arm and is closer to the four-arm radiation level.

It is important to note that since the SSH radiates a TM_{10} mode, the stored energy is primarily electric and the addition of dielectric inside the *Chu sphere* would increase the stored electric energy and the Q value. Therefore for the SSH antenna, it is important that the dielectric constant remains low, and the substrate is thin enough for improved radiation. This was also observed in [28] where Thal notes that filling the *Chu sphere* with a dielectric of permittivity ε_r corresponds to multiplying the internal region capacitances by ε_r (see Sec. 1.3.12).

1.3.11 Work of Kwon and Pozar (2005–2009)

Recent work by Kwon [4,5] and Pozar [6] aimed to consolidate the published results about small antenna gain and Q. As described in McLean [37] and Chu [11], a circularly polarized *Chu antenna* radiating equally excited TE_{10} and TM_{10} modes has a Q which is slightly greater than half

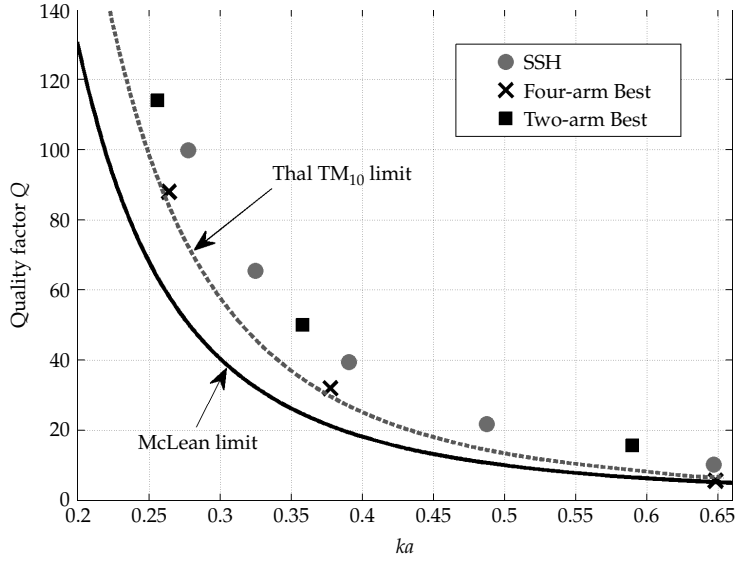

FIGURE 1.51 Quality factor for the four-arm SSH [51], four-arm [24], and two-arm [24] small antennas with the McLean limit in Eq. (1.103) and Thal TM_{10} limit in Eq. (1.170).

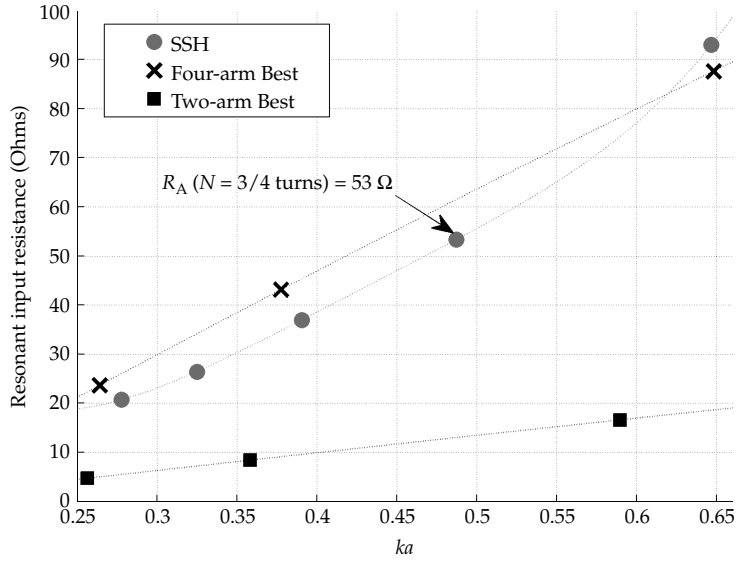

FIGURE 1.52 Resonant resistance for the four-arm SSH [51], four-arm [24], and two-arm [24] small antennas.

that of the TE_{10} or TM_{10} only case, and is given as $\hat{Q}_{\min}$ in Eq. (1.104). However, this derivation does not specify if circular polarization is a necessary condition to obtain $\hat{Q}_{\min}$ given in Eq. (1.104). Harrington [4] found that a unidirectional linearly polarized *Chu antenna* can achieve a gain of 3 and have $\hat{Q}_{\min}$ in Eq. (1.104). Also, Hansen [2] does not mention the excitation levels between the TE and TM modes for achieving Eq. (1.104). However, Fante [19] showed that $\hat{Q}_{\min}$ is possible for a *Chu antenna* with equally excited TE_{1m} and TM_{1m} modes, but did not mention the associated gain of such an antenna. On the other hand, although Geyi [21] categorized the limits of omni-directional and directional antennas, he did not specify the excitation.

To clarify the issue of excitation and polarization for the *Chu antenna*, Kwon [4,5] explored various crossed electric and magnetic dipole excitations. Later, Pozar [6] presented a summary of the gain and minimum Q values for small antennas along with the corresponding excitations. In the following sections, we provide a summary of the work by Kwon and Pozar.

1.3.11.1 Gain and *Q* for a Crossed-Dipole Chu Antenna

Kwon explored the gain and Q for a *Chu antenna* generating fields corresponding to those radiated by a pair of ideal, crossed electric and magnetic dipoles [4]. These dipoles are depicted in Fig. 1.53, with their electric and magnetic dipole moments given by

$$\boldsymbol{p_e} = \hat{\boldsymbol{z}}\, p_e \tag{1.160}$$

$$\boldsymbol{p_m} = \hat{\boldsymbol{z}}\, p_m \cos\theta_m + \hat{\boldsymbol{y}}\, p_m \sin\theta_m \tag{1.161}$$

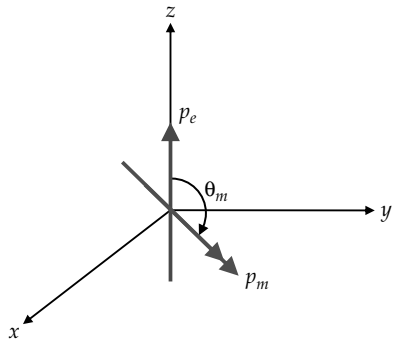

FIGURE 1.53 Set of crossed electric and magnetic dipoles about the origin, radiating the same fields as a CDCA outside the *Chu sphere*. (*After Kwon* [4].)

We will refer to this type of antenna as a *crossed-dipole Chu antenna (CDCA)*. To compute the TE_{10} and TM_{10} mode excitations corresponding to a CDCA, Kwon equated the fields due to the pair in Fig. 1.53 to the spherical mode representations. Invoking the usual mode orthogonalities of spherical wavefunctions representing the radiated field, Kwon found that the only nonzero mode coefficients excited by the crossed dipole arrangement of Fig. 1.53 are those of the TM_{10}, TE_{10}, and TE_{11} spherical modes. With the nonzero spherical mode coefficients known, the following relation between Q and polarization was obtained using Eq. (1.76)

$$Q_{\text{CDCA}} = \frac{1}{ka} + \frac{1}{(ka)^3} \cdot \frac{1}{1 + \dfrac{|\boldsymbol{p_m}|^2}{Z_0^2 |\boldsymbol{p_e}|^2}} \tag{1.162}$$

assuming $Z_0|\boldsymbol{p_e}| \geq |\boldsymbol{p_m}|$. Note the similarity to $Q_{\min}$ given in Eq. (1.103) with the one in Eq. (1.162), though Q_{CDCA} contains an extra multiplying factor. Kwon's results [4] find that:

1. Q is independent of polarization: – Both $\boldsymbol{p_e}$ and $\boldsymbol{p_m}$ are present in Q_{CDCA} as magnitude squared terms, so phase does not affect Q. That is linear, circular, and elliptical polarizations can all achieve the same Q. Also, omni-directional and directional antennas can have the same Q.
2. Equal electric and magnetic source strengths give the minimum possible Q for *Chu antenna* – That is, $Z_0|\boldsymbol{p_e}| = |\boldsymbol{p_m}|$ reduces $Q_{\text{CDCA}} = \hat{Q}_{\min}$ in Eq. (1.104).

Of course, duality also implies that interchanging magnetic and electric polarizability strengths does not impact these conclusions.

Of interest is the maximum possible gain for the arrangement in Fig. 1.53. To proceed, without loss of generality, we may choose to relate p_e and p_m from Eqs. (1.160) and (1.161) through the phase and amplitude parameters α and β, respectively. That is, we set

$$p_m = (\alpha e^{j\beta}) Z_0 p_e \tag{1.163}$$

With this choice of p_e and p_m, Kwon [4, Eq. 27] maximized the gain expression for the CDCA antenna to obtain

$$G_{\max,\text{CDCA}} = \frac{3}{2}\left(1 + \frac{2\alpha\,|\sin\theta_m \cos\beta|}{1+\alpha^2}\right) \tag{1.164}$$

with a front-to-back ratio

$$FBR = \frac{G_{\max}}{3 - G_{\max}} \tag{1.165}$$

From Eq. (1.164), it is seen that the maximum possible gain for the CDCA is 3, with $\theta_m = \pi/2$, $\beta = \pm\pi$, and $\alpha = 1$, corresponding to linear polarization. That is, the maximum (directional) gain is the sum of the gains from the ideal electric and magnetic dipoles. We also note that these excitation dipoles must be normal to each other. Further, the gain is maximum in the direction normal to the plane containing the sources.

1.3.11.2 Gain and *Q* for Dual-Set Chu Antenna (DSCA)

Kwon extended the analysis in [4] by examining the properties of a *Chu antenna* whose radiating fields correspond to more general sources. Specifically, he chose the sources $(\boldsymbol{J}_a, \boldsymbol{M}_a)$ to represent the radiating TM modes and the sources $(\boldsymbol{J}_b, \boldsymbol{M}_b)$ to radiate the spherical TE modes [5]. As usual, $\boldsymbol{J}_{a,b}$ represents an electric dipole source and $\boldsymbol{M}_{a,b}$ refers to a magnetic dipole source. To have equal power radiated from the electric and magnetic sources, Kwon [5] followed the relations

$$\boldsymbol{J}_b = -\frac{1}{Z_0} e^{j\beta} \boldsymbol{M}_a \tag{1.166}$$

$$\boldsymbol{M}_b = Z_0 e^{j\beta} \boldsymbol{J}_a \tag{1.167}$$

That is, $(\boldsymbol{J}_a, \boldsymbol{M}_a)$ are the dual of $(\boldsymbol{J}_b, \boldsymbol{M}_b)$; each set radiating equal power. We will refer to this type of antenna as the *dual-set Chu antenna (DSCA)*. We do note the DSCA is simply a linear combination of two CDCA antennas. Thus, the DSCA has the same Q as the CDCA antenna. In essence the DSCA provides more degrees of freedom in choosing the excitation sources, but the radiated mode choices are still the same. Consequently, Kwon finds the extra degrees of freedom allow for all types of polarization to be realized, simultaneously with a gain of 3 and minimum Q [5].

Table 1.5 summarizes the results derived by Kwon [4,5] for the CDCA and DSCA antennas, where $Q_{\min}$ is given in Eq. (1.103) and $\hat{Q}_{\min}$ is given in Eq. (1.104). As depicted, for all possible combinations of sources, $\hat{Q}_{\min}$ is achieved only when equally excited first order TM and TE modes are present. However, maximum gain is attained only when $\boldsymbol{J}$ and $\boldsymbol{M}$ are present. For linear polarization, maximum gain is attained when $\boldsymbol{J}$ and $\boldsymbol{M}$ are in phase but normal to each other. In the case of CP radiation, the sources must be individually CP. That is, $\boldsymbol{J} = \hat{\boldsymbol{z}} J_z$ and $\boldsymbol{M} = j\hat{\boldsymbol{y}} M_y$ will not give maximum gain. Finally, we remark that the results in Table 1.5 and the derivations by Kwon [4,5] have recently been contested by Thal as unrealizable [29]. This will be examined in Sec. 1.3.12.

Equivalent Hertzian Dipole Sources for CDCA/DSCA	Polarization/Pattern	Gain	Q
$\hat{z}J_z$(or $\hat{x}J_x$ or $\hat{y}J_y$)	Linear/Omni	1.5	$Q_{\min}$
$\hat{z}M_z$(or $\hat{x}M_x$ or $\hat{y}M_y$)	Linear/Omni	1.5	$Q_{\min}$
$\hat{z}J_z \pm \hat{z}M_z$	Linear/Omni	1.5	$\hat{Q}_{\min}$
$\hat{z}J_z \pm \hat{y}M_y$	Linear/Directional	3	$\hat{Q}_{\min}$
$\hat{z}J_z \pm j\hat{z}M_z$	Circular/Omni	1.5	$\hat{Q}_{\min}$
$\hat{z}J_z \pm j\hat{y}M_y$	Linear/Bidirectional	1.5	$\hat{Q}_{\min}$
$\hat{x}J_x \pm j\hat{y}J_y$	Circular/Bidirectional	1.5	$Q_{\min}$
$\hat{x}M_x \pm j\hat{y}M_y$	Circular/Bidirectional	1.5	$Q_{\min}$
$\hat{x}J_x \pm j\hat{y}J_y$ and $\hat{x}M_x \pm j\hat{y}M_y$	Circular/Directional	3	$\hat{Q}_{\min}$

TABLE 1.5 Summary of CDCA and DSCA *Chu Antenna* Performance. (*See Pozar* [6])

1.3.12 Work of Thal (2006–2009)

Similar to Foltz and McLean in Sec. 1.3.7, Thal set out to find a stricter Q limit to more accurately represent real antennas. Thal [28] considered the antenna geometry in Fig. 1.54, that is, an antenna with its current distribution on the *Chu sphere* surface. Thal's analysis of the antenna in Fig. 1.54 closely matches the approach taken by Chu [11]. That is, he represented each propagating mode radiated outside the Chu surface with an equivalent mode circuit. However, Thal also included in his mode representation an equivalent circuit for the mode extending inside the *Chu sphere* to account for the mode energy stored interior

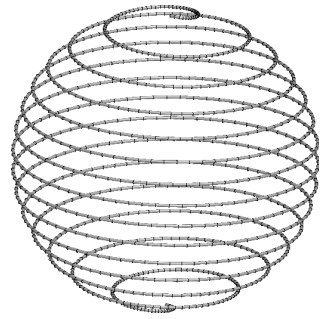

FIGURE 1.54 Possible antenna geometry considered by Thal [28] where the wiring lies on the *Chu sphere* surface.

to the sphere. We remark, that contrary to the *Chu antenna*, in Thal's analysis Q between the TM and TE modes differ significantly.

A recent publication [29] by Thal takes another approach to the problem of quantifying the energy internal to the *Chu sphere*. In [29], Thal examines the effect of TM and TE mode phases on the small antenna gain and Q limits by analyzing the time-varying component of the power in Chu's mode circuits. His results conclude, contrary to Geyi [21], Kwon [4,5], and Pozar [6], that a small antenna cannot simultaneously achieve a gain of 3 and a Q given in Eq. (1.104).

1.3.12.1 Spherical Mode Circuits at the Chu Sphere Surface

The TM and TE spherical mode wave impedances can be formulated from the orthogonal field components of Eqs. (1.51*a*) to (1.51*c*) and their duals. Table 1.6 gives the TM and TE normalized wave impedances looking outside and inside the *Chu sphere* surface [36]. As would be expected, these normalized wave impedances are independent of the azimuthal index m. We also note that for m greater than n, the associated Legendre polynomials in Eqs. (1.51*a*) to (1.51*c*) are zero. As a result, no modes for $m > n$ exist.

To construct the equivalent circuits for an antenna with its current over the *Chu sphere* surface (see Fig. 1.54), we note the recurrence relation for spherical Bessel functions $b_n(ka)$

$$\left[\frac{ka\,b_{n+1}(ka)}{j^{n+2}}\right] = \left[\frac{ka\,b_{n-1}(ka)}{j^{n}}\right] + \frac{2n+1}{jka}\left[\frac{ka\,b_n(ka)}{j^{n+1}}\right] \tag{1.168}$$

$$j\left[\frac{ka\,b_n(ka)}{j^{n+1}}\right]' = \left[\frac{ka\,b_{n-1}(ka)}{j^{n}}\right] + \frac{n}{jka}\left[\frac{ka\,b_n(ka)}{j^{n+1}}\right] \tag{1.169}$$

Using these, Thal then constructed equivalent mode networks to represent the impedances in Table 1.6 using Chu's procedure in Sec. 1.3.2 [52]. That is, he related the Bessel functions to analogous voltage and current quantities. In essence, these equivalent circuit networks are "spherical Bessel function generators" for each index n.

	$\mathbf{TM_{nm}}$	$\mathbf{TE_{nm}}$
Normalized wave impedance looking out of the sphere	$\dfrac{j\left[h_n^{(2)}(ka)\right]'}{\left[h_n^{(2)}(ka)\right]}$	$\dfrac{-j\left[h_n^{(2)}(ka)\right]}{\left[h_n^{(2)}(ka)\right]'}$
Normalized wave impedance looking into the sphere	$\dfrac{-j\,[j_n(ka)]'}{[j_n(ka)]}$	$\dfrac{j\,[j_n(ka)]}{[j_n(ka)]'}$

TABLE 1.6 Normalized Wave Impedances at Sphere $r = a$ for Spherical Mode n, with Primes Indicating Differentiation With Respect to ka

Figure 1.55 shows the two equivalent spherical mode networks for all TE_{nm} and TM_{nm} modes, with each terminal corresponding a certain TE_{nm} or TM_{nm} mode. As was in Chu [12], a is the radius of the *Chu sphere* and c is the speed of light. At a terminal, the impedance looking to the left corresponds to the wave impedance looking out of the sphere, and the impedance looking to the right corresponds to the wave impedance looking into the sphere. This is indicated in Fig. 1.55 by the exterior and interior region arrows. We note that c may be different in the interior and exterior regions if the sphere is filled with a material other than free space. We assume c is that of free space unless specified otherwise.

Given the orthogonality of the spherical modes, each antenna mode radiated by the surface current can be represented by an independent circuit of Fig. 1.55. The Q for a given mode is, of course, determined by the standard definition in Eq. (1.3). Specifically, W_E is found by summing the energies stored in all capacitors, and likewise W_M is found by summing the energies stored in all inductors. The radiated power is extracted from the termination resistance. We lastly observe that for odd n, the exterior region circuits are equivalent to Chu's circuits in Figs. 1.19 and 1.22 (Chu only found circuits for odd n). As an example, the mode circuit for a TM_{10} mode is depicted in Fig. 1.56, where the *Chu sphere* surface current exciting the TM_{10} mode is represented by a current source I_{TM10}.

1.3.12.2 Q Value for the TM_{1m} and TE_{1m} Modes

Thal [28] tabulated the Q values obtained using the mode circuits in Fig. 1.55 for the TM_{1m} and TE_{1m} modes. His results are shown in Table 1.7 where Q_{min} is the minimum possible Q for TM or TE operation given in Eq. (1.103) (McLean [3]). $Q_{TM1m,Thal}$ and $Q_{TE1m,Thal}$ are the Q values for TM_{1m} and TE_{1m} mode excitation in Fig. 1.55, respectively.

From Table 1.7, we can conclude that for $ka < 0.5$

$$Q_{TM1m,Thal} \approx 1.5 Q_{min} \tag{1.170}$$

$$Q_{TE1m,Thal} \approx 3 Q_{min} \tag{1.171}$$

It is observed that for vanishing ka, the stored energy is in the TM_{1m} mode and is dominated by the capacitors next to the current source excitation. That is, the inductors store very little magnetic energy. We can also conclude that the energy stored in the internal capacitor is half that of the external one. Therefore, the Q computed by Thal [28] is 1.5 times the McLean limit in Eq. (1.103).

Similarly, if we place a current source at the TE_{1m} port as ka decreases, the stored energy will then be dominated by the shunt inductors next to the current source since the nearby capacitors store very little electric energy. Thus, we can ignore the capacitors and conclude

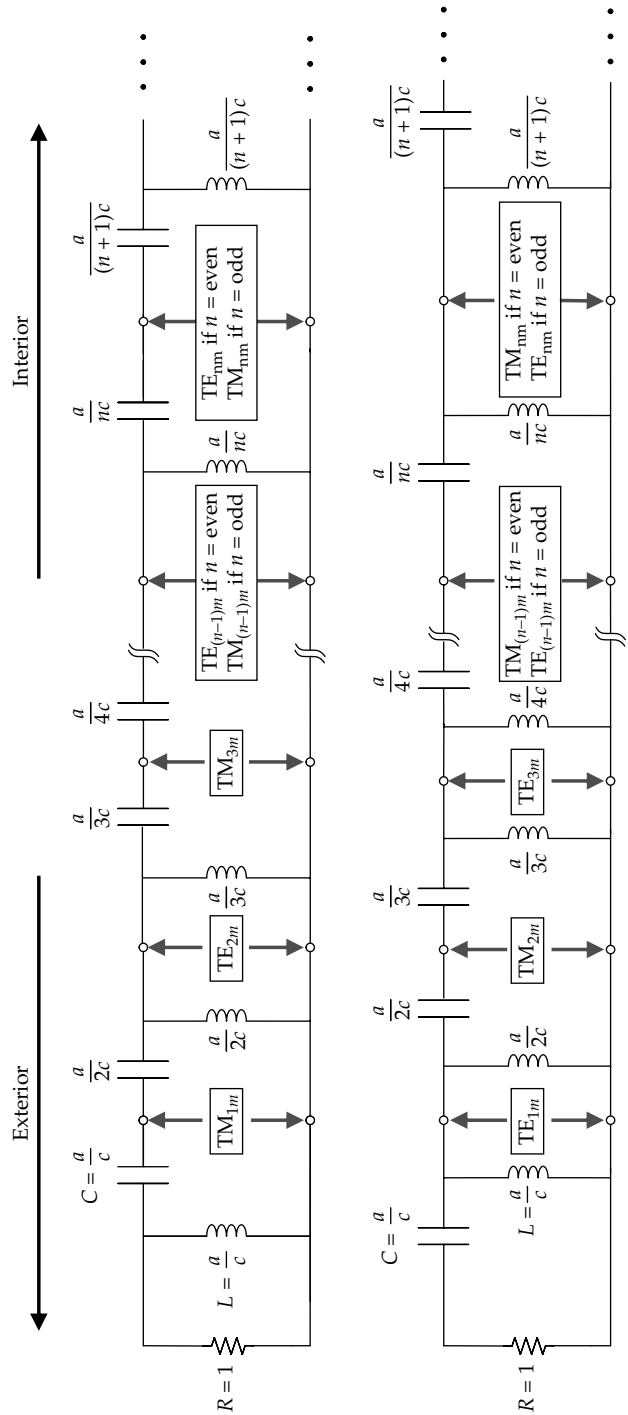

FIGURE 1.55 Spherical mode circuits at the *Chu sphere* surface. (*See Thal* [28].)

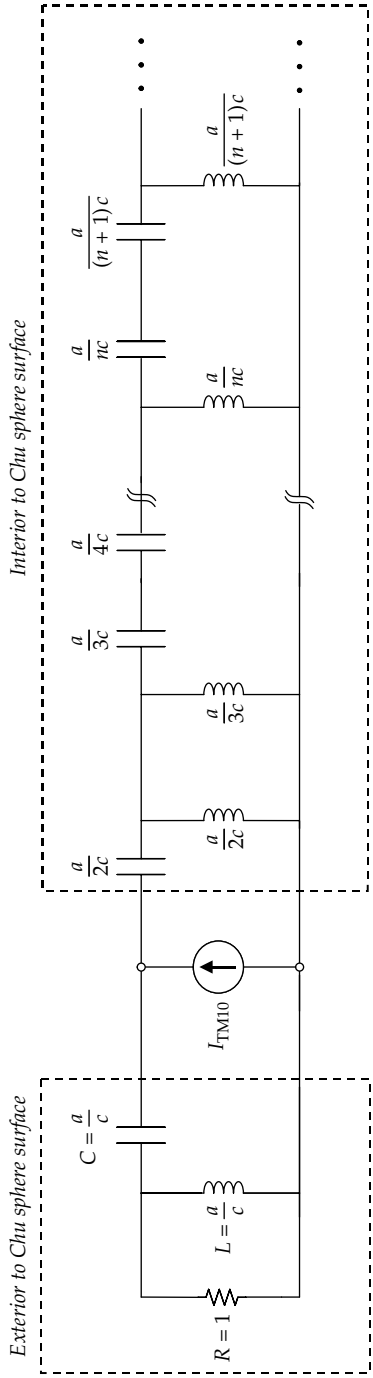

FIGURE 1.56 Spherical mode circuit for TM_{10} mode excitation at *Chu sphere* surface.

ka	$Q_{\min}$ (1.103)	$Q_{\mathrm{TM}1m,\mathrm{Thal}}$	$Q_{\mathrm{TE}1m,\mathrm{Thal}}$	$Q_{\mathrm{TM}1m,\mathrm{Thal}}/Q_{\min}$	$Q_{\mathrm{TE}1m,\mathrm{Thal}}/Q_{\min}$
0.050	8020.0	12012.1	24062.0	1.50	3.00
0.100	1010.0	1506.0	3029.9	1.49	3.00
0.200	130.0	190.6	390.0	1.47	3.00
0.300	40.4	57.7	121.1	1.43	3.00
0.400	18.1	25.1	54.4	1.39	3.00
0.500	10.0	13.4	30.0	1.34	3.00
0.600	6.3	8.2	18.9	1.30	3.00

TABLE 1.7 Comparison of McLean's $Q_{\min}$ (1.103) and the ones derived by Thal for the TE_{1m} and TM_{1m} modes in Fig. 1.55. (*See Thal* [28])

that the energy stored by the internal circuit inductor is twice that of the external inductor. Thus, the Q value using Thal's analysis is predictably three times that of McLean's limit in Eq. (1.103). We also note that there is very little variation in $Q_{\mathrm{TE}1m,\mathrm{Thal}}/Q_{\min}$ as ka increases, indicating that the ratio of magnetic stored energy to radiated power remains fairly constant in the small antenna limit. This is in contrast to the TM_{1m} case, where we see a decrease in the $Q_{\mathrm{TM}1m,\mathrm{Thal}}/Q_{\min}$ as ka increases, indicating electric stored energy to radiated power decreases.

Recently, Hansen and Collin [53] verified the accuracy of Thal's mode circuits for an antenna with its current distribution on the *Chu sphere* surface (see Fig. 1.54). After using Collin's results in [18] (see Sec. 1.3.4) to account for the exterior region energy, the internal stored energy can be found by representing the fields as spherical Bessel functions of the first kind and enforcing the tangential electric field continuity at the *Chu sphere* surface. After a curve-fitting procedure, Hansen and Collin state that Eq. (1.170) can be more accurately represented for $ka < 0.5$ as

$$Q_{\mathrm{TM}1m,\mathrm{Thal}} \approx \frac{1}{\sqrt{2}ka} + \frac{3}{2(ka)^3} \tag{1.172}$$

1.3.12.3 Self-Resonant Mode Configurations

The Q values in Table 1.7 are found using the standard Q formula of Eq. (1.3) with the assumption that the antenna is tuned to resonance using a lossless reactive element. However, the circuits of Fig. 1.55 can be used to determine the combinations of modes necessary for a self-resonant antenna described by Fig. 1.54.

TM_{10} — TE_{20} Self-Resonant Antenna Thal [28] gives two examples of self-resonant small antennas of the type described in Fig. 1.54. For a TM_{10} mode, an inductive reactance is needed to tune the antenna to resonance. Figure 1.57 shows one possible tuning solution, where the

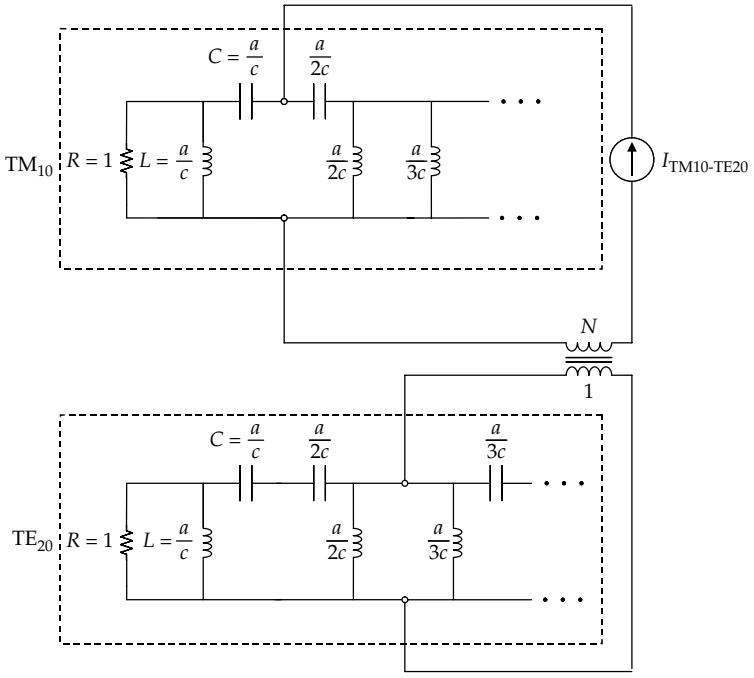

FIGURE 1.57 TM_{10} – TE_{20} mode circuit for a small antenna. (*See Thal* [28].)

surface current distribution radiates both a TM_{10} and a TE_{20} mode. The TM_{10} mode remains the primary mode of radiation, with the TE_{20} mode excited through a transformer of ratio N:1 (N is adjusted to cancel the capacitive reactance due to the TM_{10} mode). The same numerical procedure noted in [52, (Fig. 4*c*)] is used to determine the Q values using the circuits in Fig. 1.57. The results of Table 1.8 show

ka	Q_{min} (1.103)	$Q_{TM10,Thal}$	$Q_{TM10-TE20,Thal}$	TE_{20}/TM_{10} (dB)
0.050	8020.0	12012.1	12013.1	−40.80
0.100	1010.0	1506.0	1506.5	−34.80
0.200	130.0	190.6	190.8	−28.85
0.400	18.1	25.1	25.4	−23.08
0.500	10.0	13.4	13.6	−21.31
0.600	6.3	8.2	8.4	−19.90

TABLE 1.8 Comparison of McLean's Q_{min} (1.103) with the Q Derived by Thal [28] Using the TM_{10} – TE_{20} Self-Resonant Circuit in Fig. 1.57. (*See Thal* [28])

$Q_{\text{TM10, Thal}}$ (identical to that of Table 1.7) and $Q_{\text{TM10–TE20, Thal}}$ when the antenna in Fig. 1.57 is tuned to resonance by the appropriate value of N. $\text{TE}_{20}/\text{TM}_{10}$ is the ratio of the power radiated by the TE_{20} mode to the power radiated by the TM_{10} mode.

From Table 1.8 it is evident that

$$Q_{\text{TM10–TE20, Thal}} \approx Q_{\text{TM10, Thal}} \tag{1.173}$$

However, $Q_{\text{TM10–TE20, Thal}}$ remains slightly larger due to that the stored energy of the TE_{20} mode is not completely inductive. Also, the $\text{TE}_{20}/\text{TM}_{10}$ power ratio verifies that the familiar dipole pattern for small antennas remains undisturbed using this tuning technique (as the TE_{20} mode is evanescent). Of course, the TM_{10} and TE_{20} mode field patterns are given by:

$$\text{TM}_{10} \sim \sin\theta,\ E_\theta \text{ polarization (vertical)}$$

$$\text{TE}_{20} \sim \sin 2\theta,\ E_\phi \text{ polarization (horizontal)}$$

That is, the TE_{20} mode can be used to tune small antennas placed over ground planes. This is because the E_ϕ component of the electric field vanishes to zero for $\theta = 90^\circ$, automatically satisfying the PEC boundary conditions. One implementation of the $\text{TM}_{10} - \text{TE}_{20}$ in Fig. 1.57 is to use the four-arm spherical helix given by Best [24] and shown in Fig. 1.48. This antenna exhibits Q values that closely match the numerically computed $Q_{\text{TM10–TE20, Thal}}$. Additionally, the $\text{TE}_{20}/\text{TM}_{10}$ power ratio of the four-arm antenna in [24] is consistent with the values obtained in Table 1.8, as evidenced by the vertical and horizontal radiation patterns given in Fig. 1.58.

$\text{TM}_{1m} - \text{TE}_{1m}$ Self-Resonant Antenna It was shown above that if a small antenna radiates a TM_{10} mode along with a TE_{10} mode, the resulting Q can be smaller than the value obtained if the antenna radiated only the TM_{10} or TE_{10} mode. Furthermore, for a *Chu antenna*, when the radiated powers by TM_{10} and TE_{10} modes are same, the Chu limit becomes slightly greater than half the limit for the single TM_{10} mode (or TE_{10} mode) [3], as given in Eq. (1.104).

Figure 1.59 depicts the equivalent circuit for an antenna of radius a radiating both TM_{1m} and TE_{1m} modes using Thal's approach. The TM_{1m} mode remains the primary mode of radiation. As before (see Fig. 1.57), the current source representing the magnetic field discontinuity at the surface of the *Chu sphere* is coupled to the TE_{1m} mode through a transformer of ratio N:1. This ratio can be adjusted to cancel the capacitive reactance of the TM_{1m} circuit.

Using the same numerical procedure as in [52, Fig. 4c], Thal computed the Q values corresponding to the circuit in Fig. 1.59. The results of this procedure are given in Table 1.9 where $Q_{\text{TM1}m\text{–TE1}m\text{, Thal}}$ is the

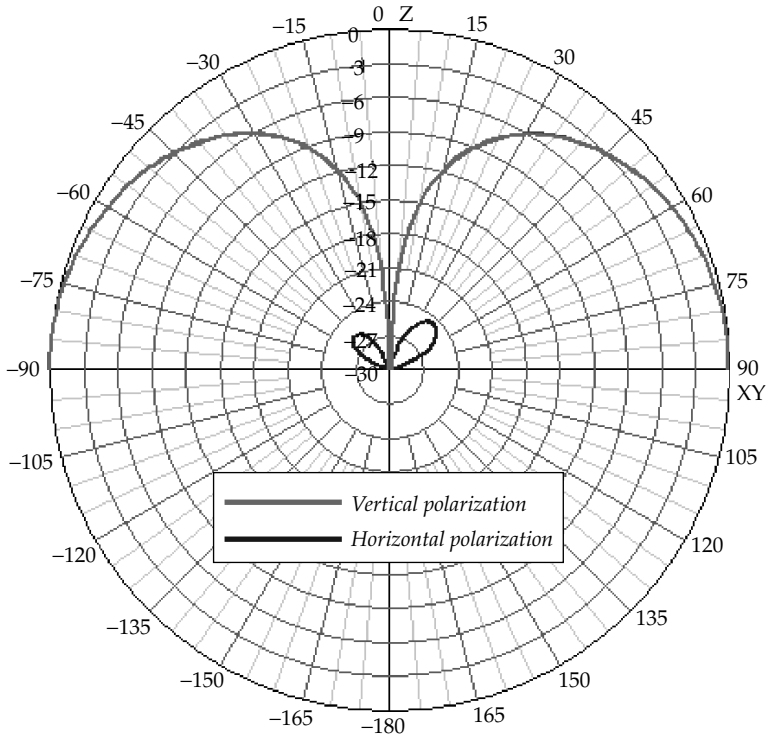

FIGURE 1.58 Vertical and horizontal patterns for the $N = 1$ turn four-arm Best antenna at resonance. (*See Best* [24].)

Q for the TM_{1m}–TE_{1m} mode circuit in Fig. 1.59 tuned to resonance by the appropriate value of N. The last column in Table 1.9 is the ratio of the power radiated by the TE_{1m} mode to the power radiated by the TM_{1m} mode.

Table 1.9 shows that the minimum Q for the TM_{1m}–TE_{1m} self-resonant antenna is approximately twice the McLean limit $\hat{Q}_{\min}$ given in Eq. (1.104)

$$Q_{\mathrm{TM}1m-\mathrm{TE}1m,\mathrm{Thal}} \approx 2\hat{Q}_{\min} \approx Q_{\min} \tag{1.174}$$

Since it was shown in Table 1.7 that $Q_{\mathrm{TM}1m,\mathrm{Thal}} < Q_{\mathrm{TE}1m,\mathrm{Thal}}$, we can conclude that $Q_{\mathrm{TM}1m-\mathrm{TE}1m,\mathrm{Thal}}$ represents the minimum possible Q for a small air-filled antenna of the type in Fig. 1.54. We should note the $\hat{Q}_{\min}$ was derived assuming a self-resonant *Chu antenna* with equally radiating TM_{1m} and TE_{1m} modes. As already noted, the results of Table 1.9 can be easily predicted by considering only the energy stored

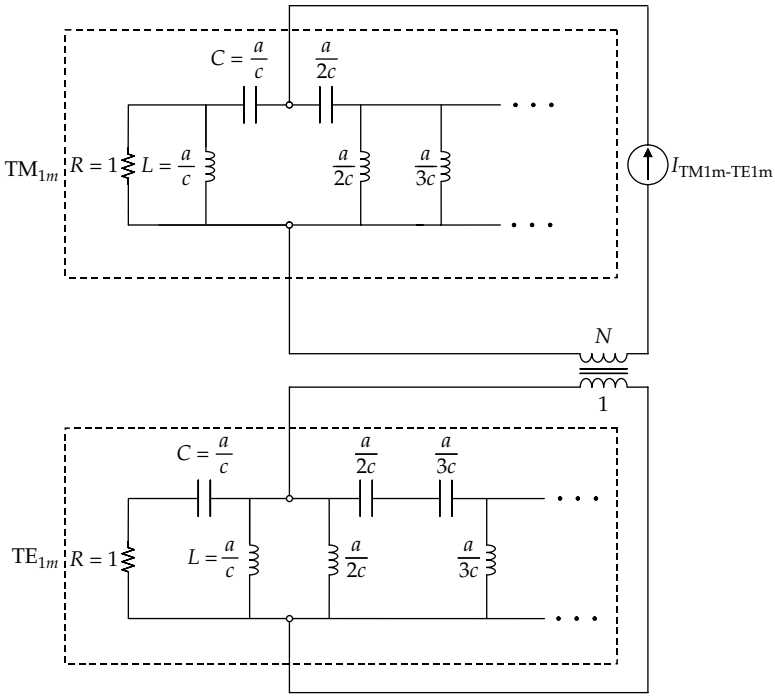

FIGURE 1.59 TM_{1m} – TE_{1m} mode circuit for a small antenna using Thal's procedure. (*See Thal* [28].)

ka	$Q_{\min}$ (1.103)	$\hat{Q}_{\min}$ (1.104)	$Q_{TM1m-TE1m,Thal}$	TE_{1m}/TM_{1m}
0.050	8020.0	4020.0	8022.5	−3.02
0.100	1010.0	510.0	1011.0	−3.05
0.200	130.0	67.5	130.5	−3.16
0.300	40.4	21.9	40.7	−3.34
0.400	18.1	10.3	18.4	−3.58
0.500	10.0	6.0	10.2	−3.85
0.600	6.3	4.0	6.5	−4.13

TABLE 1.9 Comparison of the $Q_{\min}$ (1.103) and $\hat{Q}_{\min}$ (1.104) computed by McLean [3] as compared to the Q obtained by Thal [28] for the circuit in Fig. 1.59. (*See Thal* [28].)

Radiating Mode	$Q/Q_{\min}$	Axial Ratio
TM_{10}	1.5	-
TE_{10}	3	-
$TM_{10} - TE_{10}$	1	3 dB (elliptical polarization)
$TM_{10} - TE_{20}$	1.5	≈40 dB

TABLE 1.10 Q Values Given by Thal for $ka \ll 1$ [$Q_{\min}$ is that Given by McLean in Eq. (1.103)]

by elements adjacent to the source, and by assuming all other capacitors open and all other inductors shorted. Another comment from Table 1.9 is that the power ratio TE_{1m}/TM_{1m} is approximately the inverse of $Q_{TE10,Thal}/Q_{TM10,Thal}$. Also, the power ratio TE_{1m}/TM_{1m} is no longer unity, as it was in the case for McLean's calculations with the minimum possible quality factor $\hat{Q}_{\min}$. As a result, Thal's approach predicts elliptical polarization [28].

The Q calculations by Thal [28] are summarized in Table 1.10 as compared to the $Q_{\min}$ given by McLean in Eq. (1.103). Also, Table 1.11 gives the corresponding surface current distributions necessary to excite the TM_{10}, TE_{10}, self-resonant $TM_{10} - TE_{10}$, and self-resonant $TM_{10} - TE_{20}$ modes [28] listed in Table 1.10. The necessary transformer turns N to make the resonant modes are listed in Table 1.12 [28].

1.3.12.4 Thal's Energy Lower Bound on the Mode Coupling Network

In [29], Thal seeks a relationship between small antenna gain and Q, and reexamines previous claims made on the topic. He notes that previous authors [4,6,21] who have examined the gain and Q relationship ignored any conditions on the energy inside the *Chu sphere*, and simply assumed zero internal stored energy. Consequently, it is found in [4,6,21] that it is theoretically possible for a small antenna to realize a gain of 3 and a Q given in Eq. (1.104) by equally exciting first order TE and TM modes. To find stricter limits on Q and gain, Thal begins by finding a lower bound on the energy inside the *Chu sphere*. As was in Chu [11], Thal represents the antenna system as the equivalent circuit shown in Fig. 1.60, where the input port and mode coupling network

Radiating Mode	Surface Current Distribution
TM_{10}	$\boldsymbol{J} = \pm\hat{\boldsymbol{\theta}}\,[A\sin\theta]$
TE_{10}	$\boldsymbol{J} = \pm\hat{\boldsymbol{\phi}}\,[A\sin\theta]$
$TM_{10} - TE_{10}$	$\boldsymbol{J} = -\hat{\boldsymbol{\theta}}\,[A\sin\theta] \pm \hat{\boldsymbol{\phi}}\,[NA\sin\theta]$
$TM_{10} - TE_{20}$	$\boldsymbol{J} = -\hat{\boldsymbol{\theta}}\,[A\sin\theta] \pm \hat{\boldsymbol{\phi}}[\sqrt{1.25}NA\sin 2\theta]$

TABLE 1.11 Current Distributions Over *Chu Sphere* Surface to Excite of Various Mode Configurations, with N given in Table 1.12. (*See Thal* [28])

ka	*N* for TM_{1m}-TE_{1m}	*N* for TM_{10}-TE_{20}
0.050	28.25	36.48
0.100	14.06	18.19
0.200	6.92	8.99
0.300	4.50	5.88
0.400	3.26	4.30
0.500	2.50	3.33
0.600	2.00	2.68

TABLE 1.12 Transformer Turns *N* to Achieve Self-Resonance for the Circuits Given in Figs. 1.57 and 1.59. (*See Thal* [28])

represent the antenna of *Chu sphere* radius *a*, and the radiated modes outside the *Chu sphere* are represented by the mode circuits given in Fig. 1.55 (using the exterior region circuits only). Thal states that the instantaneous power at each port is the sum of the average and time-varying powers.

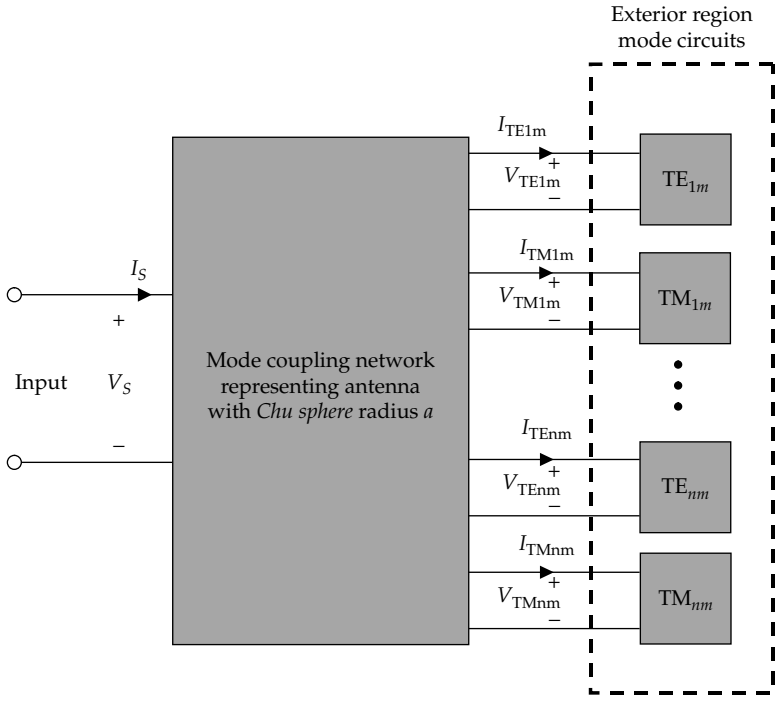

FIGURE 1.60 Equivalent network used in Thal's [29] time-varying circuit analysis to represent an arbitrary antenna with *Chu sphere* radius *a*.

Assuming a resonant antenna with no ohmic losses (zero average power in the coupling network), Thal begins his derivation of the coupling network energy bound by stating the time-varying power balance relation between the ports. Using Fig. 1.60 and assuming cosine referenced phasors for voltages and currents, Thal [28] expresses the time-varying power at the mode coupling network in terms of the voltages and currents at the ports through

$$\mathrm{Re}\left\{P_{C,\mathrm{tv}}e^{j2\omega t}\right\} = \mathrm{Re}\left\{\left(V_S I_S - \sum_{n=1}^{N} V_n I_n\right) e^{j2\omega t}\right\} \tag{1.175}$$

where $P_{C,\mathrm{tv}}$ is the time-varying power in the coupling network, V_S and I_S are the complex amplitudes of the time-varying voltage and current of the source, V_n and I_n are the complex amplitudes of the time-varying voltage and current at each of the mode circuit inputs, and N is the number of radiating modes. Thal remarks that for a resonant antenna, the instantaneous voltage and current at the source are in phase. Consequently, the time-varying power $V_S I_S$ must be the radiated power with an additional phase term $e^{j\xi}$. Suppressing the Re{ } operator and the $e^{j2\omega t}$ common to each term, Eq. (1.175) becomes

$$P_{C,\mathrm{tv}} = P_{\mathrm{rad}}e^{j\xi} - \sum_{n=1}^{N} V_n I_n \tag{1.176}$$

P_C is minimized when the phases of $P_{\mathrm{rad}}e^{j\xi}$ and $\sum_{n=1}^{N} V_n I_n$ are equal. Using Eq. (1.176) Thal forms the inequality

$$\left|P_{C,\mathrm{tv}}\right| \geq \left|P_{\mathrm{rad}} - \left|\sum_{n=1}^{N} V_n I_n\right|\right| \tag{1.177}$$

Due to the $e^{j2\omega t}$ time dependence of the time-varying components, the time-varying component of the energy in the coupling network is

$$W_{C,\mathrm{tv}} = \int P_{C,\mathrm{tv}}\,dt = \frac{P_{C,\mathrm{tv}}}{j2\omega} \tag{1.178}$$

Inserting Eq. (1.178) in (1.177) and multiplying both sides by ω, Eq. (1.177) can be written as

$$\frac{\omega \left| W_{C,\mathrm{tv}} \right|}{P_{\mathrm{rad}}} \geq \frac{1}{2} \left| 1 - \frac{\left| \sum_{n=1}^{N} V_n I_n \right|}{P_{\mathrm{rad}}} \right| \tag{1.179}$$

Thal then notes that the instantaneous energy in the coupling network can never be less than zero, thus the time-varying component of the energy in the coupling network $W_{C,\mathrm{tv}}$ can never exceed the average energy in the coupling network $W_{C,\mathrm{avg}}$. As a result, a lower bound on the coupling network energy can be found as

$$\frac{\omega_0 \left| W_{C,\mathrm{avg}} \right|}{P_{\mathrm{rad}}} \geq \frac{1}{2} \left| 1 - \frac{\left| \sum_{n=1}^{N} V_n I_n \right|}{P_{\mathrm{rad}}} \right| \tag{1.180}$$

where ω has been replaced with ω_0 to stress that the antenna is resonant. Thal states that using the minimum energy bound in Eq. (1.180), a stricter Q limit can be enforced as

$$Q = Q_{\mathrm{exterior}} + \frac{\omega_0 \left| W_{C,\mathrm{avg}} \right|}{P_{\mathrm{rad}}} \tag{1.181}$$

where Q_{exterior} is the quality factor of the antenna, assuming zero energy inside its *Chu sphere* (thus a *Chu antenna*). Q_{exterior} can be found simply by applying Eq. (1.3) to the exterior region mode circuits of Fig. 1.55 (omitting the internal region), in conjunction with knowledge of the modal excitation levels.

1.3.12.5 Applications of the Energy Lower Bound

Using the minimum energy bound Eq. (1.180) and the sharpened Q limit Eq. (1.181), Thal examines the often cited [4,6,21] result that it is theoretically possible for a small antenna to achieve both a gain of 3 and Q given in Eq. (1.104) using first order TE and TM modes. Thal considers the case where the TE_{1m} and TM_{1m} modes radiate equal power, with the phase of the TE pattern advanced by a phase angle $\Psi/2$ and the phase of the TM pattern delayed by $-\Psi/2$. This corresponds to the currents I_R in the unit terminating resistances of the exterior circuits in Fig. 1.55 having the form of

$$I_{R,\mathrm{TE}1m} = I_0 e^{j\Psi/2} \qquad I_{R,\mathrm{TM}1m} = I_0 e^{-j\Psi/2} \tag{1.182}$$

The power radiated by each mode is found as the power dissipated in the terminating resistances. With input currents and voltages at the TM_{1m} and TE_{1m} mode ports written in terms of the terminating resistance currents in Eq. (1.182), the coupling network energy bound Eq. (1.180) becomes [29]

$$\frac{\omega_0 \left| W_{C,\text{avg}} \right|}{P_{\text{rad}}} \geq \frac{1}{2} \left| 1 - \cos\Psi \sqrt{1 + 1/(ka)^6} \right| \tag{1.183}$$

For the case where the TM_{1m} and TE_{1m} modes correspond to the fields radiated by a z-polarized electric Hertzian dipole (TM) and a y-polarized magnetic Hertzian dipole (TE), respectively, the gain can be written as [29]

$$G = 3\cos^2(\Psi/2) \tag{1.184}$$

To achieve minimum possible Q, the coupling mode energy bound in Eq. (1.183) must go to zero. Under such conditions

$$\cos\Psi = (1 + 1/(\text{ka})^6)^{-1/2} \tag{1.185}$$

and from Eq. (1.184), the corresponding gain is

$$G_{\text{Qmin}} = 1.5 \left(1 + \frac{(ka)^3}{\sqrt{1 + (ka)^6}} \right) \tag{1.186}$$

with the corresponding Q given in Eq. (1.104) [29]. For a gain of 3, $\Psi = 0$ and Eq. (1.183) becomes

$$\left. \frac{\omega_0 \left| W_{C,\text{avg}} \right|}{P_{\text{rad}}} \right|_{\Psi=0} \geq \frac{1}{2} \left[\frac{\sqrt{1 + (ka)^6}}{(ka)^3} - 1 \right] \tag{1.187}$$

Using Eqs. (1.181) and (1.187), the corresponding minimum possible Q in the small antenna region is

$$Q_{\max(G)} \approx \frac{1}{ka} + \frac{1}{(ka)^3} - \frac{1}{2} \tag{1.188}$$

Equation (1.188) is nearly identical to the single mode minimum Q in Eq. (1.103). Thal concludes that the statements made in [4,6,21] proclaiming it is theoretically possible for a small antenna to achieve a gain of 3 and a Q of Eq. (1.104) are erroneous [29].

1.3.13 Work of Gustafsson (2007)

So far, spherical wave functions were used to represent the radiation outside the *Chu sphere*. In contrast, recent publications [30,53–54] considered a different approach to analyzing small antennas. As already

noted by Thiele [7], Thal [28], and Foltz and McLean [20], Chu's approach may not be suitable for practical antennas. Gustafsson et al. [30] proceeded to instead use the scattering properties of small particles (i.e., their polarizability dyads, $\bar{\bar{\gamma}}_e$ and $\bar{\bar{\gamma}}_m$) to extract the minimum Q, gain, and bandwidth of small antennas. His approach is evocative of Green's [54] work that related antenna gain to its radar cross-section.

To describe the approach in [30], it is important that we first introduce the small particle or low frequency scattering parameters found in many books and papers [57–60]. With the aid of Fig. 1.61, they are (see [55] and [56]):

- $\bar{\bar{\chi}}_e$: electric susceptibility dyad
- $\bar{\bar{\chi}}_m$: magnetic susceptibility dyad
- $\bar{\bar{\gamma}}_e$: electric polarizability dyad
- $\bar{\bar{\gamma}}_m$: magnetic polarizability dyad
- $\bar{\bar{\gamma}}_\infty$: high contrast polarizability; limiting value of $\bar{\bar{\gamma}}_e$ and $\bar{\bar{\gamma}}_m$ when the small scatterer is perfectly (electric or magnetic) conducting. It follows the $\bar{\bar{\gamma}}_\infty$ is symmetric 3×3 dyadic. It is therefore diagonalizable with its eigenvalues being $\gamma_{1,2,3}$ and $\gamma_1 > \gamma_2 > \gamma_3$.

1.3.13.1 Limitations on Small Antenna Gain-Bandwidth Product and *D/Q* Ratio

Gustafsson et al. considered the limitations on the gain-bandwidth product and D/Q ratio for a single resonance small antenna. A key

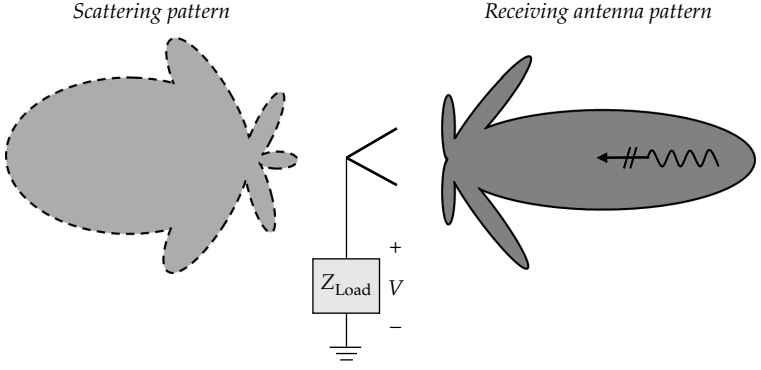

FIGURE 1.61 Antenna receiving and scattering patterns.

starting expression for the analysis is given in [30] as

$$\int_0^\infty \sigma_{\text{ext}}(\lambda)d\lambda = \pi^2 \left(\hat{\boldsymbol{p}}_e^* \bullet \bar{\bar{\gamma}}_e \bullet \hat{\boldsymbol{p}}_e + \hat{\boldsymbol{p}}_m^* \bullet \bar{\bar{\gamma}}_m \bullet \hat{\boldsymbol{p}}_m\right) \tag{1.189}$$

In this, $\hat{\boldsymbol{p}}_e = \boldsymbol{E}_0/|\boldsymbol{E}_0|$ is the polarization of the incident field to the small scatter (small antenna), and $\hat{\boldsymbol{p}}_m = \hat{\boldsymbol{k}} \times \hat{\boldsymbol{p}}_e$ where $\hat{\boldsymbol{k}}$ is the direction of propagation. It is shown in [30] that

$$\begin{aligned}\int_0^\infty \sigma_{\text{ext}}(\lambda)d\lambda &\geq \frac{1}{\tilde{\eta}} \int_{\lambda_1}^{\lambda_2} \sigma_a(\lambda)d\lambda \geq \frac{1}{\tilde{\eta}} \int_{\lambda_1}^{\lambda_2} \left(1 - |\Gamma|^2\right) \lambda^2 G(\lambda)d\lambda \\ &\geq \frac{1}{\tilde{\eta}} \min\left\{\left(1 - |\Gamma|^2\right) G\right\} \cdot \left(\int_{\lambda_1}^{\lambda_2} \lambda^2 d\lambda\right) \\ &\geq \frac{1}{\tilde{\eta}} \lambda_0^3 \min\left\{\left(1 - |\Gamma|^2\right) G\right\} \cdot B \end{aligned} \tag{1.190}$$

where $\lambda_1 = 3.10^8 f_1 =$ lower operational frequency wavelength
$\lambda_2 = 3.10^8 f_2 =$ upper operational frequency wavelength
$\lambda_0 = 2\pi/k_0 = (\lambda_1 + \lambda_2)/2 =$ average wavelength

$$\begin{aligned} B &= 2\left(\frac{\lambda_2 + \lambda_1}{\lambda_2 - \lambda_1}\right) = 2\left(\frac{k_1 - k_2}{k_2 + k_1}\right) = 2\left(\frac{f_2 - f_1}{f_2 + f_1}\right) \\ &= \text{fractional bandwidth} \end{aligned} \tag{1.191}$$

$G =$ antenna gain
$\Gamma =$ reflection coefficient at the feed port
$\tilde{\eta} =$ maximum value of the absorption efficiency over the wavelength interval $[\lambda_1, \lambda_2]$

It is also implied that $\min\left\{\left(1 - |\Gamma|^2\right) G\right\}$ is taken over the wavelength interval $[\lambda_1, \lambda_2]$. We note that in deriving Eq. (1.190) we used the approximation $\int_{\lambda_1}^{\lambda_2} \lambda^2 d\lambda = \lambda_0^3(1 + B^2/12) \approx \lambda_0^3$. It follows from Eqs. (1.189) and (1.190) that

$$\min\left\{\left(1 - |\Gamma|^2\right) G\right\} \cdot B \leq \tilde{\eta} \frac{\pi^2}{\lambda_0^3} \left(\hat{p}_e^* \bullet \bar{\bar{\gamma}}_e \bullet \hat{p}_e + \hat{p}_m^* \bullet \bar{\bar{\gamma}}_m \bullet \hat{p}_m\right) \tag{1.192}$$

and for a perfectly (electric or magnetic) conducting antenna structure, we have

$$\min\left\{\left(1 - |\Gamma|^2\right) G\right\} \cdot B \leq \tilde{\eta} \frac{\pi^2}{\lambda_0^3} \left(\hat{p}_e^* \bullet \bar{\bar{\gamma}}_\infty \bullet \hat{p}_e + \hat{p}_m^* \bullet \bar{\bar{\gamma}}_\infty \bullet \hat{p}_m\right) \tag{1.193}$$

with, of course, $\hat{p}_e \bullet \hat{p}_m = 0$. From the relations of $\bar{\bar{\gamma}}_{e,m,\infty}$, we can conclude that

$$\min\left\{\left(1-|\Gamma|^2\right)G\right\}\cdot B \le \tilde{\eta}\frac{4\pi^3}{\lambda_0^3}(\gamma_1+\gamma_2) \tag{1.194}$$

where $\gamma_{1,2}$ are the largest two eigenvalues of $\bar{\bar{\gamma}}_\infty$.

Gustafsson et al. proceeded to find a lower limit for the Q of a single resonance, lossless small antenna matched at the resonant frequency. From a single resonance model for the absorption cross-section, Gustafsson et al. argue that the antenna Q factor can be extracted [30]. Using the absorption cross-section model and Eq. (1.189), he finds that the directivity and Q for a small antenna are related through [30]

$$\frac{D}{Q} \le \tilde{\eta}\frac{k_0^3}{2\pi}(\gamma_1+\gamma_2) \tag{1.195}$$

We note the similarity of Eqs. (1.195) to (1.194), and we also remark the expected behavior that Q is inversely proportional to the antenna volume (since $\gamma_{1,2}$ are proportional to the antenna volume).

1.3.13.2 Applications of the Gustafsson Limits

Considering now an antenna being perfectly electric conducting (PEC), it follows that $\bar{\bar{\gamma}}_m$ and thus $\gamma_2 = 0$ in Eqs. (1.194) and (1.195) [30].

Also, $\gamma_1 = 4\pi a^3\gamma_1^{\text{norm}}$ [30], where a is the radius of the *Chu sphere* and γ_1^{norm} is given in Fig. 1.62 for several antenna geometries (scatterers). Further, since the directivity of single mode radiating small antennas (like the Hertzian dipole) is $D = 1.5$, it follows from Eq. (1.195) that

$$Q_{\min} = \frac{1.5}{(ka)^3\gamma_1^{\text{norm}}} \tag{1.196}$$

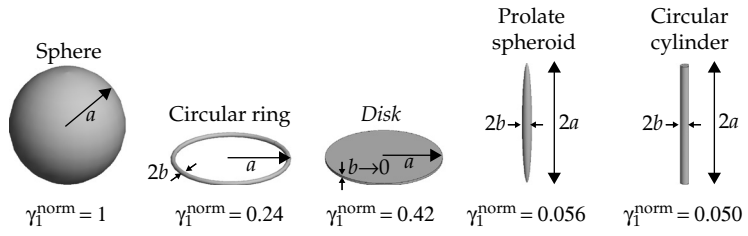

FIGURE 1.62 Normalized γ_1^{norm} eigenvalues for several small antenna geometries, with $b/a = 10^{-3}$ for the circular ring, prolate spheroid, and circular cylinder. (*See Gustafsson* [30].)

with γ_1^{norm} given in Fig. 1.62. Gustafsson also provides closed-form $\gamma_{1,2}$ expressions for prolate and oblate spheroids in [30] and shows that the oblate spheroid geometry has lower $Q_{\min}$.

For a spherical volume (*Chu sphere*), with $D = 1.5$ and $\tilde{\eta} = 0.5$, since $\gamma_1^{\text{norm}} = 1$, Eq. (1.196) gives

$$Q_{\text{Spherical,Gustafsson}} = \frac{1.5}{(ka)^3} \tag{1.197}$$

This is identical to Thal's antenna supporting a single TM_{10} mode. We also note that Gustafsson's (1.197) expression is identical to the Q values obtained by Best [24] for a N-turn four-arm spherical helix.

Another comparison to Gustafsson's analytic $Q_{\min}$ values are shown for a prolated spheroid (see Fig. 1.33). For numerical computations, the prolate spheroid (of height h and width $2a/3$) was modeled as a four-arm elongated helix antenna (see Fig. 1.63). Using the $TM_{10} - TE_{20}$ tuning technique describe in Thal [28] (varying the number of turns N in the four-arm elongated helix) the resonance was adjusted to generate the data in Fig. 1.64. The calculated values using the radiation data from the NEC code plotted in Fig. 1.64 and compared to the analytic Q in [30] with $\gamma_2 = 0$, $\tilde{\eta} = 0.5$, and $D = 1.5$. Indeed, though D/Q was derived assuming $|k| \to 0$, the Gustafsson limit and measured data of Fig. 1.64 are in close agreement even for $ka = 0.65$. From Fig. 1.64, we can conclude that unlike the limits derived using the fictitious *Chu antenna* with assumed mode excitation, Eqs. (1.194) and (1.195) allow for stricter upper bounds if the antenna is composed of purely electric material. Knowledge of the antenna's absorption characteristics are, however, necessary to use the Gustafsson limits.

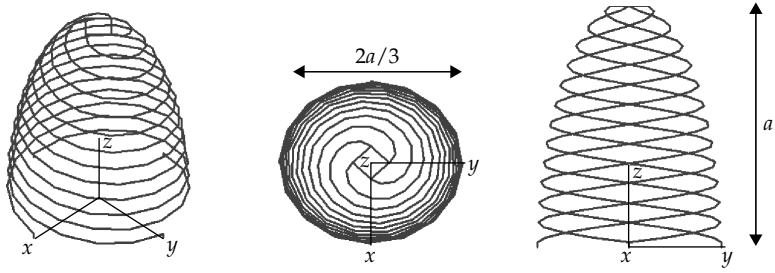

FIGURE 1.63 Three-turn four-arm elongated helix antenna with height/width = 2/3.

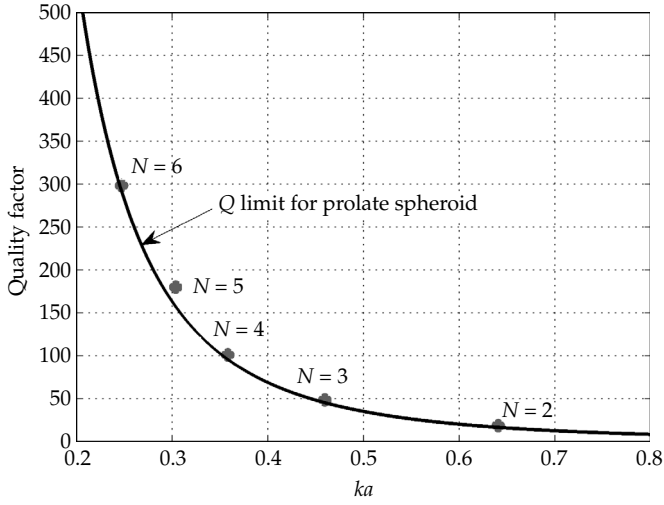

FIGURE 1.64 Gustafsson Q limit for prolate spheroid with width to height ratio 2/3 along with 4NEC2 measured N-turn four-arm elongated helix Q. (*See Fig. 1.63.*)

Comments

Though the methods used by different authors to evaluate small antenna properties have become more sophisticated, the basic principles relating antenna size and Q presented by Wheeler and Chu remain valid. The circuit approximations for the supported mode are likely most valuable in understanding small antenna parameters and their properties. Recent work has shown that the relationship between gain and Q remains a controversial topic. As seen by Chu [11], and recently by Thal [29], Gain and Q cannot be considered independent quantities in practice.

The work of Yaghjian and Best [10] provided a thorough evaluation of Q computation methods. While Q can be computed exactly through Maxwell's equations, in practical applications it is necessary to determine Q based on the antenna input impedance. Q can be easily computed from the antenna input impedance $Z_A(\omega) = R_A(\omega) + jX_A(\omega)$ as [10]

$$Q(\omega) \approx \frac{\omega}{2R_A(\omega)} \sqrt{\left(R'_A(\omega)\right)^2 + \left(X'_A(\omega) + \frac{|X_A(\omega)|}{\omega}\right)^2} \qquad (1.198)$$

Equation (1.198) remains valid for all frequency ranges and antenna sizes [10], and as a result is the most robust method for evaluating Q based on input impedance.

The minimum possible Q for a small antenna circumscribed by a *Chu sphere* (see Fig. 1.1) is a topic of significant practical relevance, as it provides a valuable reference as to how well a small antenna's bandwidth compares to an ideal case. We summarize several minimum Q formulas in Table 1.13. Notes on each formula are also provided, as it is critical to understand the underlying assumptions in each equation in order to make an appropriate comparison with the small antenna.

Recent works by Gustafsson, Best, and Thal did highlight the uncertainties in characterizing small antennas. So questions such as

- What antenna current gives the lowest Q?
- How can small antenna efficiency be increased?
- Can shape play a more important role in small antenna theory and parameter control?

although not fully addressed, are now much better understood.

Minimum Q	Reference	Notes
$\frac{1}{ka}+\frac{1}{(ka)^3}$	McLean [37]	Assumes TM or TE mode radiation only
$\frac{1}{2}\left(\frac{2}{ka}+\frac{1}{(ka)^3}\right)$	McLean [37]	Assumes TM and TE mode radiation
$\frac{1.5}{(ka)^3}$	Thal [28]	Assumes a surface current distribution over the *Chu sphere* surface radiating a TM mode
$\frac{3}{(ka)^3}$	Thal [28]	Assumes a surface current distribution over the *Chu sphere* surface radiating a TE mode
$\frac{1}{(ka)^3}$	Thal [28]	Assumes a surface current distribution over the *Chu sphere* surface radiating TM and TE modes
$\frac{G}{\tilde{\eta}}\frac{1}{2(ka)^3}$	Gustafsson et al. [30]	G = antenna gain $\tilde{\eta}$ = antenna absorption efficiency Assumes antenna composed of PEC material

TABLE 1.13 Summary of Small Antenna Q Limits for *Chu Sphere* of radius = a

References

1. H. A. Wheeler, "Fundamental limitations of small antennas," *Proceedings of the IRE*, vol. 35, December 1947, pp. 1479–1484.
2. R. C. Hansen, "Fundamental limitations in antennas," *Proceedings of the IEEE*, vol. 69, no. 2, February 1981, pp. 170–182.
3. R. F. Harrington, "Effect of antenna size on gain, bandwidth, and efficiency," *Journal of Research of the National Bureau of Standards*, vol. 64D, January–February 1960, pp. 1–12.
4. D. H. Kwon, "On the radiation *Q* and the gain of crossed electric and magnetic dipole moments," *IEEE Transactions on Antennas and Propagation*, vol. AP-53, May 2005, pp. 1681–1687.
5. D. H. Kwon, "Radiation *Q* and gain of TM and TE sources in phase-delayed rotated configurations," *IEEE Transactions on Antennas and Propagation*, vol. AP-56, August 2008, pp. 2783–2786.
6. D. M. Pozar, "New results for minimum *Q*, maximum gain, and polarization properties of electrically small arbitrary antennas," EuCAP 2009, Berlin, Germany, March 2009, pp. 23–27.
7. G. A. Thiele, P. L. Detweiler, and R. P. Penno, "On the lower bound of the radiation Q for electrically small antennas," *IEEE Transactions on Antennas and Propagation*, vol. AP-51, June 2003, pp. 1263–1269.
8. H. A. Wheeler, "Small antennas," *IEEE Transactions on Antennas and Propagation*, vol. 23, July 1975, pp. 462–469.
9. Y. Huang, R. M. Narayanan, G. R. Kadambi, "On Wheeler's method for efficiency measurement of small antennas," *IEEE International Symposium on Antennas and Propagation*, 2001, pp. 346–349.
10. A. D. Yaghjian and S. R. Best, "Impedance, bandwidth, and Q of antennas," *IEEE Transactions on Antennas and Propagation*, vol. AP-53, April 2005, pp. 1298–1324.
11. L. J. Chu, "Physical limitations on omni-directional antennas," *Journal of Applied Physics*, vol. 19, December 1948, pp. 1163–1175.
12. R. W. P. King, *The Theory of Linear Antennas*, Harvard University Press, Cambridge, Mass., 1956.
13. S. R. Best, "The performance properties of electrically small resonant multiple-arm folded wire antennas," *IEEE Antennas and Propagation Magazine*, vol. 47, no. 4, August 2005, pp. 13–27.
14. D. M. Pozar, *Microwave Engineering*, 3d ed., John Wiley & Sons, Hoboken, N.J., 2005.
15. R. E. Collin, *Foundations for Microwave Engineering*, 2d ed. McGraw-Hill, New York, 1992.
16. P. A. Rizzi, *Microwave Engineering: Passive Circuits*, Prentice Hall, Englewood Cliffs, N.J., 1987.
17. R. M. Fano, "Theoretical limitations on the broadband matching of arbitrary impedances," *Journal of the Franklin Institute*, vol. 249, Jan. 1950.
18. R. E. Collin and S. Rothschild, "Evaluation of antenna Q," *IEEE Transactions on Antennas and Propagation*, vol. AP-12, January 1964, pp. 23–27.
19. R. L. Fante, "Quality factor of general ideal antennas," *IEEE Transactions on Antennas and Propagation*, vol. AP-17, March 1969, pp. 151–155.
20. H. D. Foltz and J. S. McLean, "Limits on the radiation Q of electrically small antennas restricted to oblong bounding regions," *Proceedings of the IEEE AP-S International Symposium*, vol. 4, July 11–16, 1999, pp. 2702–2705.
21. Y. Geyi, "Physical limitation of antenna," *IEEE Transactions on Antennas and Propagation*, vol. AP-51, August 2003, pp. 2116–2123.
22. Y. Geyi, "A method for the evaluation of small antenna Q," *IEEE Transactions on Antennas and Propagation*, vol. AP-51, August 2003, pp. 2124–2129.
23. S. R. Best, "Bandwidth and the lower bound on Q for small wideband antennas," *IEEE International Symposium on Antennas and Propagation*, 2006, pp. 647–650.

24. S. R. Best, "The radiation properties of electrically small folded spherical helix antennas," *IEEE Transactions on Antennas and Propagation*, vol. AP-52, no. 4, April 2004, pp. 953–960.
25. S. R. Best, "Low Q electrically small linear and elliptical polarized spherical dipole antennas," *IEEE Transactions on Antennas and Propagation*, vol. AP-53, March 2005, pp. 1047–1053.
26. S. R. Best and J. D. Morrow, "On the significance of current vector alignment in establishing the resonant frequency of small space-filling wire antennas," *IEEE Antennas and Wireless Propagation Letters*, vol. 2, 2003, pp. 201–204.
27. H. A. Wheeler, "The spherical coil as an inductor, shield, or antenna," *Proceedings of the IRE*, vol. 46, September 1958, pp. 1595–1602.
28. H. L. Thal, "New radiation *Q* limits for spherical wire antennas," *IEEE Transactions on Antennas and Propagation*, vol. AP-54, October 2006, pp. 2757–2763.
29. H. L. Thal, "Gain and *Q* bounds for coupled TM-TE modes," *IEEE Transactions on Antennas and Propagation*, vol. AP-57, no. 7, July 2009, pp. 1879–1885.
30. M. Gustafsson, C. Sohl, and G. Kristensson, "Physical limitations on antennas of arbitrary shape," *Proceedings of the Royal Society A: Mathematical, Physical and Engineering Sciences*, vol. 463, issue 2086, 2007, pp. 2589–2607.
31. A. R. Lopez, "Fundamental limitations of small antennas: validation of Wheeler's formulas," *IEEE Antennas and Propagation Magazine*, vol. 48, no. 4, August 2006, pp. 28–36.
32. H. A. Wheeler, "The radiansphere around a small antenna," *Proceedings of the IRE*, vol. 47, August 1959, pp. 1325–1331.
33. T. Simpson, J. Cahill, "The electrically small elliptical loop with an oblate spheroidal core," *IEEE Antennas and Propagation Magazine*, vol. 49, no. 5, October 2007, pp. 83–92.
34. T. Simpson, Y. Zhu, "The electrically small multi-turn loop antenna with a spheroidal core," *IEEE Antennas and Propagation Magazine*, vol. 48, no. 5, October 2006, pp. 54–66.
35. C. A. Balanis, *Advanced Engineering Electromagnetics*, John Wiley & Sons, New York, 1989.
36. R. F. Harrington, *Time-Harmonic Electromagnetic Fields*, McGraw-Hill, New York, 1961.
37. J. S. McLean, "A re-examination of the fundamental limits on the radiation Q of electrically small antennas," *IEEE Transactions on Antennas and Propagation*, vol. AP-44, May 1996, pp. 672–675.
38. R. C. Hansen, *Electrically Small, Superdirective, and Superconducting Antennas*, Wiley, Hoboken, N.J., 2006.
39. S. R. Best, "A discussion on power factor, quality factor, and efficiency of small antennas," *IEEE International Symposium on Antennas and Propagation*, June 2007, pp. 2269–2272.
40. J. A. Stratton et al., *Spheroidal Wave Functions*, Technology Press of M.I.T. and John Wiley & Sons, New York, 1956.
41. C. Flammer, *Spheroidal Wave Functions*, Stanford Univ. Press, Stanford, Calif., 1957.
42. R. C. Hansen, *Microwave Scanning Antennas*, Peninsula, Los Altos, Calif., 1985.
43. C. A. Walter, *Traveling Wave Antennas*, 2d ed. Peninsula, Los Altos, Calif., 1990.
44. W. L. Stutzman and G. A. Thiele, *Antenna Theory & Design*, 2d ed. Wiley, New York, 1998.
45. D. R. Rhodes, *Synthesis of Planar Antenna Sources*. Clarendon, Oxford, U.K., 1974.
46. D. R. Rhodes, "On the stored energy of planar aperatures," *IEEE Transactions on Antennas and Propagation*, vol. AP-14, November 1966, pp. 676–683.
47. Y. Geyi, P. Jarmuszewski, and Y. Qi, "The Foster reactance theorem for antennas and radiation Q," *IEEE Transactions on Antennas and Propagation*, vol. AP-48, March 2000, pp. 401–408.
48. S. R. Best, "The Foster reactance theorem and quality factor for antennas," *IEEE Antennas and Wireless Propagation Letters*, vol. 3, 2004, pp. 306–309.

49. J. A. Andersen and S. Berntsen, "Comments on 'the Foster reactance theorem for antennas and radiation *Q*," *IEEE Transactions on Antennas and Propagation*, vol. AP-55, March 2007, pp. 1013–1014.
50. HFSS. ver. 11, Ansoft Corporation. Pittsbugh, PA, 2008.
51. J. Chalas and K. Sertel, The Ohio State University ElectroScience Lab, Personal Communication.
52. H. L. Thal, "Exact circuit analysis of spherical waves," *IEEE Transactions on Antennas and Propagation*, vol. AP-26, March 1978, pp. 282–287.
53. R. C. Hansen and R. E. Collin, "A new Chu formula for *Q*," *IEEE Antennas and Propagation Magazine*, vol. 51, no. 5, October 2009, pp. 38–41.
54. R. B. Green, "The general theory of antenna scattering," Ph.D thesis, The Ohio State University, November 1963.
55. C. Sohl, M. Gustafsson, and G. Kristensson, "Physical limitations on broadband scattering by heterogeneous obstacles," *Journal of Physics A: Mathematical & Theoretical*, September 2007.
56. C. Sohl, M. Gustafsson, and G. Kristensson, "Physical limitations on metamaterials: restrictions on scattering and absorption over a frequency interval," Technical Report LUTEDX/(TEAT-7154)/1-10/(2007), Lund University, Department of Electrical and Information Technology, Lund, Sweden.
57. J. B. Andersen and A. Frandsen, "Absorption efficiency of receiving antennas," *IEEE Transactions on Antennas and Propagation*, vol. AP-53, September 2005, pp. 2843–2849.
58. R. G. Newton, *Scattering Theory of Waves and Particles*, 2d ed., Springer-Verlag, New York, 1982.
59. J. R. Taylor, *Scattering theory: The Quantum Theory of Nonrelativistic Collisions*, Robert E. Krieger Publishing Company, Malabar, Fa., 1983.
60. R. Kleinman and T. Senior, "Low frequency scattering by space objects," *IEEE Transactions on Aerospace and Electronic Systems*, vol. AES-11, pp. 672–675.